The Nature of Habits in the Nonhuman Primate: The formation of sequences of eye movements and neural activity in the frontal eye field

by

Theresa M. Desrochers

B.S. Neural Science
New York University, 2000

Submitted to the Department of Brain and Cognitive Sciences
in Partial Fulfillment of the Requirements for the Degree of

Doctor of Philosophy in Neuroscience

at the

Massachusetts Institute of Technology

February 2011

Signature of Author: _____
Department of Brain and Cognitive Sciences
December 14, 2010

Certified by: _____
Ann M. Graybiel
Institute Professor and Professor in BCS
Thesis Supervisor

Accepted by: _____
Earl K. Miller
Picower Professor of Neuroscience
Director, BCS Graduate Program

The Nature of Habits in the Nonhuman Primate: The formation of sequences of eye movements and neural activity in the frontal eye field

by

Theresa M. Desrochers

Submitted to the Department of Brain and Cognitive Sciences
on December 14, 2010 in Partial Fulfillment of the
Requirements for the Degree of Doctor of Philosophy in
Neuroscience

Abstract

The nature of habits, their formation, expression, and underlying causes have been pondered for centuries. Early definitions, still in use today, posited that habits are actions associated with outcomes that, when repeated, become stimulus-response associations that can be performed automatically, or without the reinforcement of a rewarding stimulus. A prominent theory of what drives the process is reinforcement learning (RL). This definition and underlying theory may be inadequate to describe the complicated series of actions that we form and express as habits in every day life. We designed a task that would test the limits of RL by providing a nearly infinite number of action choices and no clear association with reward. We recorded using ~100 chronically implanted independently moveable electrodes from the frontal eye fields (FEF), prefrontal cortex (PFC), and caudate nucleus (CN) simultaneously as naïve monkeys performed a free-viewing scan task. Neural recordings began on the first day of this task where a random dot on a grid of targets was chosen to be baited with reward on every trial and the monkeys were free to look around until they captured the baited target. We found that monkeys formed self-guided and uninstructed sequences of eye movements that gradually evolved over months of task performance and did not appear to be driven by overall reward or cost measures. Only on a much smaller, trial-by-trial, time scale were we able to detect the RL forces at work and that the monkeys were minimizing cost on an extremely local level. We also found that neural units in the FEF showed standard single direction and non-standard multiple direction tuning very early in task acquisition. We also found a disproportionately high number of units whose tuning directions were selective for those eye movement combinations that were members of the monkeys' habitual sequences. This suggested that the FEF very rapidly adapts to the task at hand and the neural representation becomes biased towards those sequences that are repeated. Together these findings lay the foundation to understand natural habit formation and the neural mechanisms that underlie it.

Thesis Supervisor: Ann M. Graybiel
Title: Institute Professor and Professor in BCS

Acknowledgements

First, I would like to thank my family, who has been there for me through it all. To my parents, who have encouraged and supported me since day one of life. To my brothers, Paul and Peter, and my sister, Christina, who were always happy to cheer me on, through my triumphs and tribulations, and lend a helping hand whenever they could.

To my husband, Chris, who has taught me so much about living and loving science and life. He is my perfect balance and has been there at any hour of the day or night for anything from diapers to circular statistics and everything in between. To my son, Carter, who taught me how to be very efficient with my time and how to work on very little sleep, but most of all who taught me that the joys of motherhood go right along side the joys of science.

I would also like to thank members of the lab and the broader scientific community who have helped me grow. First, to my advisor, Ann, who welcomed me into the lab to do a project that was a dream for the both of us, and much more ambitious than probably either one of us imagined. She encouraged me through many difficult situations, both in the lab and out. To Joey, my comrade at arms, who has been my friend, confidant, and consultant through many years in the trenches. To Dan, who helped write a lot of code and solve many analytical puzzles. To Brian, who helped with the monkeys. To my office mate and friend, Katy, who was a sounding board for many questions. To Terra, who lived the life of successful graduate student mother at the desk next door.

To all the undergraduates: Jen, Lauren, Allison, Lulu and Geoffrey, who have worked with me and taught me about being a mentor along with contributing to my work in ways big and small. To all the members of the monkey group, past and present, who gladly gave help and advice even when it was not convenient to do so. To Henry, Yasuo, Clark, Jules, Brandy, Emily, Gila, Alex, Pat, Christine, and Margo who have offered invaluable assistance and together know just about everything about everything and try to keep us all sane. To the rest of the Graybiel lab who have helped with smiles and feedback at every point of the way.

To the members of my committee: Peter Schiller, Sebastian Seung, and Krishna Shenoy for shepherding me through the final years and chapters and offering advice and encouragement along the way. To Dr. Bob Marini and the rest of the vet and animal care staff who care for the animals with knowledge and kindness. Our work would not be possible without their understanding and willingness to work with us.

Last, but definitely not least, I would like to thank that most invaluable extended support network I have, my friends and extended family. To Amy and Rosie who almost always have time to chat, don't mind when I don't, and have been there since before I knew what neuroscience was. To Nicole who has been an inspiration in living life and being a woman physiologist. To Linda who has been so generous and caring in so many ways. To Jocelyn, Julie, Jen, Emily, Neville and my other classmates for sharing stories, struggles and triumphs. To all the rest of my friends and family who invariably brightened my days, even when time was not abundant.

Finally, to Zoltan and his family, who were there for me in a different chapter of my life.

Thank you all.

Table of Contents

Chapter I: Introduction

Habits

"We are what we repeatedly do. Excellence, then, is not an act, but a habit." – Aristotle
"Habit is either the best of servants or the worst of masters." – Nathanael Emmons

Theories about habits and how to define them have existed throughout the ages. Everyone would agree that we, as people, have habits that cover an entire spectrum of behaviors: everything from how you tap your pen when you are thinking or get to work in the morning to biting your nails or being addicted to substances. So what, then, is a habit? One could define a habit as a series of thoughts or actions that can be performed automatically, or without thinking. This rather simplistic definition of habit becomes more difficult to grapple with in the context of the behavior of animals, as it becomes more difficult to define what is done automatically.

Perhaps the first controlled experimental description of what could be considered a habit in animal behavior was by Skinner in his description of the 'superstitious' behavior of pigeons (Skinner 1948). He described that pigeons on an interval schedule of reward would show operant conditioning and even though the reinforcement was not contingent on the behavior in any way, they would repeat the behavior that came before the reward over and over again. In some animals the repeated behavior gradually changed and in others it stayed the same, but all the behaviors persisted through extinction, when actions were no longer associated with reward, and were readily reinstated when reward was reintroduced. He later describes a 'sensory superstition' whereby an arbitrarily presented stimulus could lead the pigeon to behavior that indicated a 'positive superstition', where the arbitrary stimulus led to more reinforcement, or the opposite, a 'negative superstition', where the arbitrary stimulus led to less reinforcement (Morse and Skinner 1957). There was, however, a difference between habit and these superstitions. The pigeons were not consistent in their association with a particular outcome. They switched between the 'positive' and the 'negative' over the course of the experiment. Despite this, this work was part of the establishment of behaviorism where these 'superstitious' behaviors or habits were direct results of stimulus-response (S-R) associations that were learned so that a particular stimulus would come to reflexively trigger a particular response.

Behaviorism did have its limitations, however, and one of Skinner's most famous critics was Chomsky. In his review of Skinner's Verbal behavior (1959), Chomsky points out that S-R associations are not sufficient to explain a complex organism's behavior, that the 'internal structure of the organism' is also important. He also points out that what a 'reinforcer' exactly is can be difficult to define, and indeed sometimes the relationship between reinforcer and behavior is almost impossible to decipher. He presents evidence that other 'drives' must be at play.

The next theories to emerge for the explanation of these habitual behaviors center more on the 'central motivational state' of the animal and how it works in concert with other state variables for animals to form stimulus-stimulus contingencies (Bindra 1974). In this context habit formation was viewed as a chain of successive conditioned stimuli being strung together until it could be executed as a whole and was triggered by the initial conditioned stimulus. This set of theories also explained situations that were defined to be outside the scope of behaviorism. Other early experiments also illustrated the limitations of behaviorism. It was found in pigeons that they would sustain their pecking of a key, despite it being negatively associated with reinforcement; that is, pecking the key actually prevented reinforcement (Williams and Williams 1969). This work highlighted the importance of examining the stimulus-reinforcer relationship, not just the response-reinforcer relationship as behaviorism emphasized.

Subsequent theories about habit formation, however, did not ignore behaviorism and replace those ideas with more goal-directed centric ones, but instead combined the ideas, stating that when goal-directed actions are repeated, they become S-R habits (Balleine and Dickinson 1998). This concept was supported by the introduction of an experimental procedure that illustrated that actions had become independent of the outcome or goal: reward devaluation. In brief, in this protocol, animals were trained on a particular action-outcome pair with a reinforcer (food reward). Then the reinforcer would be devalued by, for example, pairing it with sickness induced by the reinforcing stimulus and the animals would be tested for their repetition of the action. After extended training, it was shown that regardless of this devaluation of the reinforcer, animals would continue to respond (Adams 1982). Thus was the birth of an experimental protocol to test whether or not an action was habitual. Additional criteria were developed for defining action-outcome (A-O) behavior, but they are much less frequently used by experimenters as a test for whether or not a behavior is habitual. These included to what degree the action was contingent on the reinforcer (e.g. the reward being delivered with a particular timing, but with a variable contingency on if a lever was pressed) and the rate of reinforcement (Hammond 1980; Dickinson et al. 1996; Hilario and Costa 2008).

Current theories about habit formation, interestingly, have not come altered much from variations on the theme of A-O contingencies that gradually become S-R associations. There have been slight modifications, such as defining the automaticity as being between a context and a response (Wood and Neal 2007), and they have been expanded into the computational realm with theories that apply model-based (analogous to A-O) and model-free (analogous to S-R) learning algorithms to the way actions associated (Daw et al. 2005). Very few recent studies of habit formation have been conducted outside the rodent model, and studies on humans have tended to focus on addiction rather than on habit formation in and of itself (Hikosaka et al. 1995; Miyashita et al. 1996). Current theories also do not seem to be able to explain, or account for, habits and behaviors that are more complex, though there has been some work showing the conditions under which superstitions are developed in humans. The less control a person perceives there to be over a situation, the more likely a person is to perceive an illusion of pattern (Whitson and Galinsky 2008). There is a richness that has not yet been captured by the literature though there is a recognition of the existence of a much broader definition (Graybiel 2008).

Types of Eye Movements

In order to study a complex sequence of movements that can be described as a habit in the primate, it is advantageous to use as a model system one which is as simple as possible in terms of degrees of freedom of movement. With only six muscles that control the position of the eye in the orbit, and the extensive understanding of the mechanical and neural control mechanisms underlying them, eye movement sequences are the ideal simplified system in which to study habits.

There are five basic types of eye movements that are used to maintain a stable image of the world and orient to new objects: vestibulo-ocular reflex (VOR), optokinetic response (OKN), vergence, smooth pursuit, and saccades. These types of eye movements have differing neural control mechanisms. The first three types are not volitional. First, the VOR is a reflex that stabilizes the eyes as the head moves and is controlled by the vestibular system. Second, the OKN is generated when the head remains stationary and there are large fields moving across the retina, such as watching objects pass by from a moving car; the control of this is through vestibular-oculomotor circuits. Third, vergence eye movements rotate the eyes in opposite directions on a vertical axis to focus on objects near or far from the eyes. This command comes through the oculomotor nucleus (Buttner-Ennever and Horn 1997).

The remaining two types of eye movements, smooth pursuit and saccades, can be volitionally controlled. Smooth pursuit and saccades are the conjugate eye movements that are used to maintain or bring objects of interest for viewing on the fovea. The fovea is the most densely packed region of photoreceptors in the retina that produces the highest visual acuity. Smooth pursuit maintains the position of the fovea on a moving object. The sensory information for smooth pursuit comes from two parallel retinal pathways: the magnocellular (motion-sensitive) and parvocellular (form- and color-sensitive) pathways. These two streams travel through the lateral geniculate nucleus of the thalamus (LGN) and then to dorsal visual cortex (Buttner-Ennever and Horn 1997; Schiller and Tehovnik 2005). Areas that can be stimulated to elicit smooth pursuit movements are medial temporal (MT) cortex, medial superior temporal (MST) cortex, and frontal eye fields (FEF) (Gottlieb et al. 1994; Schiller 1998). Cells responding to smooth pursuit movements can also be found in area 7a of the parietal lobe and in dorsomedial frontal cortex.

Saccadic eye movements are high-velocity eye movements for the purpose of very rapidly bringing an object into foveal view. There are several brain areas capable of generating saccadic eye movements and they can be divided into the anterior and posterior systems. All areas within these systems can be stimulated to produce saccadic eye movements. The posterior system consists of the superior colliculus and occipital (V1, V2) and parietal cortices (lateral intraparietal sulcus, LIP). The anterior system contains the frontal eye fields (FEF) and medial eye fields (MEF), also known as the supplementary eye fields (SEF). Ablating the superior colliculus eliminates the ability to elicit eye movements via stimulation from the occipital and parietal corticies but not from the anterior system (FEF and MEF) (Schiller and Tehovnik 2001).

Natural Saccades

To study habitual sequences of eye movements, it is necessary to simplify the visual environment in order to elicit only one type of volitional eye movement: saccades. Two parameters are modified to produce a simplified visual environment. The first simplification uses a two-dimensional rather than a three-dimensional space in order to limit vergence movements. The second simplification effectively eliminates motion in the visual field and thus limits VOR, OKN, and smooth pursuit eye movements. Both simplifications are common in experimental paradigms and can be accomplished by presenting visual stimuli on a computer screen or other flat surface in front of the stationary subject.

Saccades have been studied in many such simplified visual environments. One common task used to study sequences of eye movements is in the visually guided saccade task. In general, visually guided saccade tasks require subjects to fixate a spot of light and then make a saccade to another spot of light that appears in the visual field. There are many instantiations of this task that vary parameters such as stimulus location, number of stimuli, the timing of the illumination of targets, and the existence of extraneous targets that are not saccaded to. For the purposes of studying habitual sequences of saccades, this task was adapted to require monkeys to perform a series of up to seven visually guided saccades (Fujii and Graybiel 2003). One-by-one, targets were illuminated within a grid of potential targets to instruct the monkey where and when to next move its eyes. These sequences were either random or repeated and the monkeys received extensive training prior to recording. The authors found phasic neural responses to the boundaries (beginning and ends) of the sequence in the prefrontal cortex.

Though this explicit timing and order of visual cues is well suited for initial questions regarding sequences of saccades, it is far more simple than the natural visual environment. Two follow up questions therefore emerge from this work: 1) do these same neural markers of the beginnings and ends of sequences exist when the monkey is not specifically instructed where or when to move its eyes; and 2) do these responses exist in the naïve, rather than over-trained animal? In order to address the first question, it is necessary to study uninstructed or "free" eye movements.

Natural eye movement patterns were first studied in detail by Yarbus, who observed that these movements were not just random, but followed particular paths based upon the task at hand (1967). This cognitive control of eye movements has now been shown numerous times in the context of natural tasks in humans (Hayhoe and Ballard 2005; Jovancevic-Misic and Hayhoe 2009). However, there is still relatively little understood about of the neural basis of these eye movement patterns, or what the eye movements themselves look like, independent of a specific task requiring motor action. There is an even smaller body of work that explicitly examines habitual eye movement patterns, as discussed below.

Some early work suggesting that humans do have habitual eye movement patterns, or scanpaths, comes from experiments examining eye movements during "pattern perception" where the patterns were "pictures" of particular objects (a line drawing of a face is the only example shown) (Noton and Stark 1971a; Noton and Stark 1971b). In this study they showed that while subjects were in the "learning phase" they tended to repeat the same scanpaths for the same objects, and then later in the "recognition phase" the initial movements again contained these

same paths. They concluded that while pattern/object perception seems habitual for each subject, it was not consistent from subject to subject.

The question then remains as to what commonalities there may be in the scanpaths that humans adopt. One study that used a two-location visual search task found that when subjects were only given enough time to search one location, all subjects scored better on finding the target when their first saccade was to the location that had been the most probable one to find the target (Araujo et al. 2001). It would seem intuitive, then, that subjects would then use the probability cue for all of the trials, but, surprisingly, this was not the case. Instead, subjects often looked first at the location that was closer to the fixation point. The authors suggest that this may have been because subjects were trying to "minimize the cognitive and attentional load" that goes along with planning. This could be viewed as a suggestion that we have a tendency to try to routenize eye movement behavior, as making a set of movements habitual is often thought of as having the effect of making it less effortful and more automatic.

Other work has shown that humans adopt scanpaths through an array of random targets when they must fixate each target in the course of going from start to goal, with the scanpaths adhering to a combination of a few basic strategies: 1) direction based 2) perceptually based on local information, or 3) perceptually based on global information (Findlay and Brown 2006). The authors show that within each subject, the strategy is consistent across arrays. They also show that the scanpaths are close to optimal within each strategy, and other work has shown that optimality in search is a unifying principle (Najemnik and Geisler 2005, 2008). However, different subjects do use different scanning strategies and in the one subject where the experiment was repeated, the authors observed a relatively low similarity between scanpaths on the two sessions (more similarity for fewer targets). They conclude that the variability they saw may be intrinsic to the system. Thus, this study points to a subset of commonalities between subjects, but does not adequately address whether these eye movement patterns can become habitual.

Across subjects, commonalities in series of eye movements have thus far only been hinted at. In one study, Gilchrist and Harvey examined the directions of eye movements as subjects scanned a 5x5 grid of triangles for the one that was oriented upwards along with two other task conditions where the triangles were less-regularly arrayed (2006). They found that in all task conditions there was a strong bias for the subjects to use horizontal eye movements, regardless of how regularly arrayed the targets were. The authors used this to suggest that there was a common strategy for how subjects performed this task, but precisely what the strategy was or what the strategy in any task that requires scanning a visual scene with similar objects, still remains to be identified.

Very few studies have examined free scanning eye movements in monkeys. An early study observed consistent latencies in visual search through many targets which was taken to indicate consistent scan paths (Latto 1978b). Another study had monkeys make scanning eye movements on a grid of nine fixation stimuli for the purposes of examining the incidence of different saccade latencies in the context of a target appearing at random for the monkey to acquire after a natural fixation (Sommer 1994). Though the scanning movements were not systematically examined for patterns the author did indicate that they existed (personal communication, Sommer 2006). Other

studies have examined natural eye movements without the use of a display of targets but the observations regarding patterns of eye movements were limited to the fact that horizontal saccades were more prevalent (Henn and Cohen 1973).

We therefore designed a task that utilized natural eye movements, but allowed the analysis of sequences of saccades. The naturalistic scan task we designed for monkeys required them to scan a grid of dots until they passed through or fixated on a dot that had been randomly chosen to be the target baited with reward. There was a delay imposed before the monkey could "find" the baited target to ensure a sufficient number of eye movements with which to examine their sequence properties. Therefore, the scan task was as natural as possible while somewhat constraining the dimensionality of the visual space. We placed no restrictions on where or when the monkey could move its eyes and the targets themselves were placed within the amplitudes of saccades that humans and monkeys make naturally (Henn and Cohen 1973; Bahill et al. 1975). This experimental design would allow us to address the question of whether neural activity like that found by Fujii and Graybiel (2003), that marks the boundaries of habitual eye movement sequences, exists if the monkey is not explicitly instructed to move its eyes.

Habits in the Brain

In order to examine the second question raised by Fujii and Graybiel (2003), whether neural activity related to habitual sequences of movements exists in the naïve animal, two things were necessary. One was to be able to record from target brain regions chronically, over the course of extended task acquisition and performance. Individual, daily penetrations are not only impractical for recording from multiple brain regions simultaneously, but they do not enable the tracking of the neural properties of very small cortical regions (i.e., without moving the electrode) over the long term. The second was to identify those brain regions that participate in the acquisition and performance of habitual eye movement sequences and record from them starting from the very beginning of task acquisition.

In order to address the issue of chronic recording, we developed in the lab a system for recording from ~100 or more independently moveable electrodes for months at a time. This system is discussed further in the *Appendix*.

There are many brain areas that could be of interest in studying habitual sequences of saccadic eye movements. First, one would want to study a region involved in generating those saccades. There are many areas capable of this, and they are members of either the anterior or posterior system of saccade generation. Whereas the posterior system seems to be for generating saccades rapidly, the anterior system, and in particular the frontal eye field (FEF), seems to be for target selection and slightly more complex tasks where the temporal order of saccades is important (Schiller and Tehovnik 2001). Other brain regions have also been shown to participate in sequences of eye movements, but perhaps in a less generative fashion (Schiller and Chou 1998). Work in our own lab has demonstrated neural responses in the prefrontal cortex (PFC) at the beginnings and ends of sequences (Fujii and Graybiel 2003). Thus the FEF and PFC were good candidate brain regions in which to target recordings.

Recordings examining the neural activity underlying habitual sequences of movement would be incomplete with only recordings from neocortical sites. Habits are thought to be controlled by "loops" between cortical and subcortical structures which include the basal ganglia (Alexander et al. 1986; Graybiel 2008). We would therefore want to record from an area connected to the FEF and PFC that participates in habitual behavior acquisition: the caudate nucleus (CN) (Parthasarathy et al. 1992). The CN has been shown to be involved in natural sequences of monkey behaviors such as grooming, eating, and threatening (Van den Bercken and Cools 1982), sequences of target presses (Kermadi and Joseph 1995; Miyachi et al. 1997), sequences of visually guided saccades (Fujii and Graybiel 2005), and the acquisition of new behaviors (Jog et al. 1999; Barnes et al. 2005; Pasupathy and Miller 2005; Williams and Eskandar 2006).

Chronic recordings of units in the FEF, PFC, and CN were made, starting with experimentally naïve animals, throughout the months of task acquisition and performance. However, only a subset of these recordings were included for analyses for this thesis. The recordings were originally designed to record from the entire circuit, with an emphasis (in numbers of electrodes) on recording from the brain area thought to be most influential in habit formation and thought to be interconnected with those areas related to eye movements, the CN. However, to begin to analyze these data recorded from the initially naïve animal in the context of a relatively unconstrained task (free eye movements), it was necessary to begin with analyses of a region where the physiological responses to number of visually guided saccade tasks was well established. The FEF is just such a region, and previous work provided benchmarks by which to assess neural responses. Comparatively little is known about the specifics of all cell types in the CN and how it participates in the acquisition of habits. Similarly, there have been a wide variety of neural responses categorized in the PFC, and responses often seem to be very task specific indicating the adaptability of the region. This would make it difficult to categorize neural responses in a novel and uninstructed task without first having a nearby region to compare to. With all these factors in mind, the neural recordings analyzed for this thesis were from the FEF. An obvious future direction will be to analyze those recordings from the PFC and CN that were made simultaneously, and this will be discussed further in the *Discussion* (*Chapter IV*).

Frontal Eye Field

The first experiment to characterize the firing properties of neurons in the FEF of an awake monkey without stimulation found that neurons only discharged after the initiation of an eye movement, and it was therefore thought that these neurons were not involved in voluntary eye movements (Bizzi 1967). This study was then expanded upon by early work that examined general responses of cells in the FEF during head movements, visually guided saccades, and after ablations of the FEF and SC (Bizzi and Schiller 1970; Mohler et al. 1973; Schiller et al. 1979). A subsequent study cataloged the responses of neurons in the intact FEF as monkeys fixated a single target on the screen and then made saccades to another target (Bruce and Goldberg 1985). They categorized FEF cells into those that responded pre-saccade, post-saccade or as having no-saccade response, and then further categorized the responses of the pre-saccadic neurons as visual (V), visuomovement (VM), or movement (M) responses. These categories persisted for quite some time. Later studies performed a more quantitative analysis of exactly when neurons in the FEF discharged in relation to saccades, including a description of multiple bursts of activity, particularly in VM cells (Schall 1991).

Single direction tuning – two saccades

Studies of saccades to single targets were soon augmented by studies that required the animal to make two saccades. The first of these tasks, the "double-step" task required the monkey to saccade to two successively flashed targets which were both extinguished before the first saccade. The endpoint of the second saccade was arranged so that it was either in the receptive field of the cell at the beginning fixation, or during the fixation between the first and second saccades. Cells in the FEF preferred the latter condition and were relatively independent of the eye's initial position. These results suggested that the direction of the saccade, and not the retinal or spatial location of a target, was what the neurons in the FEF primarily signaled (Goldberg and Bruce 1990).

The next questions in the context of executing two saccades centered on whether saccade execution is necessary to see a response in the FEF and what the involvement of the FEF might be in the planning of saccades. A "continuous stimulus" task addressed these questions. In this task the monkey made two saccades in the same direction, and at the appearance of the second fixation point a "behaviorally irrelevant" stimulus also appeared in the future receptive field of the cell. Approximately 30% of V and VM cells showed a predictive visual response; that is, cells responded when the upcoming saccade would bring a stimulus into the cell's receptive field (Umeno and Goldberg 1997). This predictive visual response was observed regardless of whether a saccade was prepared to go to the target in the receptive field. A subsequent study flashed the "irrelevant" target and found responses in the FEF to the remembered location not only in trials were the target was flashed, but also in trials that followed a block of trials when the target was flashed (Umeno and Goldberg 2001). This illustrated the rapid plasticity of the FEF in adapting to the expectations of the task. Both studies also suggested that saccade preparation is not necessary to evoke activity in the FEF, though with such a limited display (only three targets), it was difficult to judge what was "relevant" and "irrelevant" to the monkey.

Lesions – two saccades

The preceding studies suggested that the FEF was involved in the planning and execution of more than one saccade (or possible saccade). This was further supported by lesion work that showed large and lasting deficits with unilateral lesions to the FEF of single saccades to paired targets and two saccades to a sequence of sequentially presented targets (Schiller and Chou 1998). Studies that inactivated the FEF corroborated this result and produced a deficit in both single-step and double-step saccades, saccades made to two sequentially flashed visual targets (Sommer and Tehovnik 1997, 1999). Whereas deficits in single saccade tasks eventually recovered after lesions to the FEF, saccades to two or more sequentially presented targets did not recover, nor did the selection of simultaneously presented targets (Tehovnik et al. 2000). This finding further supports these neurons being involved in sequences of saccades.

Visual search - one saccade, many targets

The compliment to studies of FEF cells while monkeys performed multiple saccades to single targets are studies that examined the neural responses when the monkeys were asked to "search" for a single target to saccade to amongst multiple distracters and report its location using a saccade to that target. The first study to record activity from the FEF while the monkey performed visually guided saccades with multiple targets on the screen found that response properties were more complex than previously thought; activity related to the location of the

target in the array evolved through time and could be dissociated from saccade initiation, indicating a possible role in target selection (Schall and Hanes 1993; Schall et al. 1995). The participation of the FEF in learning habitual, stimulus-response associations was illustrated by results showing that they modulated their selectivity according to the color of the stimulus set the monkeys had been trained on (Bichot et al. 1996). These results collectively showed the participation of the FEF in target selection, specific even to the stimulus set trained on.

More recently, studies on the FEF have used visual search tasks that do not require an eye movement to report the location of the target. This resolves a potential confound in the previous studies where saccade preparation and target selection occurred simultaneously, though previous work had shown an example FEF cell that signaled the presence of the target in the receptive field when a saccade was not made (Schall et al. 1995). Such "covert" search tasks that require the shifting of attention and not eye position itself have supported that target selection emerges in the FEF without explicit saccade preparation by showing that selectivity for the target emerged in spiking activity before it did in the local field potential (LFP), which is thought to represent the inputs to the area (Monosov et al. 2008). A task which required monkeys to remember a cued target location through a delay and then detect a change at that cued location within an array without making any saccades found that cells in the FEF had delay period activity that was predictive of whether or not the monkey would detect a change (Armstrong et al. 2009). The shifts of attention required by visual search were also found to potentially be carried out by the FEF (Buschman and Miller 2009).

Sequences

These studies that used many targets with and without saccade preparation still left open the question of what role the FEF plays in more than two saccades. The preceding tasks utilized more than one saccade for the purposes of trying to understand the participation of the FEF in the planning, execution, or mapping out of space for single saccades. One of the first studies to explicitly examine activity in the FEF during sequences of three saccades focused on the population of cells in the FEF that are activated by the appearance of a target in their future receptive field, without preparing a saccade to that location, termed quasi-visual (QV) neurons. The authors found that these cells fired in a "triple step" (three-saccade) paradigm the most after the first saccade, regardless of whether the subsequent saccade was toward or away from the receptive field of the cell. This provided evidence of a "map" hypothesis of these cells, as they appeared to indicate all possible upcoming targets, regardless of saccades made directly to them (Tian et al. 2000). However, if the second saccade did not enter the receptive field, then the third saccade did, and it is possible that this activity could represent not a map, but the fact that the monkey knew after extensive training that it would make a saccade into the receptive field of that cell in two steps instead of one. A study that specifically examined sequences three center-out-center saccades found a small fraction of neurons with pre-saccadic activity in the FEF responded selectively in relation to the rank of the eye movement (what order it came in, 5%), both the rank and direction (15%), or the entire sequence (9%), though this was significantly less than the proportions found in the SEF (Isoda and Tanji 2003). Stimulating during sequences of two saccades found a similar difference: sequences of two saccades were more affected by stimulation in the SEF than in the FEF (Histed and Miller 2006). These studies suggested that the FEF played an active role in sequences of eye movements, even if it was potentially less than other brain regions (but see Schiller and Chou 1998).

Natural sequences

The finding that neurons in the FEF respond to sequences of instructed eye movements then leads to the question of what occurs during natural sequences. Very early work examined the effects of FEF lesions on the performance of a well-learned search task where the monkey freely looked for a circle among ~30 other shapes. FEF lesioned monkeys showed an increased time to find the target along with a small increase in incorrect responses, but deficits were minor and the animals could still perform the task. Further, the extent of the impairment in the FEF lesioned animals was proportional to the amount of training the animal had received preoperatively: the more training, the less of an impairment (Latto 1978b, a). Though these results were suggestive, they were not conclusive as the monkeys' eye position had not been recorded throughout task execution.

The first paper to report on neural responses in the FEF during natural scanning eye movements demonstrated visual- and movement-related activity and found that cells increased their activity during scanning when a portion of the image in the receptive field was the target for the next saccade, but decreased if the target was outside the cell's receptive field (Burman and Segraves 1994). A significant conclusion of this study was that the visual activity of the neurons during natural scene scanning could not have been predicted from the responses during more conventional tasks. A second study of neural activity in the FEF during natural scanning eye movements found cells with V and VM activity had activity that predicted the next saccade prior to when the current visual input would have produced such activity. Also the authors found "advance" predictive activity which occurred later in the fixation period prior to a sequence of two saccades that predicted the direction or goal of the second saccade in the sequence (Phillips and Segraves 2009). Such a result could be construed as sequence selectivity during natural scanning eye movements. However, the role of the FEF in habitual, repeated sequences of natural eye movements remains unclear.

Other responses

Neurons in the FEF, though they predominantly have shown responses to saccades, also show a wide variety of responses to other stimuli such as foveal fixation, smooth pursuit, head turning, orbital position, and auditory stimuli (Bizzi and Schiller 1970; Bruce and Goldberg 1985). Smooth pursuit neurons have been found to occupy a particular region of FEF and are selective for a particular direction of pursuit with and without microstimulation (Gottlieb et al. 1994). Reward modulation has also been seen in the FEF, but it was spatially selective unlike in the CN where it could be spatially nonselective (Ding and Hikosaka 2006). The vast majority of work has focused on a two-dimensional world displayed in front of a monkey, but clearly we do not move about in such a world. The existence of activity related to the depth of stimuli in FEF was shown when it was found that approximately two-thirds of V and VM cells were broadly tuned to near or far disparities (Ferraina et al. 2000). Subsequent work showed that cells in the FEF also have three-dimensional selectivity that combines vergence and smooth pursuit movement signals (Fukushima et al. 2002).

It is clear that neurons the FEF do not have one simply defined function, but do show a variety of response that have a common theme. Neural activity related to one, two or more visually guided saccades, natural sequences of eye movements, searching an array of targets, saccading to objects in depth, tracking a moving object, and even perhaps responses auditory stumuli share

the potential functions of assessing space for objects of interest and mapping how to move the eyes to best see those objects. Given this multi-functioning, it is important to try to understand the neural responses in the FEF in a context that is as close to natural behavior as possible. Very few studies have done this for the FEF or any other brain region because it necessitates studying a behavior that is natural, yet still tractable in terms of analyses. We have developed a task to elicit just such a behavior for this purpose.

Chapter II: Behavior

Abstract

Habits and rituals are expressed universally across animal species. These behaviors are advantageous in allowing sequential behaviors to be performed without cognitive overload, and appear to rely on neural circuits that are relatively benign but vulnerable to takeover by extreme contexts, neuropsychiatric sequelae, and processes leading to addiction. Reinforcement learning (RL) is thought to underlie the formation of optimal habits. However, this theoretic formulation has principally been tested experimentally in simple stimulus-response tasks with relatively few available responses. We asked whether RL could also account for the emergence of habitual action sequences in realistically complex situations in which no repetitive stimulus-response links were present and in which many response options were present. We exposed naïve macaque monkeys to such experimental conditions by introducing a unique free saccade scan task. Despite the highly uncertain conditions and no instruction, the monkeys developed a succession of stereotypical, self-chosen saccade sequence patterns. Remarkably, these continued to morph for months, long after session-averaged reward and cost (eye movement distance) reached asymptote. Prima facie, these continued behavioral changes appeared to challenge RL. However, trial-by-trial analysis showed that pattern changes on adjacent trials were predicted by lowered cost, and RL simulations that reduced the cost reproduced the monkeys' behavior. Ultimately, the patterns settled into stereotypical saccade sequences that minimized the cost of obtaining the reward on average. These findings suggest that brain mechanisms underlying the emergence of habits, and perhaps unwanted repetitive behaviors in clinical disorders, could follow RL algorithms capturing extremely local explore/exploit tradeoffs.

Introduction

Reinforcement learning (RL) theory formalizes the process by which rewards and punishments can shape the behaviors of a goal-seeking agent—person, animal, or robot—toward optimality (Sutton and Barto 1998). RL algorithms have been widely applied in neuroscience to characterize neural activity in animals and human subjects, most famously for the dopamine-containing systems of the brain and related brain regions (Schultz et al. 1997; Bayer and Glimcher 2005; Samejima et al. 2005; Morris et al. 2006). These ideas have also been influential in the study of habit learning, in which habits are typically thought to arise when behaviors, through repetition, eventually become reinforcement-independent, stimulus-response (S-R) associations that can be executed in a semi-automatic manner (Dickinson 1985).

In most learning experiments designed to test these ideas, a small range of relationships between actions and reward is imposed, cost-benefit ratios are explicit, and fixed and usually limited numbers of response choices are available, as for example when human subjects are asked to move a cursor in one direction to receive a monetary reward in a computer game, or when rodents are trained to press one or a small set of levers to receive a food reward. RL algorithms of varying complexity robustly account for decision-making behavior in many such experiments (Montague et al. 1995; Barraclough et al. 2004; Daw et al. 2006). But what if the actions needed to receive the reward were sequential, there were an exponentially large number of choices, the rewards were not predictable, and no explicit instructions were given to the agent? Such conditions occur in everyday life (Noser and Byrne 2010; Song et al. 2010). In computer science, the challenge of forming optimal sequential behaviors due to the vast number of possibilities has been highlighted by the traveling salesman problem, in which the goal is to minimize the total distance of visiting a given number of cities exactly once; this optimization problem has been difficult to solve (Applegate 2006). It is still unclear whether, and how, animals and humans learn optimal habits facing analogous challenging situations (Montague et al. 1995; Noser and Byrne 2010).

We designed a task to incorporate such extreme uncertainty, we applied this task to experiments in macaque monkeys, and we then tested whether RL algorithms could account for the observed behaviors. In this free-viewing scan task, experimentally naïve monkeys were free to choose their own saccadic sequences to scan a grid of dots, one of which was randomly baited. In each experimental trial, the monkeys could not predict when or where the target would become baited. Thus, no particular saccade or saccade sequence could be relied upon to produce a reward, meaning that no fixed S-R "habit" could be acquired to solve the task. Moreover, the reward in every trial was identical, so that the only way to improve cost-benefit ratios was to minimize cost by reducing as much as possible the total length of scanning before reward delivery. As such, the task had many similarities to the traveling salesman problem.

Despite this complexity, monkeys, without instruction, developed repetitive scan patterns that were optimal or near-optimal for solving the task. Moreover, the evolution of their preferred scanning patterns changed markedly through months of task performance, despite the fact that the monkeys maximized total rewards per session and minimized total travel distance (cost) per

session relatively early on. With standard session-based analysis, the habitual behaviors appeared to change without reinforcement as a driving force.

However, within session, trial-by-trial analysis of the monkeys' scan-path transition probabilities showed that their behaviors could be accounted for, and closely simulated, by simple RL algorithms emphasizing local, trial-by-trial cost reduction. These findings demonstrate the power of short-time RL analysis and suggest that, even under highly uncertain conditions, relatively simple learning rules can govern the formation and optimization of habits. This deep-structure of habit formation may be critical not only for the emergence of habits and mannerisms in everyday life, but also for the insistent quality of repetitive behaviors occurring in neuropsychiatric disorders.

Results

Task overview

We recorded the eye movements of two experimentally naïve monkeys as they were exposed to a free-viewing scan task that they performed during daily sessions across months (**Figure 1**). Each monkey was head-fixed and seated in front of a computer screen on which a grid of 4 or 9 green target dots was presented. The monkey was free to move its eyes in any way as long as its gaze remained in the space occupied by the green grid. After a variable 1-2 sec Delay Scan period, which prevented the monkey from receiving reward immediately, one of the dots was chosen to be the baited target according to a pseudorandom schedule. The start of this Reward Scan period was not signaled to the monkey. Capture of the baited target when the monkey's gaze entered the target window immediately extinguished the green targets (processing delay, mean 61 ms ± 61 ms SD). The trial then proceeded through reward delay, reward, and the intertrial interval (ITI) as illustrated in **Figure 1**. Because the monkeys were naïve, to improve performance during initial sessions, behavioral shaping such as gradually lengthening the Delay Scan periods was employed (see **Figure 2**, also *Chapter V: Methods*), but the monkeys were never given instruction. Both monkeys learned the 4- and 9-target tasks, averaging ~ 70% rewarded trials overall (**Figure 2A**). The total Scan Time was typically 1.5-4 s and contained 7-20 fixations (**Figure 3**).

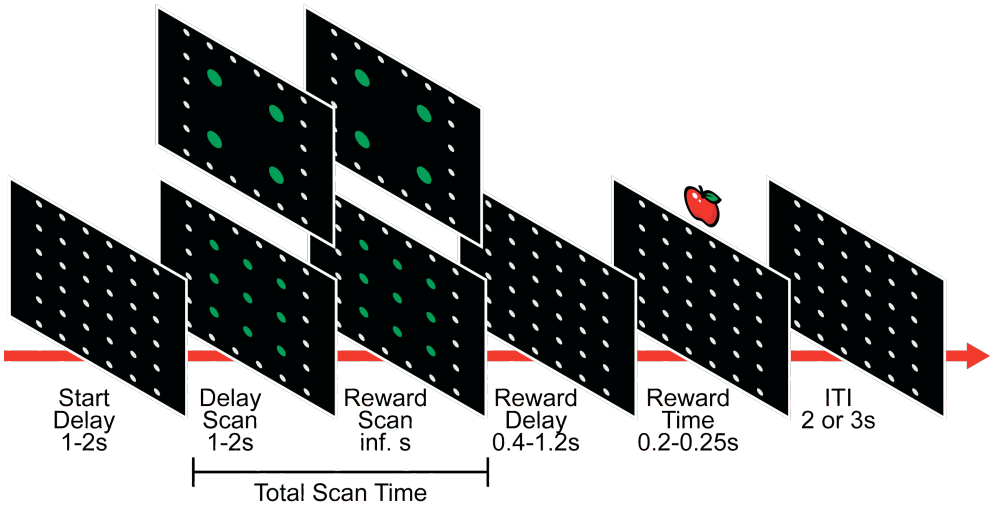

Figure 1. Schematic of the free-viewing scan task. There was no requirement for the monkey's eye position when the gray grid was displayed. After a variable Start Delay, the green target grid was presented indicating the start of the Scan Time. When the green target grid was displayed, and once the monkey's gaze entered the area defined by the green grid, the only requirement was that the eye position remained in that space. After the variable Delay Scan, the Reward Scan began when a randomly chosen target was baited without any indication to the monkey. There was no time limit on the duration of the Reward Scan. Once the monkey captured the baited target by fixating or saccading through it, the green grid immediately turned off and the trial proceeded through the remaining task periods as illustrated. If the monkey's eye position exited the green grid area before capturing the baited target, the trial was immediately aborted by extinguishing the green target grid and no reward was delivered.

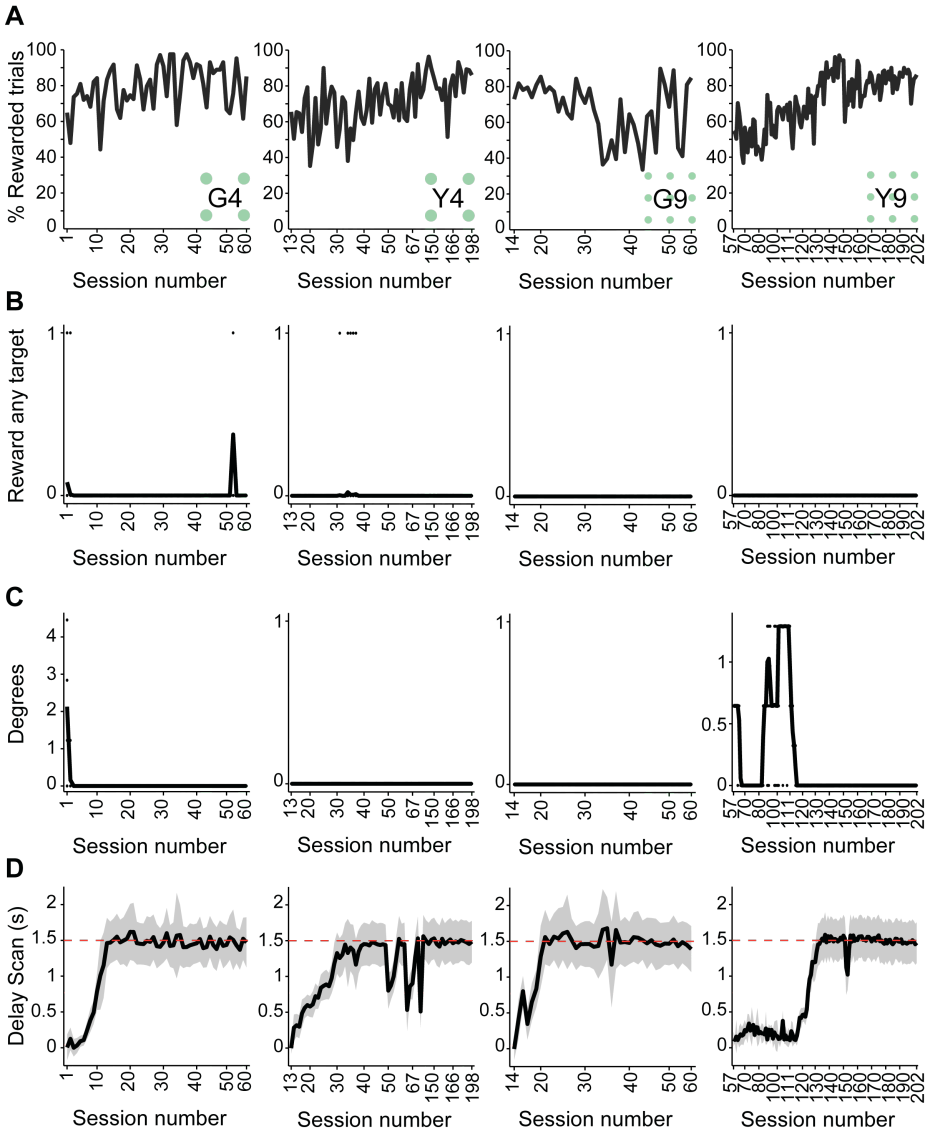

Figure 2. Task performance and shaping parameters. All rows show the monkeys and the conditions in the following order: G4 (monkey G in 4-target task), G9, Y4, and Y9. (A) Percent of rewarded trials per session. (B,C) Dots indicate values of parameters in each session, lines indicate the average of the values. (B) Indicates for each session the presence (1) or absence (0) of the parameter rewarding any target entered after the Delay Scan. Note this parameter was not used in G9 or Y9. (C) In each session the number of degrees the radius of the acceptable window around the target was greater than the radius of the target. Note this parameter was not used in G9 or Y4. (D) Mean ± SD Delay Scan time for each session. Red dashed line for all plots indicates the mean of 1.5 s that is reached when the monkey completes task acquisition and performs the full 1-2 s Delay Scan.

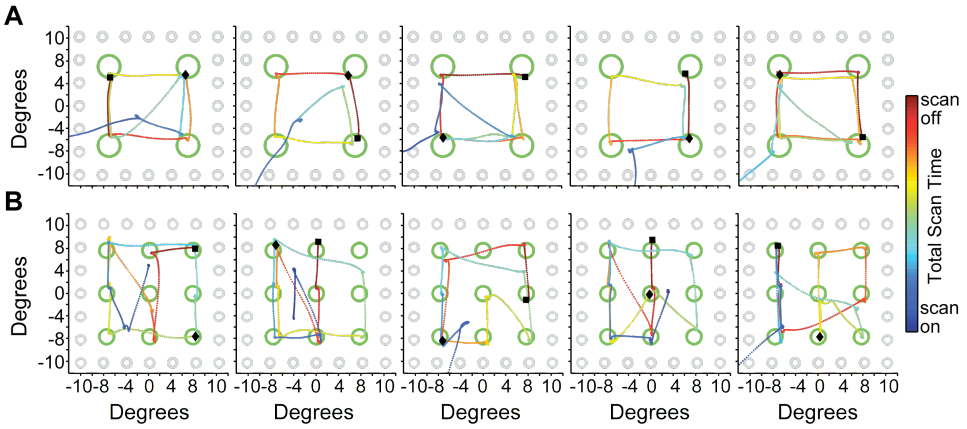

Figure 3. Example trials. (A,B) Eye movements of monkey G for five sequential trials during the Total Scan Time. Time is represented by color from dark blue (green targets on) to dark red (green targets off). (A) Session 12, 4-target task. (B) Session 21, 9-target task.

Sequences of eye movements

Despite the absence of explicit training on how or when to move their eyes in the task, the monkeys developed particular repeated patterns of saccades to scan the target grids (e.g., **Figure 3**). To examine these patterns, we selected the most frequent 'loop' sequences: sequences that began and ended on the same target compiled from a pool of the top 20 most frequent 5-fixation sequences across all rewarded trials and sessions (see *Chapter V: Methods*). We calculated the percentage of trials in each session that contained each loop sequence. The percentages for the loop sequences were not constant across sessions. Instead, the loop sequences were acquired and dropped throughout the months of task performance (**Figure 4**).

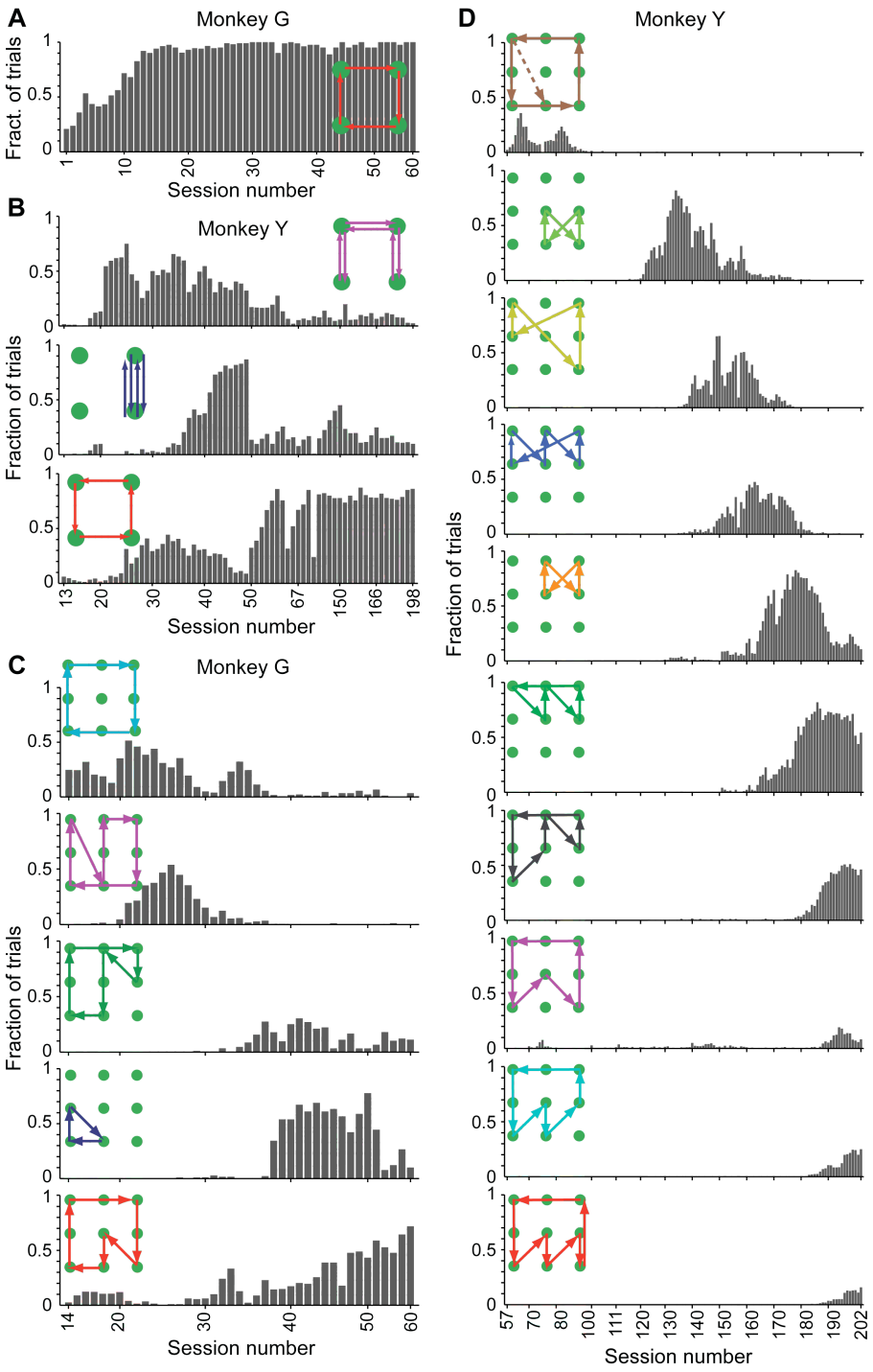

Figure 4. Loop sequences emerge and shift during prolonged task performance. Each plot shows the fraction of rewarded trials per session containing the most frequent saccade paths that form a closed loop (start and stop on the same target), regardless of start or stop position during Total Scan Time. (A) Monkey G, 4-target task (G4). (B) Monkey Y, 4-target task (Y4). (C) Monkey G, 9-target task (G9). (D) Monkey Y, 9-target task (Y9). Dashed line in first panel indicates slight variation from main pattern included in the fraction.

To further investigate the loop sequences, we examined when, during trial time, the sequences tended to occur. To visualize this we created fixation 'rasters' with those fixations that were members of the loop sequences in **Figure 4** highlighted in the same color (**Figure 5**, **Figure 6**). From this we observed that often the loop sequences did not account for all the fixations in a given trial. Also, individual loop sequences were often performed preferentially at a particular time during the trial. For example, the aqua sequence in **Figure 5A** and the light green sequence in **Figure 6A** tended to be performed at the beginnings of trials. Across task performance sessions the fraction of fixations that were members of loop sequences increased until reaching ~ 70% of Total Scan Time fixations (**Figure 7**). This observation suggested that in addition to the loop sequences gradually shifting from one to another, the monkeys' eye movement patterns were becoming more repetitive as task performance progressed.

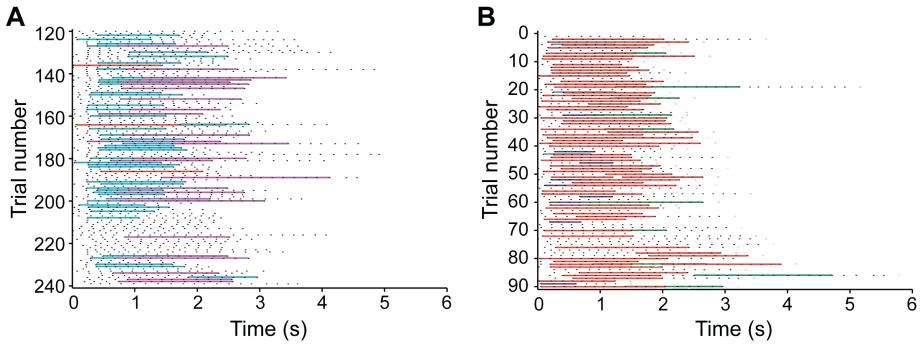

Figure 5. Fixation rasters with loop sequences highlighted. Each horizontal line represents the Total Scan Time for each rewarded trial for G9 trials during session 21 (C) and session 60 (D). Time zero is the onset of the green target grid. Black dots indicate fixation onset times. Horizontal colored lines indicate fixations that are members of the loop sequences shown in loop sequences Figure, with the same color code.

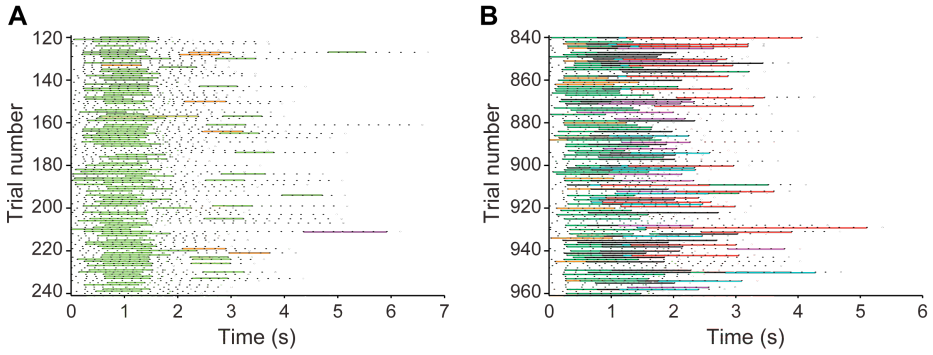

Figure 6. Fixation rasters with loop sequences highlighted. Each horizontal line represents the Total Scan Time for each rewarded trial for Y9 trials during session 133 (C) and session 202 (D). Time zero is the onset of the green target grid. Black dots indicate fixation onset times. Horizontal colored lines indicate fixations that are members of the loop sequences shown in loop sequences Figure, with the same color code.

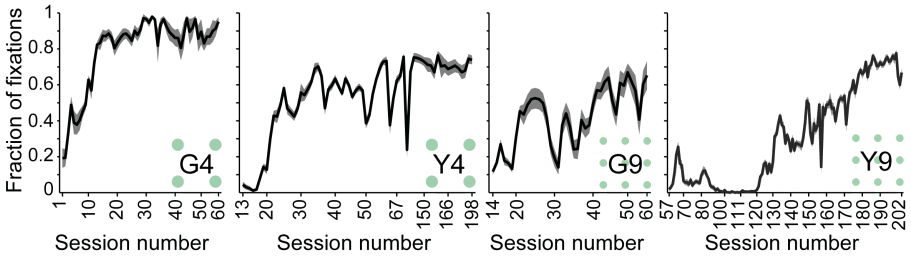

Figure 7. Mean fraction of fixations per trial during the Total Scan time that are members of any of the loop sequences for each monkey in each task condition (e.g. Y4 shows fraction of fixations per trial that are members of any of the three paths diagramed in loop sequences Figure, B). Dark gray horizontal shading indicates approximate confidence limits (±1.96 × SEM).

To test this conclusion without assuming either fixed-length sequences or deterministic scan patterns that did not account for all saccades (**Figure 7**), we turned to a probabilistic analysis of the scanning behaviors. We compiled for each session the transition probabilities of saccades between all pairs of targets. The single-step transition probabilities from two example sessions are shown (**Figure 8**). We used these transition probabilities for two analyses. The first was to calculate what the most probable, rather than most frequent, loop sequence was that started on the lower left corner target. These most probable loops (**Figure 9**) shared many features of the most frequent loop sequences (**Figure 4**). The second analysis was to decompose the transition probabilities using nonnegative matrix factorization (NMF) into positive mixtures of transition components (Lee and Seung 1999). These transition components represent the most explanatory parts of the overall transition patterns (deterministic or not) that could be seen at the level of saccades between adjacent targets.

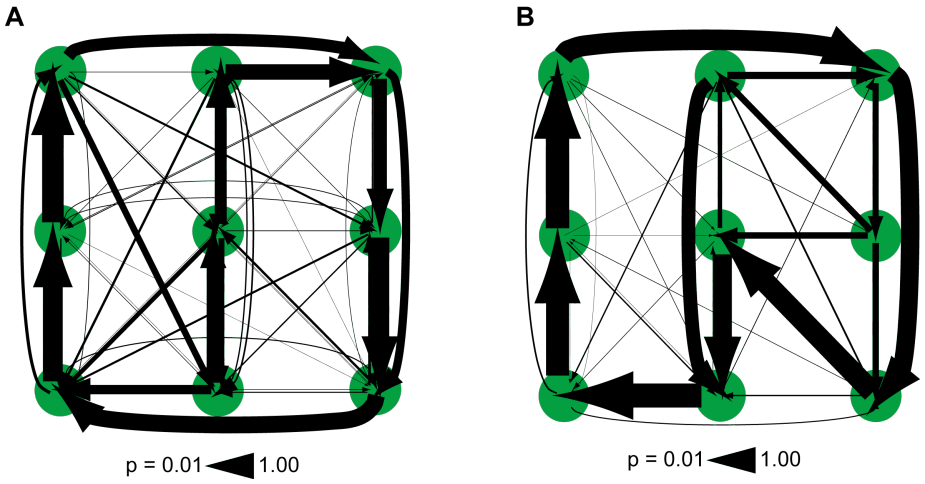

Figure 8. Single step Markov model for two example sessions in monkey G. The probability of each transition is indicated by the thickness of the vector. (A) Session 21, early in G9 task performance (8th 9-target session). (B) Session 60, late in G9 task performance (47th 9-target session).

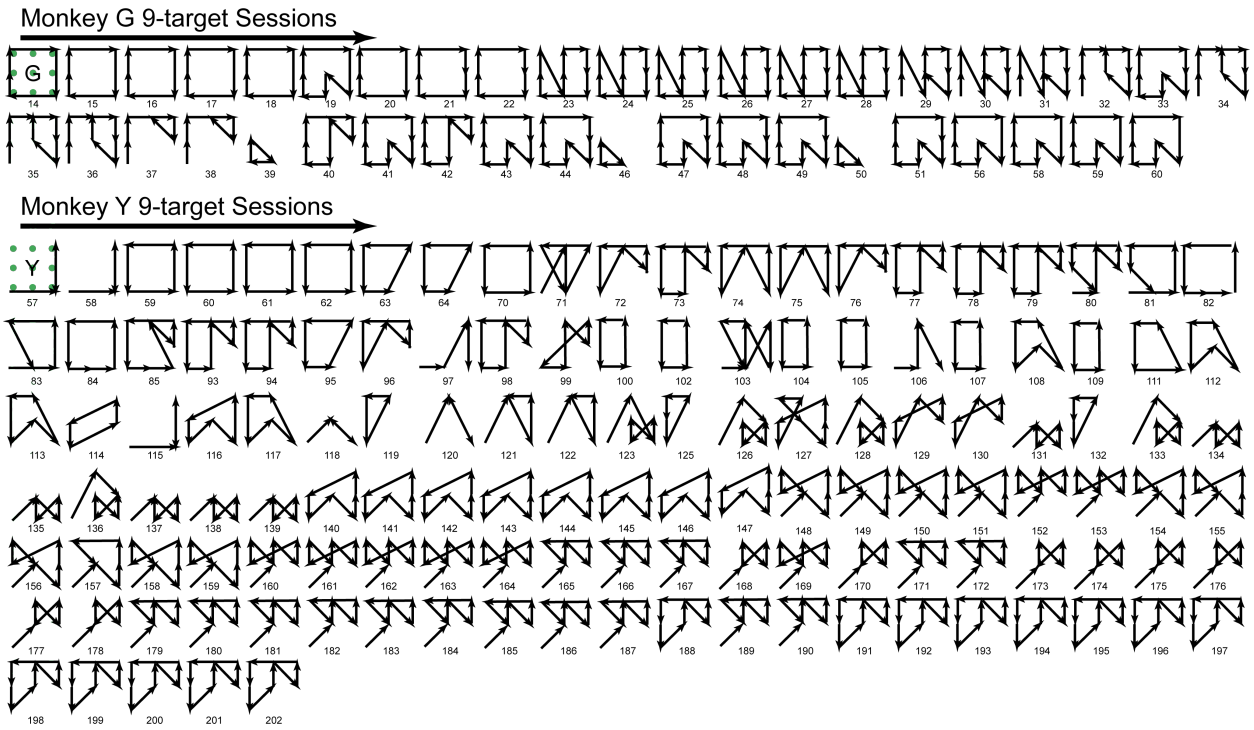

Figure 9. Most probable loop sequences. The most probable loop of saccade vectors, defined as starting at the lower left corner target and finishing when any target in the sequence is visited for a second time, using a single step Markov model is depicted. Each icon, starting in the upper left, represents the most probable loop for a single session in the 9-target task for monkey G (upper) and monkey Y (lower) with the session number noted below each.

Using this decomposition we found that the weights of the NMF factors, like the most frequent loop sequences (**Figure 4**), changed over time and were clustered into epochs across sessions rather than being randomly distributed (**Figure 10**). This clustering into temporally localized epochs exceeded chance, as tested by applying the same NMF analysis to random permutations of the saccade data ($P < 0.01$, dispersion permutations test, *Chapter V: Methods*). The NMF analysis thus also suggested that the monkeys' repeated scan patterns systematically shifted until eventually they settled into particular habitual scan patterns.

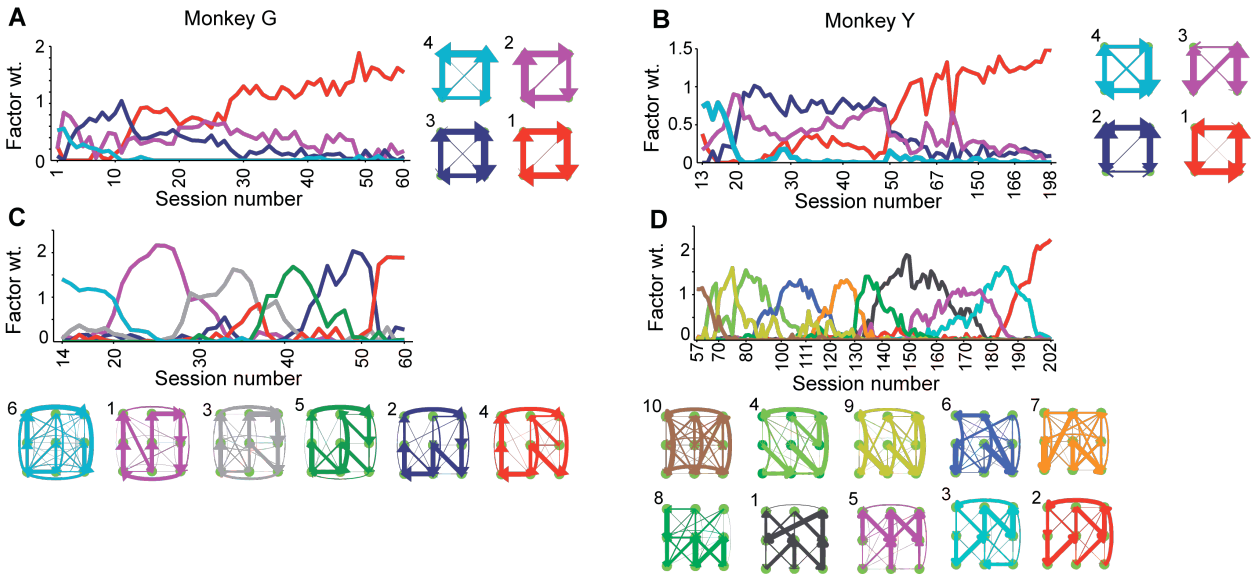

Figure 10. Nonnegative matrix factorization (NMF) shows successive appearance of factors resembling loop sequences. Each panel displays the weight of each factor during Total Scan Time on all rewarded trials through task performance. Factors are diagrammed in colors to show similarity to the loop sequences in loop sequences Figure. Numbers on upper corner of the factors indicate their rank order by total magnitude (i.e., sum of the weight across sessions). (A) G4, root mean squared (rms) error of factorization = 0.02673. (B) Y4, rms error = 0.02452. (C) G9, rms error = 0.0225. (D) Y9, rms error = 0.01728.

Behavioral driving forces

We next asked whether reward and cost, key drivers in RL models, could account for the shifts of scan patterns. We calculated reward rate as the number of rewards earned in each session divided by the total amount of time spent in the Reward Scan for rewarded trials (**Figure 11A**). Because the energy required by the extraocular muscles to maintain fixation is relatively little in comparison to that required by saccades and these muscles contract in proportion to saccade amplitude (Robinson 1964), we used the mean total distance that the monkeys' eyes traveled during the Reward Scan per trial for each session as an estimate of the cost of the scanning (**Figure 11B**). Despite the fact that the scan patterns continued to change across the entire experimental time, both reward rate and cost per session reached asymptote early in the sessions. For the 4-target task, asymptotic reward and distance were reached by session 9 for G4 in both measures, and by sessions 10 and 20, respectively in Y4. In the 9-target task, G9 had a relatively steady rate and Y9 reached asymptote for the final 18 sessions (see *Chapter V: Methods*).

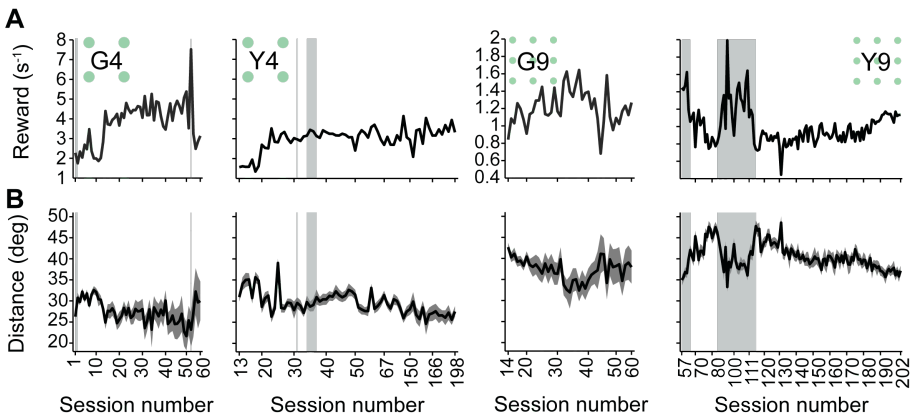

Figure 11. Session-averaged behavioral measures. All rows show monkeys and conditions in the order depicted in A (G4, Y4, G9, and Y9). (A) Reward rate measured as number of rewards per total Reward Scan time in each session. (B) Mean saccade distance during Reward Scan per session with shading indicating approximate confidence limits (±1.96×standard error of the mean, SEM). Gray vertical bars in A-B indicate sessions containing shaping periods when the task was made easier for the monkey (see Chapter V: Methods, task parameters and shaping Figure).

We also examined other possible measures of cost and found all measures to have similar trends. The mean Reward Scan duration (**Figure 12**), the mean number of saccades during the Reward Scan time (**Figure 13**), mean number of fixations during the Reward Scan time (**Figure 14**), mean fixation durations (**Figure 15**), and mean time to cover all the targets (**Figure 16**) were calculated. We examined the mean across task performance sessions of all these measures and found that they individually bore little or no relation to shifts in the performance of the monkey's most frequent loop sequences.

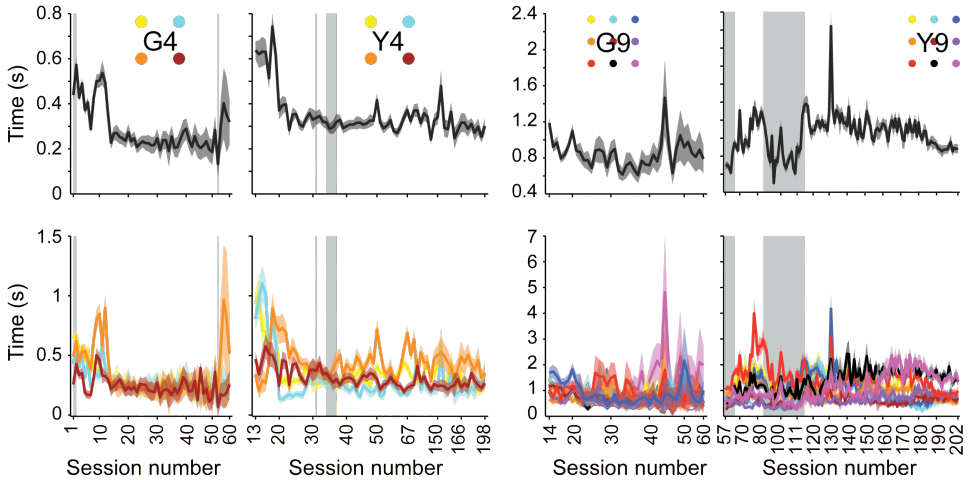

Figure 12. Mean Reward Scan duration across sessions. Shading shows approximate confidence limits (±1.96 × SEM). Top row shows overall mean, bottom row shows the same but separated out by baited target. Gray vertical bars in indicate sessions containing shaping periods when the task was made easier for the monkey.

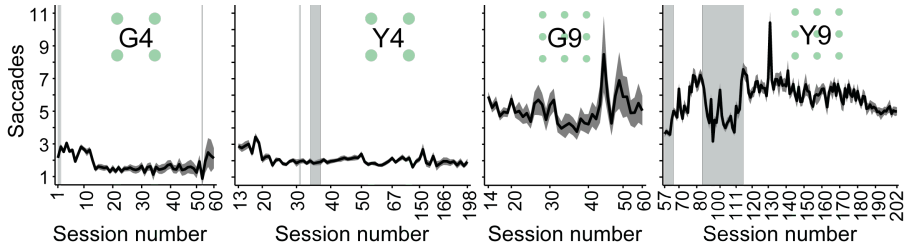

Figure 13. Mean number of saccades per Reward Scan period. Gray shaded vertical bars indicate sessions containing shaping periods when the task was made easier for the monkey (see Chapter V: Methods, Figure 2).

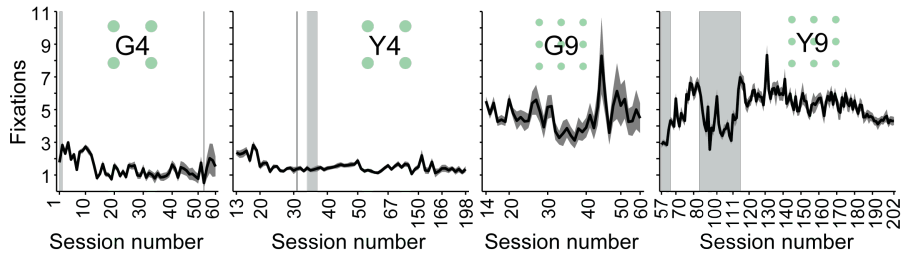

Figure 14. Mean number of fixations to complete the trial (during Scan Time) for monkeys G and Y through training. Dark gray horizontal shading shows approximate confidence limits (±1.96 × SEM). Gray vertical bars in indicate sessions containing shaping periods when the task was made easier for the monkey.

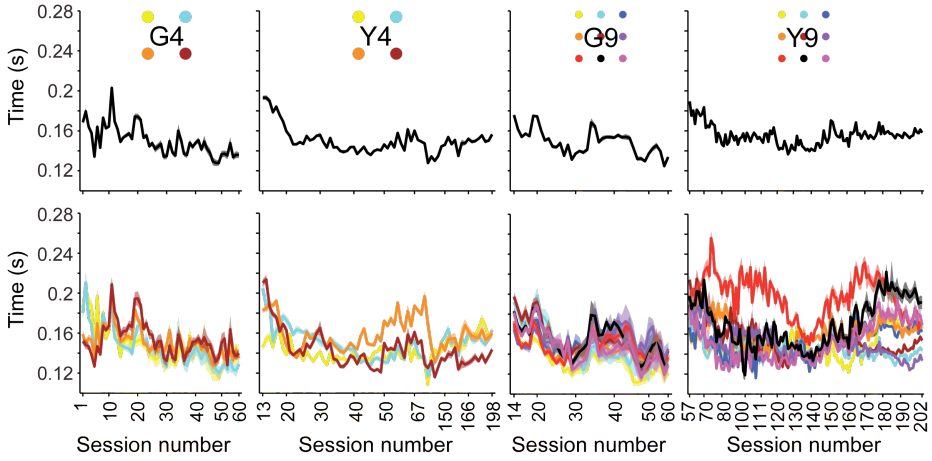

Figure 15. Mean fixation durations across training for monkey G and Y. Top row shows overall mean, bottom row shows the same but separated out by target fixated. Diagram indicating money and task condition is color-coded to indicate target identity. Shading shows approximate confidence limits (±1.96 × SEM).

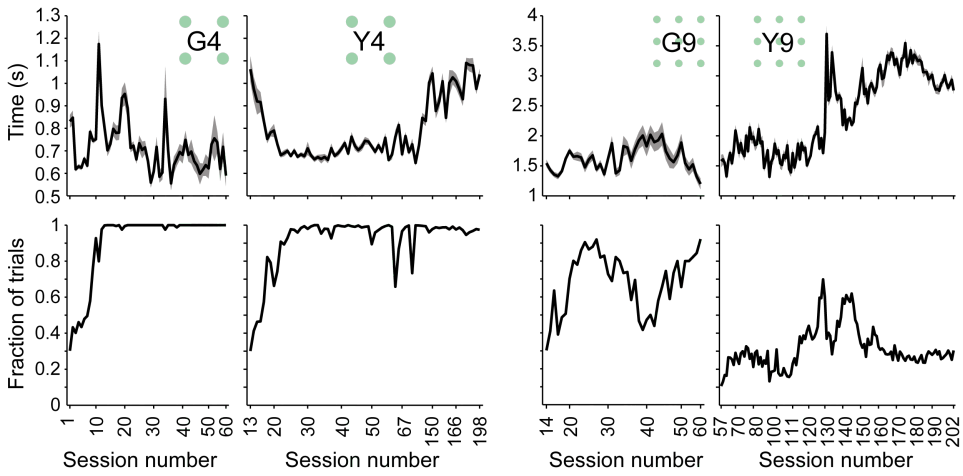

Figure 16. Top row: Mean time for monkey's gaze to land on or pass through ("cover") all targets in the display. Dark gray shading shows approximate confidence limits (±1.96 × SEM). Bottom row: Percentage of rewarded trials where all the targets were covered. Monkey and task condition as diagrammed in top row.

These results appeared to challenge RL models. Both reward and cost evolved to asymptotic levels, yet the scanning patterns of the monkeys continued to change long past the time that these values reached steady state. A further result, however, suggested that the session averages might not have the resolution to show the effects of changing reward or cost. The scan patterns became more repetitive and habitual through the months of task performance, as evidenced by the steady decline of the entropy of the monkeys' eye movements (*Chapter V: Methods*, **Eqn. 1**) (**Figure 17**). These entropy measurements suggested that, if the habitual patterns became optimal or nearly so, the pattern shifts might still conform to RL theory. In the face of the large variability intrinsic to the task, local changes in reinforcement might take over the learning if shifts in the sequences of saccades performed were "local" in time.

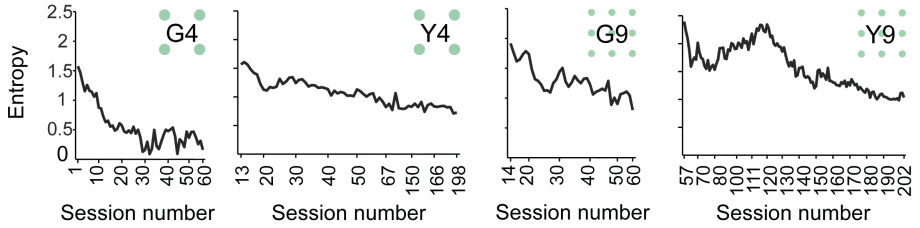

Figure 17. Entropy of transition probabilities during Total Scan Time for each session through training for monkeys G and Y.

Optimal scan paths

To investigate this possibility, we first asked whether the monkeys achieved optimal habitual scanning patterns. We computed the optimal scan path, defined as that which minimized the total distance to obtain the reward in a single trial on average. One simple component of an optimal solution to this task would involve the monkeys not making saccades during the Delay Scan period, when no target was baited. This strategy, however, was apparently not used by either monkey: both performed a nearly equal average number of saccades in the first second and the last second of each trial (**Figure 18**). A second possible optimality would be for the monkey to maximize the number of saccades that passed through, rather than fixated on, targets. The

monkeys did not use this strategy either; the percentage of saccades that passed through targets tended to decrease across sessions, not increase (**Figure 19**). Therefore, the optimal realized solution to this task must involve the eyes moving all through the Delay and Reward Scan periods.

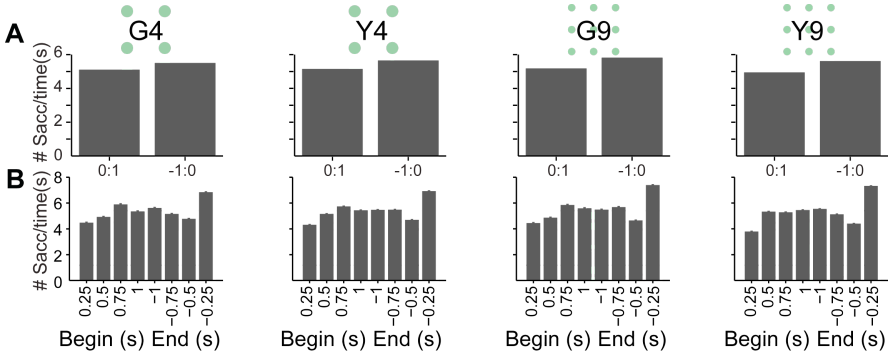

Figure 18. Mean saccade rate. (A) Mean number of saccades per second (±1.96 × SEM, note error bars are too small to be seen) in the first second after the green target grid turns on (begin range 0:1 s) and the last second before the baited target is captured and the green target grid turns off (end range -1:0 s). (B) Same as in A with saccade rate in the first and last seconds shown in 0.25 s bins with greater bin edge listed for each bin, e.g. begin range 0:0.25 s, 0.25:0.5 s, end range -0.5:-0.25 s, -0.25:0 s, etc. Note the last bin (-0.25:0 s) for each monkey and task condition is likely the largest because by definition the green targets will turn off when the baited target is captured with a saccade thus making the minimum number of saccades in that bin 1 instead of 0.

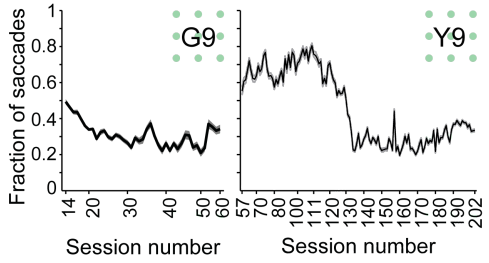

Figure 19. Mean fraction of saccades per trial that pass through intervening targets. Dark gray horizontal shading indicates approximate confidence limits (±1.96 × SEM).

During the Reward Scan period, revisiting a previously scanned target did not lead to reward. Thus, the optimal strategy would be to scan each target exactly once. Given that the onset of the Reward Scan was unpredictable and that there was no evidence of different behaviors in the Delay Scan and Reward Scan periods, we assumed that the monkeys treated the entire period as the reward period. This assumption necessarily means that the optimal scanning pattern was a loop pattern in which each target was visited once before returning to the original target. Among such patterns, the one with the minimum total distance should be the optimal policy.

We determined the optimal loop scan patterns that covered all targets once (**Figure 20**) by using an exhaustive search algorithm (*Chapter V: Methods*), and then compared them to the habitual patterns reached by the monkeys. Both monkeys reached the optimal pattern in the 4-target task, and monkey G did so in the 9-target task (**Figure 4A-C**). Moreover, G9 reached the optimal path after transitioning through the sixth most optimal pattern (**Figure 4C**, **Figure 20B** purple path). Y9 gradually approached the optimum by progressively covering more of the targets in the loop

sequences, and her final pattern was near optimal, as it was the fifth most optimal (**Figure 4D**, **Figure 20B**). The monkeys thus not only generated habitual behaviors de-novo and without explicit instruction, but also were able eventually to 'solve' this task in the most optimal manner.

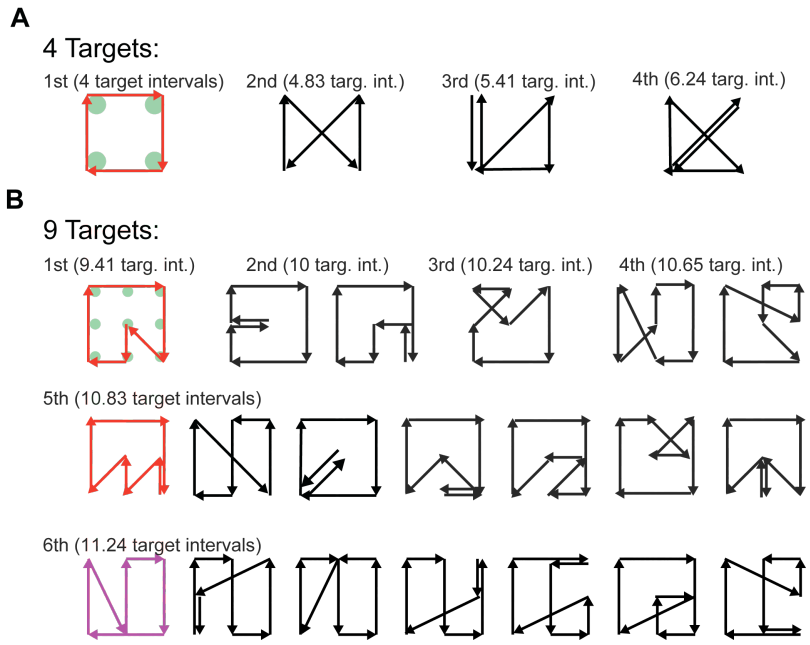

Figure 20. Monkeys converge on efficient deterministic patterns. The most efficient deterministic patterns for the 4-target (A) and 9-target (B) tasks as computed using an exhaustive search algorithm are shown. Total geometric distance to cover all the targets using the depicted path is noted. Only one of many possible equivalent rotations and reflections is shown for each path. Paths the monkeys performed are colored red or purple to correspond with loop sequences.

Trial-by-trial analyses

To determine whether RL was the driving force behind the evolution towards the optimal pattern, despite initial indications from session-averaged data, we performed trial-by-trial analysis of the effects of cost on the changes of the scan patterns. We excluded only initial trials on which behavioral shaping occurred (see *Chapter V: Methods*). The analysis was based on the explore-exploit principle central to RL algorithms (Williams 1992; Sutton and Barto 1998). A fluctuation of the scan pattern from the previous trial was taken to represent exploration. If the monkey was 'rewarded' with a shorter scan distance in the current trial (k) than the previous trial (k-1), the monkey could attribute the success to the differences between the scan patterns in the two trials (k-1 to k, *Chapter V: Methods* **Eqn. 3**). The monkey would then strengthen the differences between the scan patterns, and similar differences would likely occur again in the next trial (k to k+1). In contrast, if the distance were increased, the changes in the scan patterns should be extinguished so that similar changes would not likely occur in the next trial. This pattern represents exploitation. Therefore, a positive correlation should exist between the reduction in distance from trial k-1 to trial k and the similarity in the changes of the scan patterns between trials k-1 to k and k to k+1 (*Chapter V: Methods* **Eqn. 4**).

Taking the transition probabilities to represent a given trial's scan pattern, we computed the correlation between the change in distance (cost) and the similarity of changes in scan patterns for each successive set of three contiguous trials (k-1, k, k+1). With this "reinforcement test", we

found that the cost vs. similarity correlations were small but highly significant for both monkeys in both conditions ($P < 0.002$, shuffle test) (**Figure 21**). These results from trial-by-trial analyses of the data strongly suggested that, contrary to the results based on session-averaged data, RL analysis could account for the changes in scanning behavior of the monkeys.

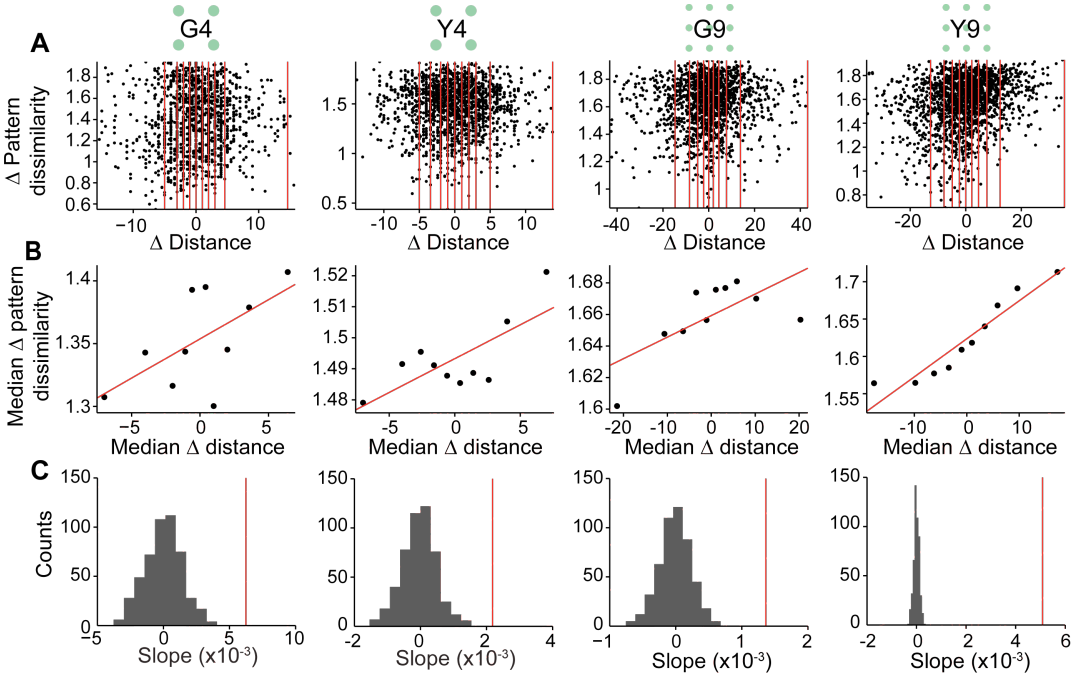

Figure 21. Trial-by-trial reinforcement test shows correlation between cost and change in pattern. Each column corresponds to the monkey and task conditions as depicted above row A. Distances were simplified to be the geometric distance: one unit is the horizontal or vertical distance between adjacent targets. (A) The overall distribution of change in geometric distance and dissimilarity of the change in pattern, where pattern is the set of transition probabilities representing a single trial. Each point represents one trial: G4: N = 6,109 trials; Y4: N = 25,113 trials; G9: N = 5,912; and Y9: N = 54,214. (B) Trials were then binned into 10 equal bins. The median of each of the ten bins was plotted and used to compute the correlation (red line) between the change in distance and the pattern dissimilarity. The total number of trials (N), correlation coefficients (R) and correlation p-values are listed below. Note this p-value is different than the P-value reported to indicate significance resulting from the shuffle test in the text. G4: N = 6,109 trials; R = 0.613, p = 0.060; slope = 0.006. Y4: N = 25,113; R = 0.737, p = 0.015; slope = 0.002. G9: N = 5,912; R = 0.672, p = 0.033; slope = 0.001. Y9: N = 54,214; R = 0.951, p < 0.0001; slope = 0.005. (C) Histogram of slopes resulting from shuffling the dissimilarity of change in the patterns 500 times and computing the resulting slope for each. Actual slope indicated by red line and depicted in B. All shuffled slopes were found to be less than the actual slope indicating a significance of P < 0.002.

As an extension of the reinforcement test, which showed a correlation between change in pattern and change in distance, we examined what effect the trial-by-trial changes in the distance that the eyes traveled during the Reward Scan period (cost) would have on the loop sequences. We hypothesized that if cost had an effect on loop sequence performance then a cost benefit would result in the monkey performing a sequence sooner (i.e. after fewer trials) whereas detrimental cost would result in the monkey performing a sequence later (i.e. after many trials). To test this hypothesis, for each trial on which a loop sequence was performed we calculated the inter-sequence interval (ISI): the number of trials that transpired before the loop sequence was

performed again. The ISI for the current trial was then compared to the change in cost from the previous trial.

We found a significant positive correlation between the mean ISI and the mean change in distance (shuffle test $P \leq 0.05$, **Figure 22**, see *Chapter V: Methods* for more details). This result indicates that when the monkey performed a loop sequence (e.g. G9 purple and Y9 yellow (**Figure 22A-B**), if the monkey's eyes traveled a shorter distance during the Reward Scan on that trial compared to the previous trial (negative cost), then the monkey would repeat that same loop sequence in a fewer number of trials than if there had been a greater cost. This finding held for the pool of loop sequences illustrated in **Figure 4** across both monkeys for both grid sizes (**Figure 22C-D**).

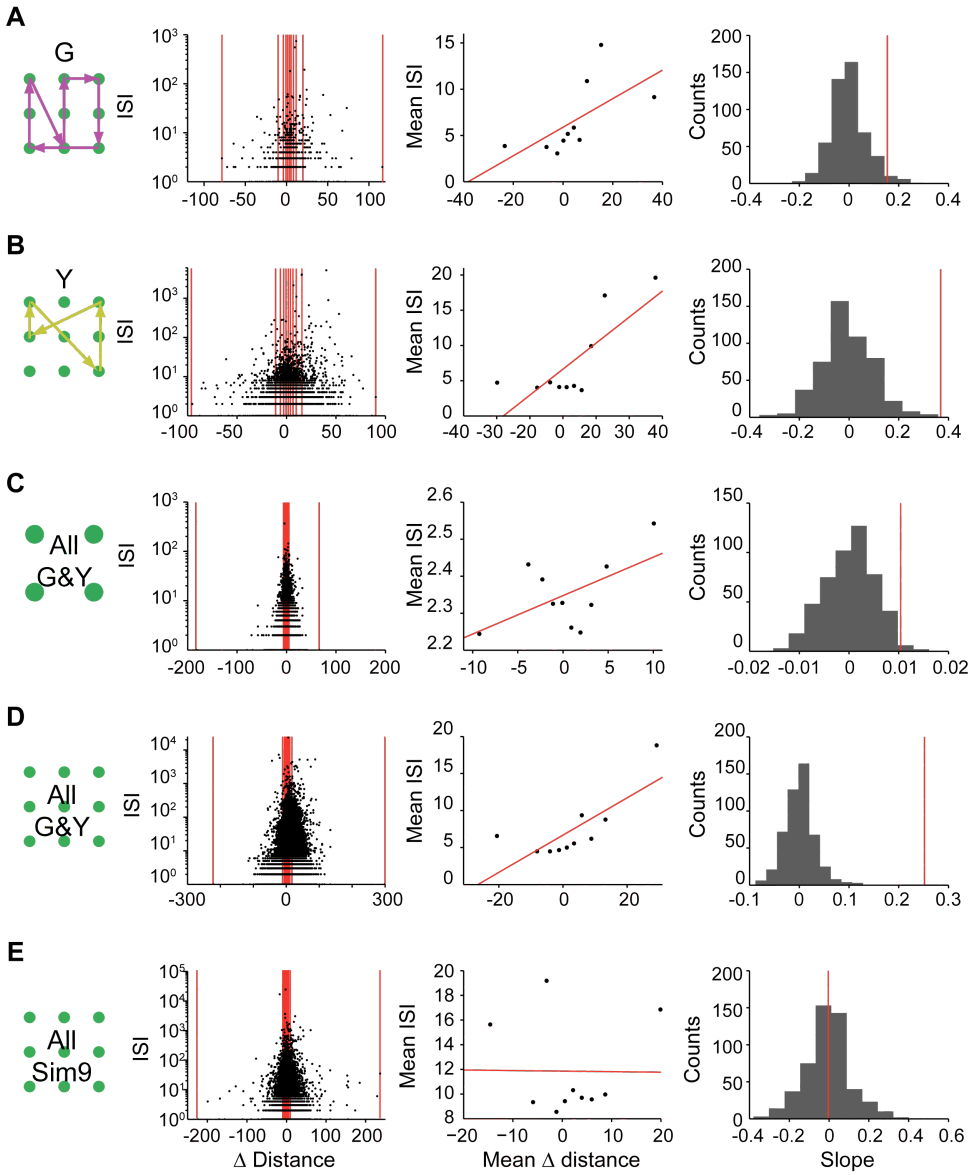

Figure 22. Correlation between trial-by-trial change in distance and inter-sequence interval. All rows contain the same three elements as follows. Left column: the overall distribution of change in geometric distance and inter-sequence interval (ISI) across all trials containing the pattern(s). Each data point is a trial with the number of trials

(N) listed below. Center column: the mean and line fit of each of ten bins each containing the same number of trials (bin edges indicated by red lines in left column). Linear correlation coefficient (R) and correlation p-value listed below. Right column: Histogram of slopes resulting from shuffling the ISI and change in distance 500 times and computing the resulting slope for each. Actual slope illustrated in middle column indicated by red line. P-value listed is fraction of shuffled slopes greater than actual. (A) ISI correlation for an example G9 path: N = 878; R = 0.625, p = 0.053, slope = 0.15; P = 0.03. (B) ISI correlation for an example Y9 path: N = 6,702; R = 0.787, p = 0.007, slope = 0.37; P < 0.002. (C) Pool of all trials containing any of the 4-target loop sequences: N = 35,350; R = 0.564, p = 0.089, slope = 0.01; P = 0.01. (D) Pool of all trials containing any of the 9-target paths loop sequences: N = 76,885; R = 0.766, p = 0.010, slope = 0.25; P < 0.002. (E) Pool of all trials containing any of the simulated 9-target task (Sim9) loop sequences; note there is no correlation: N = 29,953; R = -0.011, p = 0.976, slope = -0.005, P = 0.49.

Simulation

To demonstrate directly that RL could lead to the shifts of the monkeys' repetitive scanning patterns, we simulated an agent that performed the scan task and changed the agent's scan patterns according to a RL algorithm. The agent generated saccades according to transition probabilities that were determined by the action values of making the transitions. If an action value was large, the corresponding transition probability was also large. We implemented the REINFORCE algorithm developed by Williams (Williams 1992) to perform RL (*Chapter V: Methods*). At each trial, the action values shifted randomly around the mean to produce explorations. The transition probabilities were used to generate a sequence of saccades. The baited target was randomly chosen and the reward was obtained as in the experiments. At the end of the trial, the mean action values were shifted toward the values at the beginning of the trial if the total scan distance was smaller than the previous trial, and otherwise, the values were shifted away. This protocol represented the exploitation stage.

The simulations closely resembled the performance of the monkeys on this task (**Figure 23**). The reward rate, the distance the eyes traveled, and the entropy of the paths (**Figure 23A-C**) all paralleled those measured for the monkeys' behavior (**Figure 11**, **Figure 17**). Reward rate and distance showed large changes only in the earlier sessions run, whereas entropy continued to decrease through task performance. The final most probable loops reached by the simulations (**Figure 23D-E**) were equivalent to the final loop sequences in the monkeys (**Figure 4**). Different runs of the simulation had different convergence rates, but they nevertheless converged on the same paths (**Figure 24**). In addition, the session-by-session structure of the shifts from one pattern to another was strikingly similar between monkeys (**Figure 10**) and the simulations (**Figure 23F-G**). The statistical dispersion of the weight of all but one Sim4 factor (#3) and one Sim9 factor (#9) was significantly lower than expected by chance ($P < 0.0001$, 10,000-session permutations test), much the same as found for the NMF factors in the monkeys. These results demonstrate that the relatively simple RL model we used captured the essence of the monkeys' complex behavior in this task.

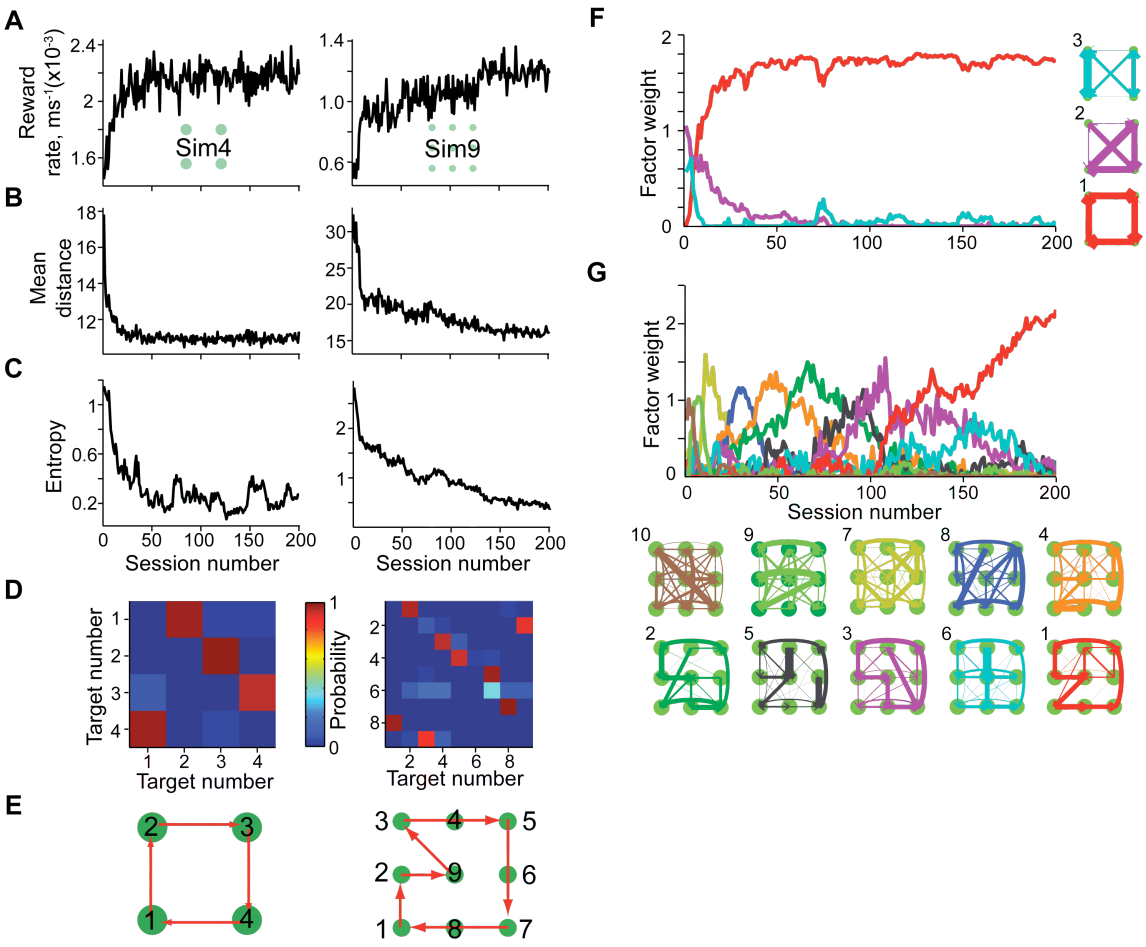

Figure 23. The REINFORCE algorithm simulation performs similarly to the monkeys. (A-E) For each row, columns represent conditions depicted in A: REINFORCE simulation of the 4-target task (Sim4) and REINFORCE simulation of the 9-target task (Sim9). Reward rate measured as number of rewards per total simulated trial time in each session (A); mean geometric distance per session (B); entropy of transition probabilities per session (C); final transition probabilities (D) and resulting most probable pattern (E). (F,G) NMF of simulations as in NMF of monkey data Figure: Sim4 (F, rms = 0.02314) and Sim9 (G, rms = 0.03655).

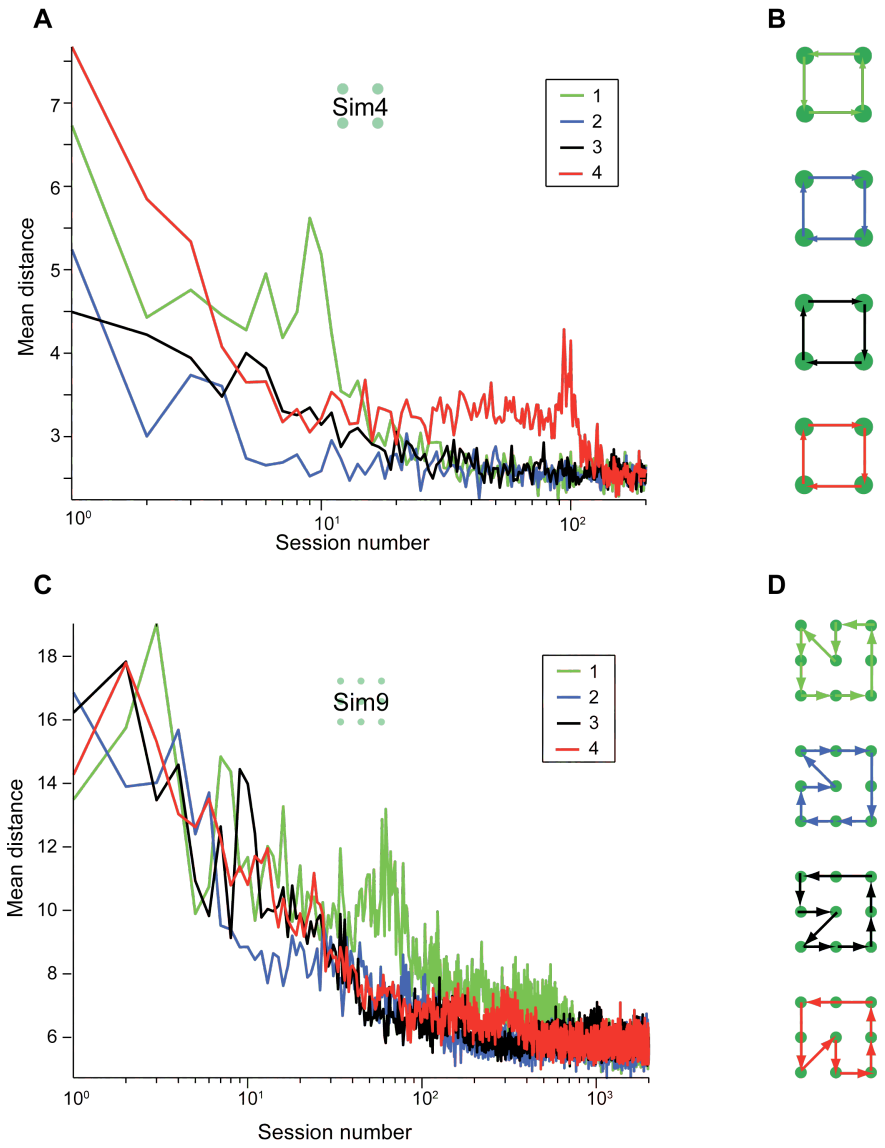

Figure 24. Simulations have different learning rates but converge on the same paths. (A) Mean geometric distance over 200 sessions, each containing 200 trials, of four REINFORCE algorithm simulations of the 4-target task with corresponding final paths shown in B. (C) Mean geometric distance over 2,000 sessions containing 200 trials each of four REINFORCE algorithm simulations of the 9-target task with corresponding final paths shown in D.

In contrast to the parallel between the monkeys' and the modeled behavior in all previous analyses, the correlation between ISI and cost was not seen in the REINFORCE algorithm simulated data (**Figure 22E**). This result suggests that RL could account for the shifts in the loop sequences as performed by the monkeys and leaves an avenue for the possible expansion of the RL model.

We used the data produced by the REINFORCE algorithm to validate the reinforcement test used on the monkey data in several ways. First, we used the reinforcement test on the simulated data to confirm the presence of RL in the same manner as in the monkeys (**Figure 25** left columns). The presence of RL was not detected in the simulated data when the reward (negative geometric

distance) on each trial was randomly assigned to be a number between 10 and 15, which was approximately the same range as the distances on the REINFORCE simulated trials (**Figure 25** right columns).

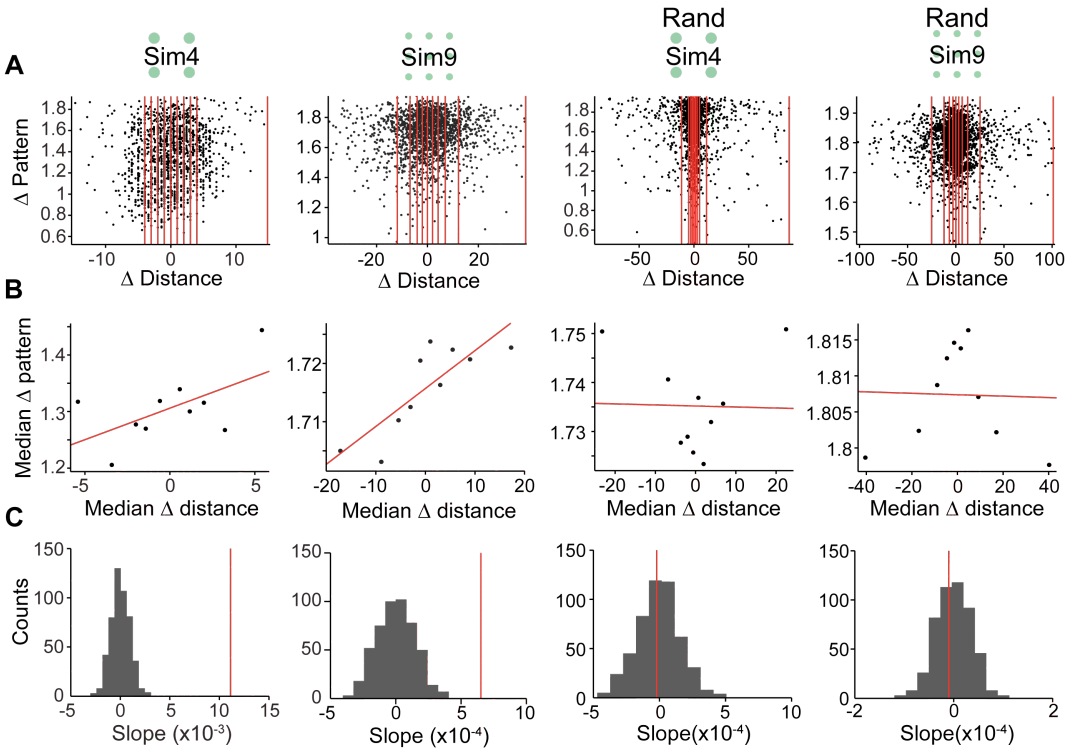

Figure 25. Trial-by-trial reinforcement test shows correlation between cost and change in pattern for REINFORCE but not random simulations. Each column corresponds to the simulation and task conditions as depicted above row A: 4-target simulation (Sim4), 9-target simulation (Sim9), 4-target simulation with random reward (Rand Sim4), and 9-target simulation with random reward (Rand Sim9). (A) Overall distribution of change in geometric distance and dissimilarity of the change in pattern, where pattern is the set of transition probabilities representing a trial, across all trials (N): Sim4, N = 16,715; Sim9, N = 16,732; Rand Sim4, N = 16,144; Rand Sim9, N = 16,350. (B) Median change in geometric distance and dissimilarity of pattern change for each of ten bins containing equal numbers of trials. Bin edges indicated by red lines in A. Slope of line fit to the ten points shown with correlation coefficient (R) and p-value listed: Sim4, R = 0.580, p = 0.079, slope = 0.01; Sim9, R = 0.825, p = 0.003, slope = 0.0007; Rand Sim4, R = -0.025, p = 0.946, slope = -2.1×10-5; Rand Sim9, R = -0.031, p = 0.933, slope = -9.9×10-6. (C) Histogram of slopes resulting from shuffling the dissimilarity and change in distance 500 times and computing the resulting slope for each. Actual slope as found in B indicated by red line. P-value listed is fraction of shuffled slopes greater than actual. Note left two columns (REINFORCE simulations) show significant slope ($P < 0.002$) and right two columns do not (random reward simulations, P = 0.58 and P = 0.60 respectively).

Second, to examine how accurate the reinforcement test was, we performed multiple simulations and randomly assigned each simulation to either use REINFORCE or have random reward as described above. Each of the 300 simulations had 100 sessions with 200 trials each session. For each simulation the reinforcement test was used to calculate the *P*-value of the slope of the correlation between the change in distance and the dissimilarity in the change of patterns. For the 4- and 9-target simulations, the false positive rate was less than 0.3 percent with none of the slopes in the random reward condition simulations having a *P*-value of less than 0.01 (**Figure 26**). Receiver operating characteristic (ROC) analysis showed there was an improvement in the

true positive rate when more sessions were used (200 sessions per simulation), but there were still no false positives, further supporting the use of this test to detect RL.

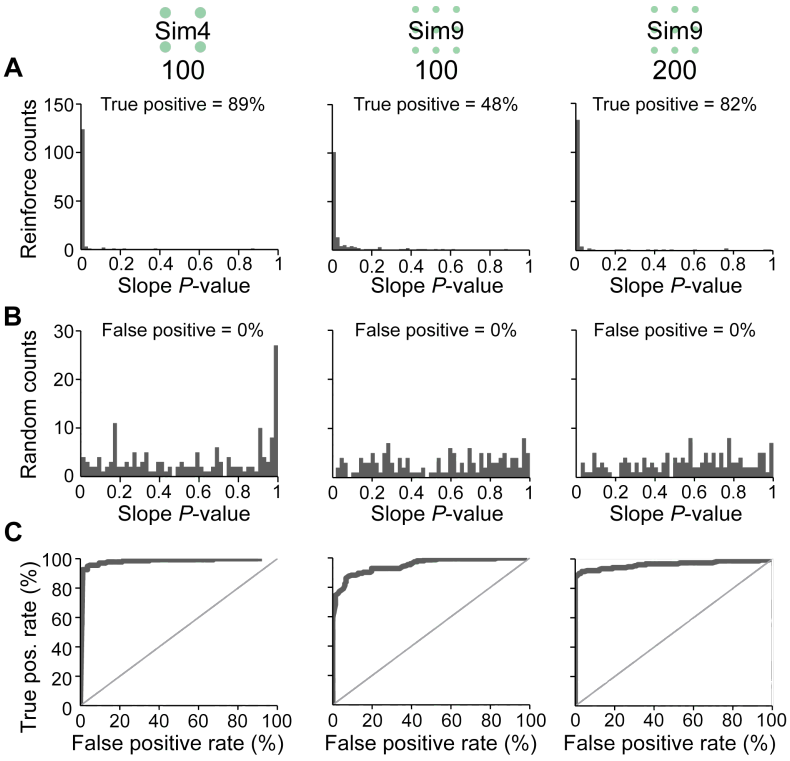

Figure 26. Reinforcement test detects RL with almost no false positives. Simulation and task condition depicted above row A: Sim4 100, 300 simulations of 100 sessions each; Sim9 100, 300 simulations of 100 sessions each; Sim9 200, 300 simulations of 200 sessions each. All simulated sessions contained 200 trials. Each simulation was randomly assigned to the REINFORCE algorithm or random reward algorithm (A) Histogram of the P-values of the slopes obtained using the reinforcement test on each of the simulations assigned to the REINFORCE algorithm. True positive rates noted are the percentage of P-value counts where $P < 0.01$. (B) Histogram of the P-values of the slopes obtained using the reinforcement test on each of the simulations assigned to the random reward algorithm. False positive rates noted are the percentage of P-value counts where $P < 0.01$. (C) Receiver operating characteristic (ROC) curve for the results of the 300 simulations in each condition.

In this task, measures of distance, reward rate, and number of saccades/fixations were all correlated. Consequently, there existed the possibility that a parameter other than distance would be the best drive for reinforcement learning. Because there was one reward at the end of each trial (reward was constant), reward rate is inversely proportional to the time required to capture the baited target. Similarly, because each saccade was surrounded by two fixations that occupied a larger fraction of time (~150 ms per fixation vs. ~30 ms per saccade), the number of saccades is approximately proportional to the time.

To disambiguate these factors, we used the REINFORCE algorithm and simulated 5,000 sessions of 200 trials each using the reward rate as the reinforcement drive with the goal being to maximize the reward rate. Reward rate was calculated as one over the time to capture the baited target, with the duration of each fixation set to 150 ms and the duration of each saccade set to 30 ms times the geometric distance of the saccade (one unit equals the horizontal or vertical

distance between adjacent targets). We found that the session-averaged reward rate, distance, and entropy took a greater number of sessions to reach steady-state than when the distance was used as the reinforcement drive in the simulations (**Figure 27A-C**). More strikingly, by the 5,000th session the reward rate-based simulation had not converged on the optimal path (**Figure 27D-E**, black) as had the distance-based simulations (**Figure 23E**).

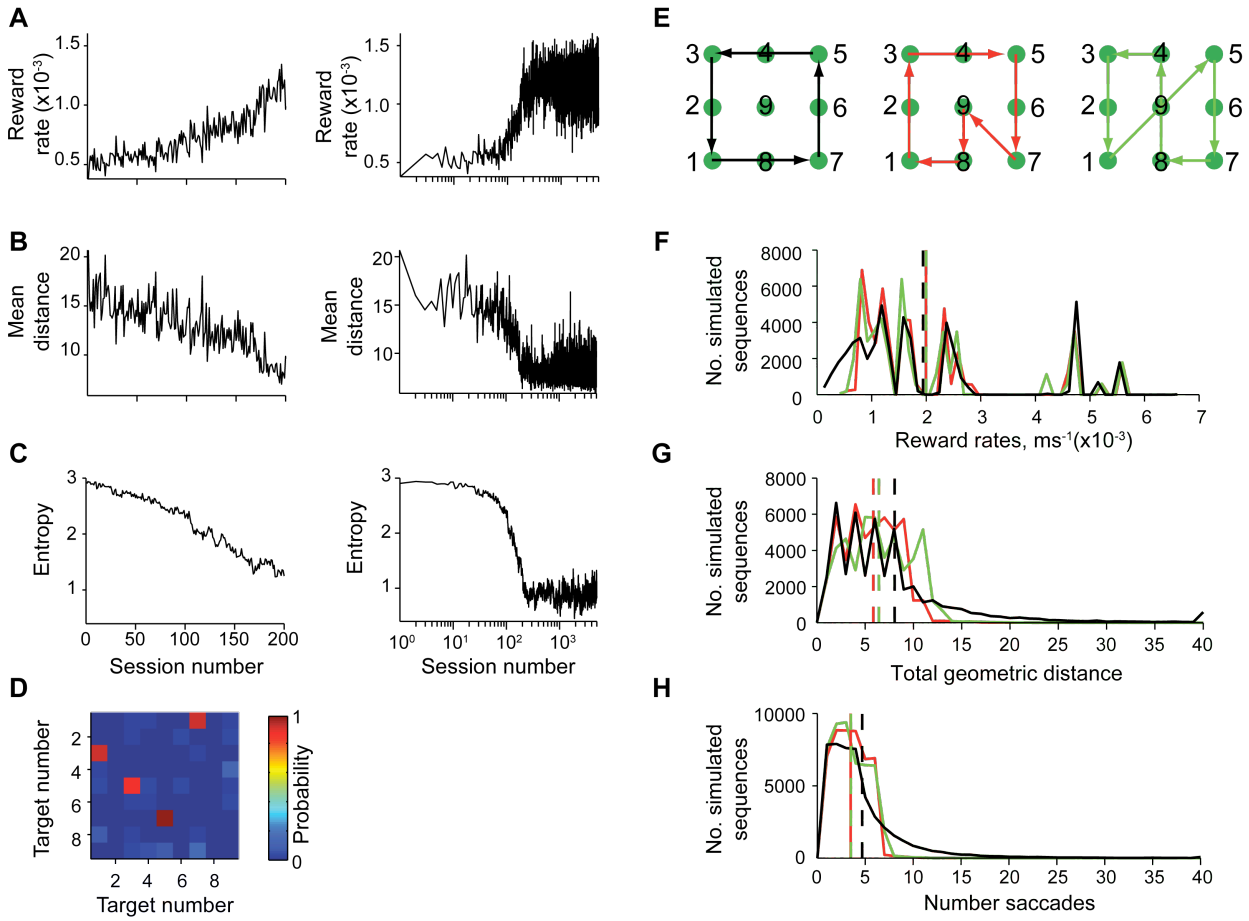

Figure 27. REINFORCE algorithm simulation using reward rate instead of distance does not converge on optimal path. Simulation of 5,000 9-target sessions, 200 trials each using reward rate (1/trial time with fixations = 150 ms and unit distance saccades = 30 ms) as the reward signal. (A-C) Left column is the first 200 simulated sessions and right column is all 5,000 simulated sessions. (A) Mean reward rate per session. (B) Mean geometric distance per session. (C) Entropy per session. (D) Final transition probabilities in the 5,000th session. Note the very low probability of visiting the center target. (E) Black: most probable path corresponding to D. Red: optimal distance path (see optimal paths Figure). Green: near-optimal distance path (see optimal paths Figure) with the same number of fixations as the optimal path. (F-H) Histogram of reward rates generated by 50,000 saccade sequences in Monte-Carlo simulations of the task using the paths depicted in E. Vertical dashed lines indicate the mean of each distribution. (F) Histogram of reward rates. Note the mean reward rate is nearly identical for all three paths. (G) Histogram of total geometric distance. (H) Histogram of the total number of saccades.

The final transition probabilities reached by the reward maximizing REINFORCE simulation, despite not having converged on the most optimal path, could have been close to optimal. To test the performance of the final set of transition probabilities (**Figure 27E** black) in comparison with the optimal (**Figure 27E** red) or a nearly optimal (**Figure 27E** green) in distance path, we

generated 50,000 saccades sequences using Monte-Carlo simulations and calculated the mean reward rate of each set of transitions. We found that the mean reward rates were nearly equivalent for all three paths: 0.0019422, 0.0019962, and 0.0019986 rewards per ms respectively (**Figure 27F**). Thus the reward maximizing simulation did indeed yield a set of transitions that produced a comparable mean reward rate; however, there were too many patterns that also had close to optimal reward rates and the optimal distance path was not converged upon. In contrast, minimizing the distance using REINFORCE had a unique pattern that the monkey also converged on.

For the same three sets of transitions discussed above, the total geometric distance means were 8.0553, 5.8462, and 6.4445 respectively (**Figure 27G**). The mean simulated number of saccades to complete the trial was similar with the final reward maximizing simulation transitions being the greatest and the optimal and nearly optimal distance paths had a mean of fewer saccades (**Figure 27H**). Therefore, to simulate this task, minimizing distance more closely approximated the monkeys' behavior and converged on the optimal policy, whereas maximizing reward rate did not.

Discussion

Strong associations between stimulus and response characterize many habitual behaviors. Through repeated trials and reinforcement learning, the associations are formed and strengthened. The S-R paradigm has been the focus of most experimental studies of habit learning, in which the tasks performed involved a limited number of stimuli and responses. But habits can consist of extensive sequences of behaviors, not just single responses, and the number of possible sequences can be enormous. The learning mechanisms underlying such habitual action sequences have rarely been studied experimentally. RL algorithms have been employed in computer simulations to learn sequential actions such as in playing games (Barraclough et al. 2004; Daw et al. 2006), and in a hippocampus-dependent water-maze learning in rats (Foster et al. 2000). Here we asked whether RL could account for learning such sequential habits and individualized rituals under conditions of extreme uncertainty.

Our task was designed to study the formation of such sequential habits. The stimulus was a simple grid of dots, but because the responses were self-generated saccade sequences, the number of possible sequences was virtually infinite. Given that the baited target was chosen at random in each trial, simply saccading to a particular target or a particular set of targets in sequence did not lead to the reward each time. Despite the uncertainty intrinsic to the task, the monkeys formed repetitive scan patterns without instructions, and the patterns evolved through months of performing the task. Eventually, the monkeys settled into highly stereotypical scanning patterns with low entropy, characteristic to habitual behaviors.

We did not test whether reward devaluation affected the patterns, but the pervasiveness of these repetitive scanning patterns, especially in the many sessions of the 4-target task, clearly suggests that the patterns were habitual. The monkeys achieved optimal or nearly optimal scan patterns near the end of the experimental sessions. Despite there being many equivalent loop patterns for each level of optimality (rotations and reflections of **Figure 20**), the monkeys chose to perform a

single instance of each pattern. This fact again suggests that the monkeys have formed habitual sequences of eye movements without instruction.

It is remarkable that the monkeys 'solved' this task at all, given their lack of instruction. This finding may mean that there is an innate drive toward optimality. Our experiments indicate that the monkeys could not have been using session-averaged reward amounts or cost to shape their behavior successfully—these mostly reached asymptote early in the experiments. But trial-by-trial analysis demonstrated that the changes in saccade patterns were correlated with the fluctuations of the total distances to capture the baited target and earn reward, itself the same for each trial. A simple RL algorithm simulating the task captured the richness of a naïve monkey's performance: the total cost (saccade distance) to obtain the reward in a single trial was, on average, minimized. Our findings thus suggest that even for sequences of actions made to receive a singular, identical reward in a highly uncertain context, non-human primates can use RL to acquire habitual optimal sequences of behavior.

There were large individual differences in the rates at which the monkeys learned the optimal patterns, both across monkeys and across task versions. Our RL simulations showed that the scan task has complex cost structure in the space of scan patterns. An unfortunate choice of actions during the learning could lead to long detours from the optimal patterns due to local minima. Consequently, the rates of convergence to the optimal patterns varied greatly from run to run in the simulations, even with exactly the same parameters (**Figure 24**). The choices of the simulation parameters, especially the degrees of exploration and exploitation in each trial, also influenced the convergence rates, perhaps mirroring the effects of innate individual differences.

The reinforcement test we devised demonstrated that cost reduction is positively correlated with the similarity of the pattern changes on a trial-by-trial basis, as expected from the exploration-exploitation tradeoff inherent to RL learning. The correlation tended to be weak for at least three main reasons: 1) the shift in the patterns was the consequence of both learning and random exploration in each trial; 2) the estimates of the transition probabilities in each trial, used to compute the similarities between the shifts of the scan patterns in consecutive trials, could be inaccurate due to the limited number of saccades; and 3) the distance to capture the baited target fluctuated over a wide range due to its random assignment in each trial. Consequently, a large number of trials was required to show that the correlations were significant. It is also possible that the simplifying assumptions made in the corresponding simulations, such as the creation of saccade sequences using the limited trial-by-trial transition probabilities, were not entirely adequate to mimic the monkey behaviors in great detail (e.g., **Figure 22E**). Nevertheless, this analysis and relatively simple algorithm captured much of the richness of the monkeys' behaviors.

Habits, mannerisms, routines, and repetitive behaviors of any sort can share the feature of semi-automaticity. We found that monkeys can acquire such habitual behaviors without training and without a simple or explicit S-R environment, and that the habitual behaviors acquired were near-optimal in minimizing cost. Repetitive behaviors are not always advantageous, however. They can be dangerous when they allow predators to predict behavior. Further, repetitive behaviors frequently occur in disorders ranging from the stereotypies expressed in some neuropsychiatric conditions to the repetitive behaviors triggered as responses to anxiety-

provoking situations (Ridley 1994; Graybiel 2008). Our findings suggesting that there may be a spontaneous drive to repetitiveness should thus have implications for a broad range of both normal and abnormal behaviors.

Chapter III: Frontal Eye Fields

Introduction

The visual system is perhaps the most-studied system in the primate brain. Neural responses throughout this system have been recorded and categorized, ranging from the effects of light on photoreceptors in the retina to the responses in primary visual cortex, to the firing of motor neurons in the brainstem that control the eye muscles. To examine the role of the visual system in generating the sequences of saccades that naïve animals perform in a free-viewing scan task, we analyzed neural recordings from the frontal eye fields (FEF).

Because the neural responses to saccadic eye movements have been well characterized in the FEF in well-trained animals, it was an ideal brain region to begin to classify the neural recordings from the (initially) naïve animals used in this study. Early work categorized the general types of responses found in the FEF. In classic single saccade tasks, 54.3% of neurons responded presaccadically, 18.9% postsaccadically, 19.7% responded to non-saccades, and 7% were unresponsive (Bruce and Goldberg 1985). In the same study, 8.6% of neurons with presaccadic activity also had postsaccadic activity, and neurons with presaccadic activity were further classified into 40% visual (V), 40% visuomovement (VM), and 20% movement (M) categories. Early studies such as this one showed the wide variety of neural responses found in the FEF and laid the foundation for later studies that focused on the functioning of a particular subtype of cell.

As the Bruce and Goldburg study suggested, presaccadic and postsaccadic were soon found not to be mutually exclusive categories of cells in the FEF. Later work by these authors showed that nine percent of M cells, 43% of VM cells, and 54% of V cells also had postsaccadic activity in addition to their presaccadic activity (Goldberg and Bruce 1990). Further, cells were found to have responses outside the time frame immediately preceding or following saccades. Thirty four percent of V cells and 31% of VM cells were found to have predictive visual responses where the latency in response to a target's appearance in the future receptive field was less than the latency of a target just appearing in the receptive field (Umeno and Goldberg 1997). Cells in the FEF were also shown to have memory for these predictive visual responses. Cells that showed a predictive response when the target was flashed in the future receptive field for a block of trials would then continue to show a response when no target was flashed in the following block for 20 or more trials. This kind of memory was seen in 35% of V and VM cells with predictive visual responses in the FEF (Umeno and Goldberg 2001).

This work shows that FEF cells can display behavior highly specialized for saccade-related tasks, at least in a highly trained animal. This specialization also was found to evolve throughout

different phases of single trials. The majority of the 20% of all cells recorded in a visual search task found to be V or VM related did not differentiate whether the object in the receptive field was a target or distracter in the initial visual response, but evolved to do so later in the trial, before a saccade was initiated (Schall et al. 1995). However, even this seemingly non-selective initial visual response showed learning effects and task sensitivity. In a subsequent study by the same group, of the 80 neurons recorded in the FEF with visually evoked activity, 47 were further categorized as having visual responses and 21 out of those 47 neurons (44%) discriminated between target and distracter when the difference was indicated by color (Bichot et al. 1996). FEF cells signaling more complex properties of the task were also seen: 5% and 15% of presaccadic cells where selective for the rank or direction and rank respectively of particular saccades in a sequence saccade task, with 9% of cells showing a preference for the entire sequence (Isoda and Tanji 2003).

Given the nearly exclusive use of well-defined and abstract tasks, it is difficult to predict the activity of these neurons in more natural tasks. An early study of the activity of FEF cells in a natural scanning task found that 74% of cells with saccade related activity (pre or post) were as active during natural scanning as during conventional tasks; also, 67% increased their activity during scanning when portions of the image entered the receptive field (Burman and Segraves 1994). A subsequent study found that of presaccadic direction selective cells (V or VM type), 55% showed predictive activity related to the goal or direction of a second saccade (Phillips and Segraves 2009). These two studies by Segraves and colleagues give evidence that the same types of standard and predicative visual responses that have found in classic instructed saccade tasks could also be found in the FEF during natural scanning tasks.

The experiment we conducted expands on previous work in two main ways. First, recordings were made throughout task acquisition, starting with naïve animals that had not been previously exposed to any experimental tasks. Second, though the animals were permitted to engage in freely selected saccades, the task was arranged such that self-generated, repetitive sequences of saccades were made throughout. This repetition gave greater opportunity to characterize those firing properties that required a large number of samples, and additionally provided a unique opportunity to examine the possible role of the FEF in habitual, natural saccade behaviors, which has not been done before. Here, we describe how units in the FEF were found to have classic, single direction tuning; tuning that was modulated by an additional saccade before or after in a sequence of two saccades; sharpness of tuning that was specific to a particular subtype of cells; modulation across task periods; tuning sharpness that evolved over the course of task performance; and a subpopulation of cells that were most selective for directions that were parts of habitual sequences of saccades.

Results

We recorded from a total of 538 units localized to the FEF in two hemispheres across a total of 55 data acquisition sessions in monkey G, and a total of 568 units localized to FEF in two hemispheres across a total of 181 data acquisition sessions in monkey Y for a total of 1106 units across four hemispheres in two monkeys (**Figure 28**, **Figure 29**, see also **Figure 45** in *Appendix*). The FEF was defined prior to recording as a region in the anterior bank of the arcuate sulcus in which microstimulation evoked low-threshold (< 50 μA) saccadic eye movements. As

described in the Discussion, post-hoc anatomical localization of recording sites suggests that recordings from the two monkeys may have been conducted in different sub-regions of the anterior bank of the arcuate sulcus.

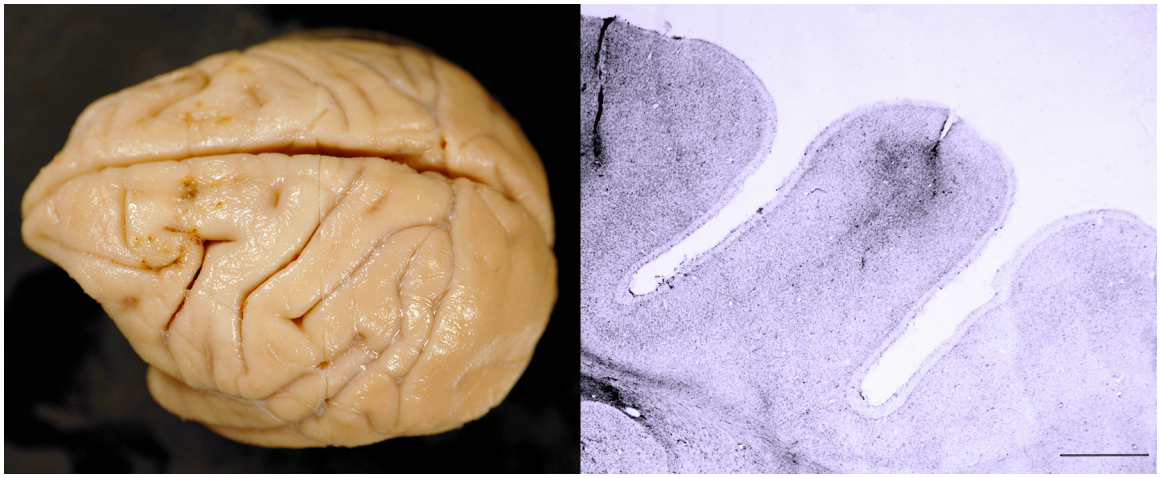

Figure 28. Monkey G brain surface and slice. Left image: surface of left hemisphere of monkey G. Left = anterior, right = posterior. Slight damage from electrodes targeting the FEF, PFC, and CN is visible. A blocking cut dividing the brain nearly in half on the anterior/posterior axis is also visible. Right image: Coronal cresyl violet-stained section from monkey G showing an electrode track between the superior and inferior arcuate sulcus at approximately AP 21. Scale bar = 2 mm.

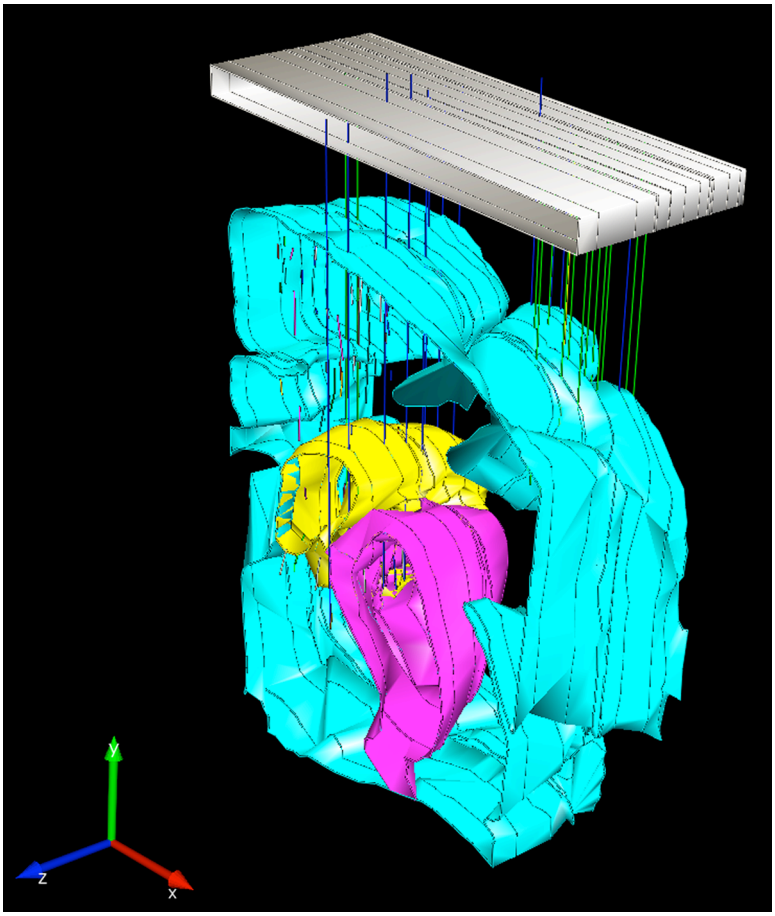

Figure 29. Three-dimensional reconstruction of electrode tracks in monkey G, right hemisphere. Icon in lower left corner indicates direction of plane of view: X (red) = lateral, Y (green) = dorsal, Z (blue) = posterior. White rectangle above the brain represents the plane of the grid used to guide electrode penetrations. Aqua is the outline of each section. Anterior and medial portions represent the surface of the brain; lateral and ventral portions represent where the sections were trimmed to fit on the glass mounting slides. Yellow outline is the caudate nucleus. Magenta outline is the putamen.

Recordings began at the start of a naïve monkey's acquisition of a free-viewing scan task where the monkey made free scanning eye movements to capture, after a delay, a target randomly chosen to be baited with reward (see *Chapter II: Behavior*, **Figure 1**). We first wanted to determine if cells recorded in the FEF during performance of the free-viewing scan task exhibited properties similar to those found in monkeys extensively trained on instructed visually guided saccade tasks. In these prior studies, the most common responses are those that show selectivity for firing before or after saccadic eye movements of a particular direction; in other words, they are tuned for a particular saccade direction.

Single direction tuning

We therefore first examined the tuning of cells to a single saccade direction. All saccade directions were binned into 8 bins with bin centers at 0°, 45°, 90°, 135°, 180°, 225°, 270°, and 315°. We binned the direction of saccades regardless of saccade amplitude for two reasons: 1) FEF cells have been shown to respond to all saccades greater than a given amplitude in a given direction, and that beyond this amplitude the response of the cell does not significantly change (Bruce and Goldberg 1985); and 2) all of the saccades during the Total Scan Time were within the ~18° square covered by the green target grid and most of the saccades in other task periods were within the ~25° square covered by the gray target grid. After binning, the firing rate was taken from two windows around every saccade. The PRE window was defined from the onset of the previous fixation to the onset of the saccade, and the POST window from saccade onset to the end of the subsequent fixation. An example cell's single direction tuning is shown in the following figure for the PRE and the POST windows (**Figure 30**). A one-way ANOVA was performed to asses the significance of the tuning ($p \leq 0.01$ corrected for multiple comparisons, see *Chapter V: Methods*).

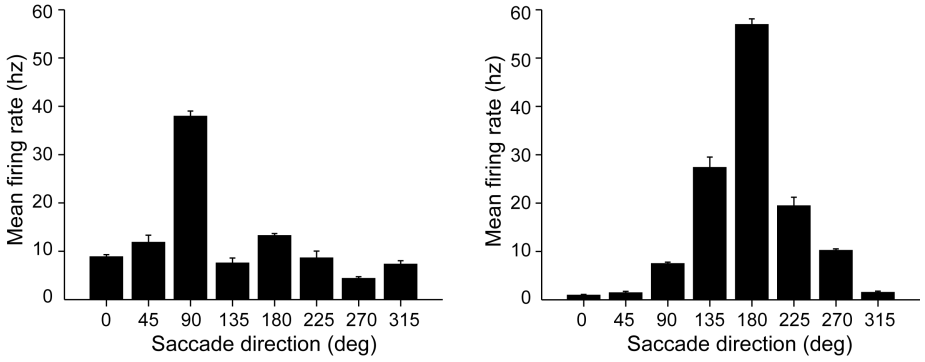

Figure 30. Single direction tuning of an example cell (monkey G, session 60, 13c1). Mean firing rate in each of eight direction bins (±1.96 * sem) in the PRE (left) and POST (right) saccade windows.

The example cell (**Figure 30**) is significantly tuned in the PRE and POST windows, and prefers 90° (up) saccades in the PRE window and 180° (left) saccades in the POST window. This cell appears to be tuned differently than prior studies that find FEF cells tuned for only one saccade direction (Goldberg and Bruce 1990). However, the design of the current task is, we currently believe, likely the cause for this apparent differential tuning PRE and POST. In our task, a unit could appear to have tuning to two different saccade directions in the two perisaccadic windows due to the underlying frequencies of which saccade directions are typically executed in sequence with each other. During the session that the above unit was recorded, it was very common for the monkey to execute a saccade left (180°) and then up (90°). Activity that was POST a leftward saccade would then appear to be PRE an upward saccade. It is in this manner that there could be the appearance of tuning for different directions in different windows.

To disambiguate whether a neuron was PRE versus POST saccade tuned, we utilized sequences of two saccades and performed a correlation analysis on the tuning curves from the PRE windows before each saccade in the sequence (PRE saccade 1 and PRE saccade 2) and from the POST windows after each saccade in the sequence. We expected that units would be most consistent in their responses, i.e. show the highest correlation, during the perisaccadic window they were tuned for. For example, if a cell preferred the POST period, then the response after saccade 1 (s1) and after saccade 2 (s2) would be highly correlated as opposed to the response PRE s1 and PRE s2 that would change based upon the frequency of the saccades that came before and after s1 and s2. Each unit was therefore classified as preferring the window (PRE or POST) that was found to have the higher correlation between the s1 and s2 epochs. For the example cell shown in **Figure 30**, the results of the correlation analysis are shown in **Figure 31**. This example cell has a higher correlation in the POST window and was therefore classified as being a POST cell. We found 312 units in monkey G and 152 units in monkey Y that showed significant direction tuning in either the PRE or POST window (**Table 1** and **2**). This result shows that units in the FEF of monkeys performing a free-viewing scan task exhibit classic single direction tuning.

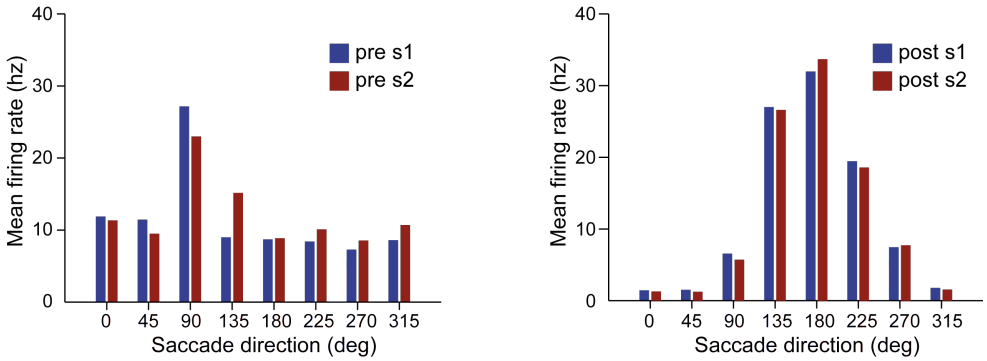

Figure 31. The tuning of an example cell in windows surrounding sequences of two saccades (s1 and s2). This cell (G, s60, 13c1) was classified as preferring the POST window because the correlation was stronger for the POST window (right, R = 0.998) than in the PRE window (left, 0.895).

	All	*1 Dir*	*2 Dir Bf*	*2 Dir Af*	*Both (B,A)*	*Neither (B,A)*	*Either (B,A)*
PRE		154 (49%)	89 (52%)	45 (39%)	36 (40%)	56 (49%)	98 (50%)
POST		158 (51%)	83 (48%)	69 (61%)	53 (60%)	59 (51%)	99 (50%)
Total	538	312 (58%)	172 (32%)	114 (21%)	89 (17%)	115 (21%)	197 (37%)

Table 1. Monkey G tuning results from all units recorded. Percentages in *PRE* and *POST* rows are out of total units for each column. Percentages in *Total* row are out of *All* units.

	All	*1 Dir*	*2 Dir Bf*	*2 Dir Af*	*Both (B,A)*	*Neither (B,A)*	*Either (B,A)*
PRE		64 (42%)	5 (22%)	0	0	59 (47%)	5 (19%)
POST		88 (58%)	18 (78%)	9	6	67 (53%)	21 (80%)
Total	568	152 (27%)	23 (4%)	9 (2%)	6 (1%)	126 (22%)	26 (5%)

Table 2. Monkey Y tuning results from all units recorded. Percentages in *PRE* and *POST* rows are out of total units for each column. Percentages in *Total* row are out of *All* units.

These results, however, could have been a biased representation of the population as a whole because these data were recorded using independently moveable, chronically implanted electrodes that were not necessarily moved to a new recording location before each recording session. A single electrode could remain in place over multiple recording sessions. This aspect of our method has the simultaneous advantage and disadvantage of sampling the same small region of brain over many recording sessions. In the context of understanding the makeup of the population as a whole, it was necessary to remove potential bias that was a result of sampling the same location multiple times by examining a subset of the population we were certain would contain different samples.

To produce a conservative estimate of the population, we selected a single representative unit from each stable stretch of recording sessions where the electrode was not moved or moved less than 75 microns. In other words, the electrode had to have been moved at least 75 microns to be considered a sample from a new location, though most locations were separated by at least 160 microns. We then bootstrapped this selection to ensure that the sample was not biased by which units were randomly selected to represent a given stable stretch of recording (see *Chapter V: Methods* for more details). Population percentages found using these bootstrapped "unique" units were lower (**Tables 3** and **4**), but not substantially different than percentages found using the population as a whole (**Tables 1** and **2**). However, we used the unique units for the majority subsequent analyses because we believed them to be a more accurate representation of the underlying distribution of FEF cells. Using the unique units, we found 49% of units (19% PRE and 30% POST) in monkey G and 22% of units (6% PRE and 15% POST) in monkey Y to be tuned to a single direction. Thus, FEF neurons recorded during performance of our free-viewing scan task showed tuning for both perisaccadic windows examined.

	All	*1 Dir*	*2 Dir Bf*	*2 Dir Af*	*Both (B,A)*	*Neither (B,A)*	*Either (B,A)*
PRE		17.5 (38%)	7.4 (35%)	4 (25%)	2.9 (24%)	8.9 (44%)	8.5 (34%)
POST		28.1 (62%)	13.9 (65%)	11.9 (75%)	9.1 (75%)	11.3 (56%)	16.7 (66%)
Total	93	45.5 (49%)	21.4 (23%)	15.9 (17%)	12.1 (13%)	20.3 (22%)	25.3 (27%)

Table 3. Monkey G unique unit population tuning. Results after bootstrapping the selection of a single unit from each stretch of recording. Percentages in *PRE* and *POST* rows are out of total units for each column. Percentages in *Total* row are out of *All* units.

	All	*1 Dir*	*2 Dir Bf*	*2 Dir Af*	*Both (B,A)*	*Neither (B,A)*	*Either (B,A)*
PRE		4 (29%)	0.2	0	0	3.8 (33%)	0.2
POST		9.7 (71%)	1.8	0.6	0.4	7.7 (67%)	2
Total	63	13.7 (22%)	2 (3%)	0.6 (1%)	0.4 (1%)	11.5 (18%)	2.2 (3%)

Table 4. Monkey Y unique unit population tuning. Results after bootstrapping the selection of a single unit from each stretch of recording. Percentages in *PRE* and *POST* rows are out of total units for each column. Percentages in *Total* row are out of *All* units.

Double direction tuning

Because the monkeys were not just performing single saccades, but performed continuous sequences of saccades, we next asked how single direction tuning was affected by the saccade preceding or following the preferred direction. We examined the firing rate in response to all possible sequences of two saccades (64 in total) in three windows surrounding the two saccades: from the onset of the fixation previous to saccade one (s1) to the onset of s1, from the onset of s1 to the onset of saccade two (s2) (encompassing the fixation POST s1 and PRE s2), and from the onset of s2 to the end of the fixation following s2 (**Figure 32**).

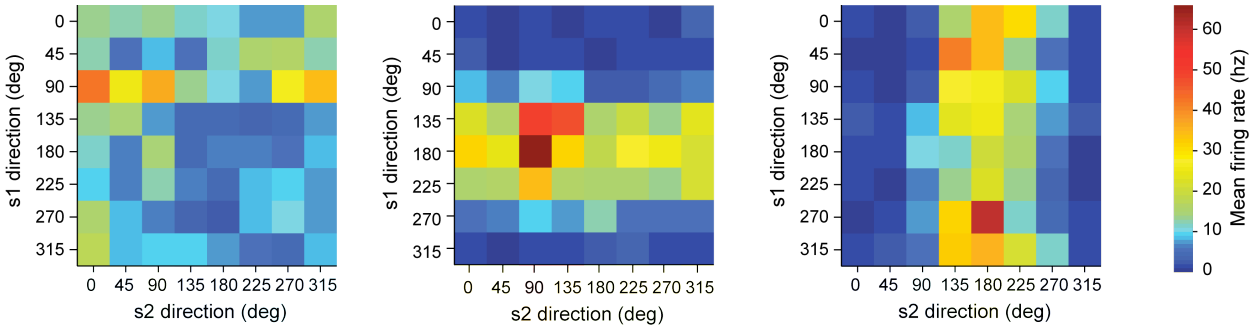

Figure 32. Double direction tuning of an example cell (G, s60, 13c1). Mean firing rate in each of 64 direction combinations of saccade 1 (s1) and saccade 2 (s2) across three windows: PRE s1 (left), POST s1/PRE s2 (middle), and POST s2 (right).

To determine if the preferred single direction (1Dir) tuning of a unit was significantly modulated by the direction of the saccade before or after, we examined "slices" through the 8x8 space of all possible two saccade combinations that held either s1 or s2 to be the preferred 1Dir direction and examined the effect of the saccade not held constant. The perisaccadic windows used for this analysis were determined by the unit's 1Dir classification as either PRE or POST. For PRE cells the windows of interest were PRE s1 and PRE s2 (same as POST s1). For POST cells the windows of interest were POST s1 (same as PRE s2) and POST s2. If there was a significant effect of interaction between s1 and s2 in a given perisaccadic window (two-way ANOVA, factors: firing rate in s1 direction and firing rate in s2 direction, $p \leq 0.01$ corrected for multiple comparisons), then the slice through the window of interest (PRE s1, POST s1/PRE s2, or POST s2) was evaluated for significant modulation by an additional saccade (one-way ANOVA of firing rate across direction, $p \leq 0.01$ corrected for multiple comparisons). If, in a given perisaccadic window of interest, a unit had both a significant interaction between s1 and s2 and a significant modulation of the activity in response to the preferred 1Dir tuning by an additional saccade, then the unit was classified as having double direction (2Dir) tuning. This process was repeated for both perisaccadic windows of interest for every unit and it was possible for units to have 2Dir tuning to both the saccade before and the saccade after the preferred 1Dir saccade.

For the example cell shown in **Figure 30, Figure 31** and **Figure 32** that was found to be a POST cell and preferred leftward (180°) saccades, the process described above proceeded as follows. We assessed the modulation by the saccade before the preferred direction by analyzing the perisaccadic window POST s2 (**Figure 32** right). The interaction between s1 and s2 was found to be significant. A slice along the s1 axis at 180° on the s2 axis (holding 2s constant at the preferred 1Dir saccade) was found to have significant modulation. The maximum within that slice was found to be down (270°), and therefore the unit was found to prefer a downward saccade before a leftward saccade and have significant 2Dir tuning (**Figure 33**, left). Using the same procedure to analyze the POST s1/PRE s2 widow showed this cell to also have significant modulation by the saccade after, with the preferred direction of modulation being up (90°) (**Figure 33**, right).

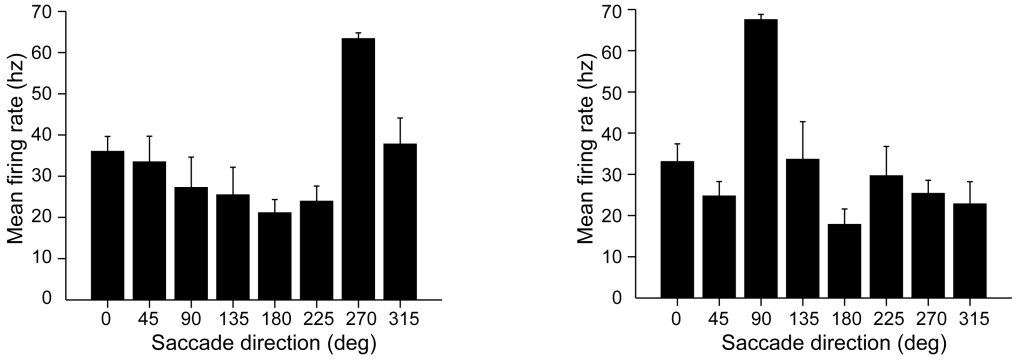

Figure 33. Double-direction tuning of an example cell (G, s60, 13c1). Left: mean firing rate (±1.96 * sem) as modulated by the saccade before. Slice taken from the POST s2 window with s2 held at the preferred single-direction tuning (180 deg) and s1 allowed to vary. Right: mean firing rate (±1.96 * sem) as modulated by the saccade after. Slice taken from the POST s1/PRE s2 window with s1 held at the preferred single-direction tuning (180 deg) and s2 allowed to vary.

The results of analyzing all cells in this manner for double direction tuning (or modulation of the preferred direction by another direction) are shown in **Tables 1** and **2** for all units and **Tables 3** and **4** for unique units. We found 23% of all unique units in monkey G to have significant 2Dir modulation by the saccade direction before, and 17% had 2Dir modulation by the saccade after (3% and 1% respectively in monkey Y). Further, we found 13% and 1% of units to be selective for both the direction before and the direction after in monkey G and Y respectively (**Tables 3** and **4**, column *Both (B,A)*). It is possible, though not explicitly tested here, that such units showing 2Dir tuning for both the saccade before and saccade after could be selective for the entire sequence of three saccades. This suggests a mechanism by which units in the FEF can be biased for the directions of multiple saccades, while still maintaining classic single direction tuning in the context of a free-viewing task.

Once we had determined the 1Dir and 2Dir tuning for all units, we next wanted to gauge the strength of the tuning, and determine if there were any differences among cells that were tuned in different perisaccadic windows. We calculated the tuning score as the firing rate in the maximum (preferred) direction bin divided by the mean firing rate across all the direction bins for all units with significant 1Dir or 2Dir tuning. In 2Dir tuning this score was performed on the slice through all possible two saccade sequences that was used to evaluate the significance of the 2Dir tuning. Both 1Dir and 2Dir tuning had eight direction bins, therefore the minimum tuning score was 1, and the maximum tuning score was 8, though this would require the unit to have a firing rate of zero for all directions except the maximum direction and this did not occur in our data set. The mean tuning score across all units recorded with significant 1Dir tuning was 1.45 with a minimum score of 1.07 and a maximum score of 2.75. The mean tuning score across all units recorded with significant 2Dir tuning, either before or after, was 1.75 with a minimum score of 1.11 and a maximum score of 3.66.

Across all units recorded, significant differences were found between groups of cells preferentially tuned to the different perisaccadic time windows (one-way ANOVA, $p < 0.01$ corrected for multiple comparisons). Overall, PRE 1Dir cells had significantly higher tuning scores than POST 1Dir cells (**Figure 34** single star). The highest mean tuning scores were found for those cells that had 2Dir tuning for the saccade before regardless of whether it was PRE or POST, and those scores were significantly different from the 1Dir tuning scores (**Figure 34** double star). There was a general trend towards the tuning scores of the PRE 1Dir and before 2Dir tuned units being higher than the tuning scores of the POST 1Dir and after 2Dir units, but this trend did not reach significance (**Figure 34**). The unique units showed the same trends, but did not reach significance. The result that 1Dir tuning for PRE was sharper than POST suggests that the map of retinotopic space already visited is not as precise as the map for space about to be visited, and this fits with the idea that the eye position signal must be more specific to generate a saccade to an exact location. The fact that the sharpest tuning was seen for 2Dir cells modulated by the saccade before suggests that, for habitual sequences of saccades in this task, the FEF more precisely keeps a tally of where the eyes have been. It could be that because the movements are habitual, less precise ‘planning’ is necessary by the cells in the FEF.

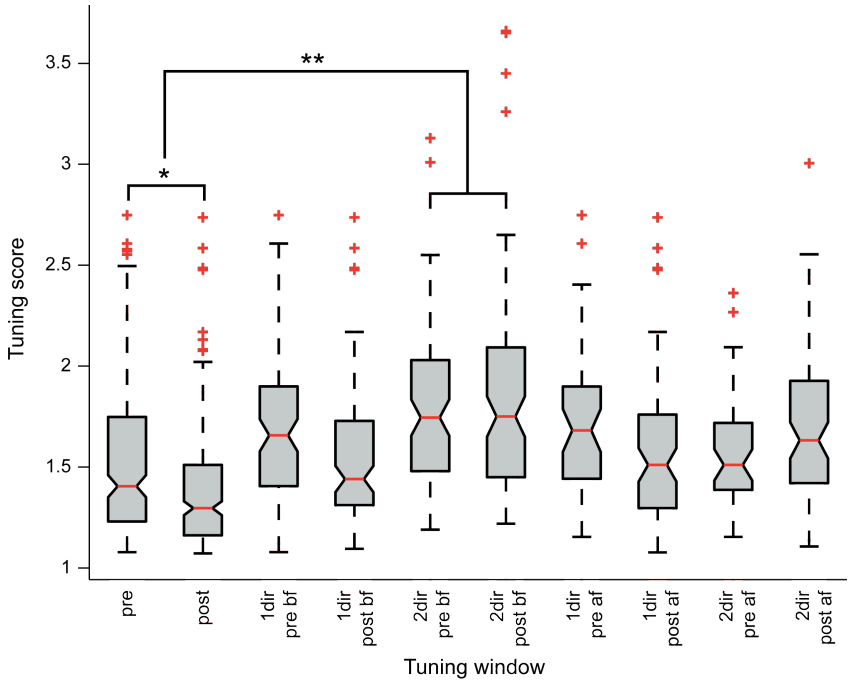

Figure 34. Box plot comparison of tuning scores across windows for all units (monkeys G and Y). Red line indicates median. Notches above and below red lines indicate 5% significance level. Tops and bottoms of each box (gray shaded region) are the 25th and 75th percentiles. Black dashed whiskers are drawn from the ends of the interquartile ranges to the furthest observations within the whisker length. Red pluses are outliers, values that are more than 1.5 times the interquartile range away from the top or bottom of the box. PRE and POST columns are the tuning scores for all units significantly tuned in either the PRE or POST window. For double direction tuning columns the tuning scores for both the primary direction (1dir) and the modulated, double direction (2dir) are shown (bf = saccade before, af = saccade after). Black stars indicate significant differences between groups.

We next examined the relationship between individual unit's 1Dir and 2Dir tuning. We found a significant, positive correlation between the 1Dir and 2Dir tuning scores of unique units in monkey G (bootstrapped correlation: slope = 0.9, R = 0.6, p = 0). In other words, the greater the tuning score was for 1Dir tuning, then the greater the tuning score was for 2Dir tuning. A representative example set of unique units across recording in monkey G is shown in **Figure 35**. As can be seen, there did not appear to be any relationship between the perisaccadic window preferred by a given unit and the correlation between 1Dir and 2Dir tuning scores. Because of the low numbers of units that were 2Dir tuned, it was not possible to accurately perform this correlation with data from monkey Y (see **Table 4**). This result points to cells in the FEF being generally more or less selective in a proportional manner across 1Dir and 2Dir tuning.

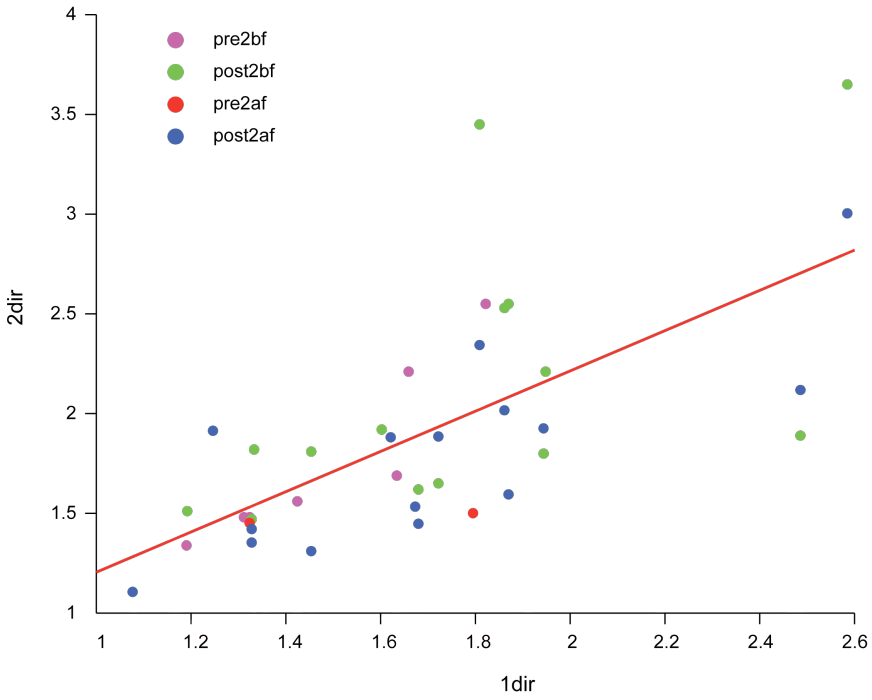

Figure 35. Correlation between single direction and double direction tuning scores. Each point represents a single unit chosen from each stretch of recording in monkey G. Unit taken was the one with the greatest signal-to-noise ratio on the second day of a stretch of recording, unless there was only one day, in which case a unit from that day was taken. Slope = 1.01, R = 0.68, $p = 2.7\times10^{-6}$ for this sample. Pre2bf = presaccadic single direction tuning, score of modulation by the saccade before; post = postsaccadic single direction tuning; af = score of modulation by the saccade after.

Task period modulation

Previous work has shown that cells in the FEF can be affected by factors such as attention (e.g., Armstrong et al. 2009; Buschman and Miller 2009), and it was reasonable to assume that a factor such as attention would not be consistent throughout all epochs of the free-viewing scan task. Therefore, we next asked for those units that were significantly 1Dir or 2Dir tuned if there was significant modulation of the unit's firing rate in response to the preferred direction(s) in different epochs of the free-viewing scan task (ANOVA, $p \leq 0.01$ corrected for multiple comparisons). The epochs examined were before the scan targets turned on (Start Delay), while the green scan targets were on (Total Scan Time), and after the green scan targets turned off (Reward Delay, Reward Time, and ITI; see **Figure 1** for illustration of task periods).

We found 88% and 48% of all 1Dir tuned cells to be modulated by task period in monkeys G and Y respectively (**Tables 5** and **Table 6**). In monkey G we found 15% of the direction tuned units were selective for the pre-scan period, 78% for the scan period, and 8% for the post-scan period. These percentages were slightly shifted for 2Dir tuning to both the saccade before and after with 4% preferring pre-scan, 95% preferring scan, and 1% preferring post-scan. Units from monkey Y showed the same trends as those from monkey G and there were units that were significantly modulated by task period, but it was difficult to make statements about the overall population given the low numbers of units. Though there are many possible explanations for differences in firing rate for the preferred direction(s) across task periods, one could account for these effects if cells in the FEF were modulated by attention. We did not explicitly test for the attentional state

of the monkeys as they performed this task; however, it is reasonable to assume that they would be most engaged during the scan period, when there were behavioral requirements placed upon the position of their eyes and reward was associated with eye movements. This result suggests that cells in the FEF modulate their firing rate to the preferred direction(s) in response to the amount of attention required, and that this occurs naturally. The existence of cells that prefer other task periods also suggests that there could be global modulation of signals in the FEF that signal the anticipation of a task about to begin or the completion of a task.

	PRE	*POST*	*2Dir Bf*	*2Dir Af*	***Total 1Dir***
Pre Scan	1.8	4.2	0.7 (4%)	0.5 (4%)	6 (15%)
Scan	12.1	18.9	15.5 (95%)	12.7 (95%)	31 (78%)
Post Scan	1.1	2	0.2 (1%)	0.1 (1%)	3.1 (8%)
Total	15 (86%)	25 (89%)	16.3 (76%)	13.3 (84%)	40 (88%)
All	17.5	28.1	21.4	15.9	45.5

Table 5. Task period selectivity for Monkey G bootstrapped unique units. Results after bootstrapping the selection of a single unit from each stretch of recording. The numbers of units found to have significant modulation in each task period are shown. *Total* column is total of either *PRE* or *POST* selective units. Percentages in *Pre Scan*, *Scan*, and *Post Scan* rows are out of *Total* units for each column. Percentages in *Total* row are out of *All* units.

	PRE	*POST*	*2Dir Bf*	*2Dir Af*	***Total 1Dir***
Pre Scan	0	0.2	0	0	0.2 (3%)
Scan	1.1	2.4	1.1	0.4	3.5 (53%)
Post Scan	0.4	2.5	0	0	2.9 (44%)
Total	1.5 (38%)	5.1 (53%)	1.1 (55%)	0.4 (67%)	6.6 (48%)
All	4	9.7	2	0.6	13.7

Table 6. Task period selectivity for Monkey Y bootstrapped unique units. Results after bootstrapping the selection of a single unit from each stretch of recording. The numbers of units found to have significant modulation in each task period are shown. *Total* column is total of either *PRE* or *POST* selective units. Percentages in *Pre Scan*, *Scan*, and *Post Scan* rows are out of *Total* units for each column. Percentages in *Total* row are out of *All* units.

Tuning across sessions

After we illustrated that direction selectivity in the FEF and the modulation thereof goes beyond simple single direction tuning or even tuning for two directions in its modulation by task performance periods, we wanted to know if units in the FEF changed their response properties over the course of task performance sessions. The first measure we examined was how the tuning score (max FR/ mean FR) evolved through time. It was possible that as the monkeys became more predictable or habitual in the sequences of saccades that they executed (see **Figure 17** *Chapter II: Behavior*), that the tuning of the cells became more specific by showing sharper tuning (i.e. higher tuning scores). We evaluated the tuning score across sessions using units that had been recorded on multiple sessions from the same recording location, without moving the electrode. For every stable stretch with two or more sessions of recordings on a single channel we calculated the slope of a linear regression line through all the tuning scores for that channel during that stretch.

Out of all stable stretches on all channels with 1Dir tuning in monkey G, 68% (23/34, $p = 0.058$ two-tailed sign test) were found to have positive slopes with a weighted mean slope of 0.14 (see

Chapter V: Methods) (**Figure 36**). The same measure in 2Dir tuned cells in monkey G showed that 83% (15/18, p = 0.008 two-tailed sign test) had positive slopes for modulation by the saccade before, and 73% (11/15, p = 0.118 two-tailed sign test) had positive slopes for modulation by the saccade after with weighted mean slopes of 0.30 and 0.23 respectively (**Figure 37**). Units recorded from monkey Y showed the same trend with 78% (7/9, p = 0.180 two-tailed sign test) having positive slope for single direction tuning and a weighted mean slope of 0.06 (**Figure 38**). There was very sparse data for double direction tuning in monkey Y, but 2 out of 3 slopes were positive for modulation by the saccade before and 2 out of 2 for the saccade after (data not shown). This analysis thus showed a trend across all classes of cells towards units becoming more sharply tuned at individual recording locations as task performance progressed with perhaps the most rapid changes occurring in the first ~10 sessions. Additionally, only one subclass of cells, those with 2Dir tuning modulated by the saccade before, showed a significant number of increases in tuning sharpness across stretches of recordings. It is interesting to note that this same subclass of units (2Dir Bf) was also the subclass that showed the sharpest overall tuning. It is possible that this sharper tuning could reflect the increased specificity of the patterns of saccades that the monkeys executed as task performance progressed and that these cells in the FEF might play a role in the process of forming habitual sequences of saccades.

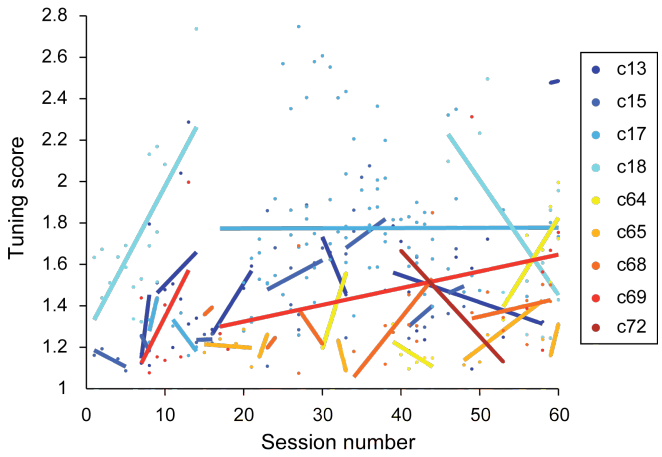

Figure 36. G 1Dir tuning through time. Session number vs. tuning score is plotted for each session a unit with significant single direction tuning was recorded for two or more sessions on each channel. Linear regression lines shown for the points recorded without moving the electrode.

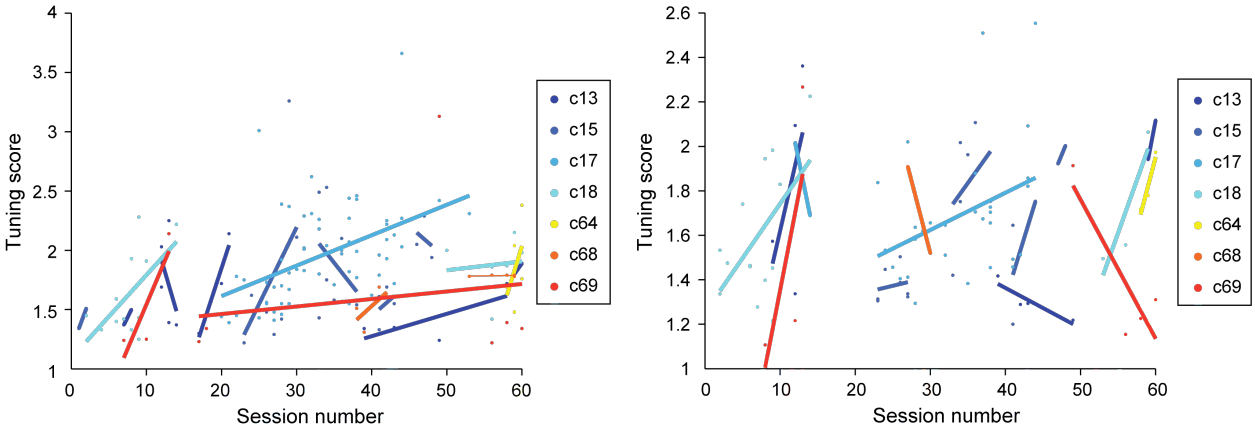

Figure 37. G 2Dir tuning through time. Session number vs. tuning score is plotted for each session a unit with significant double direction tuning was recorded for two or more sessions on each channel. Linear regression lines shown for the points recorded without moving the electrode. Left: modulation by saccade before. Right: modulation by saccade after.

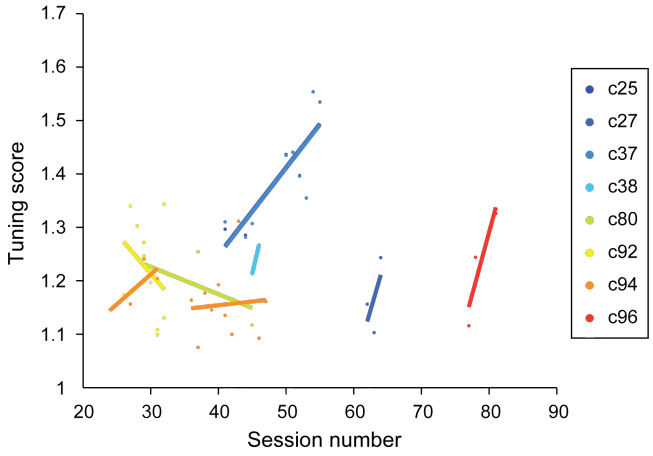

Figure 38. Y 1Dir tuning through time. Session number vs. tuning score is plotted for each session a unit with significant single direction tuning was recorded for two or more sessions on each channel. Linear regression lines shown for the points recorded without moving the electrode.

We next examined more specifically how the tuning of individual FEF units related to the habitual sequences of saccades that evolved over the course of task performance sessions. We first asked if in the beginning of task acquisition (the first 10 sessions), when a relatively low percentage of trials contained a loop sequence (*Chapter II: Behavior* **Figure 4**), we saw the same kinds of 1Dir and 2Dir tuning that we saw in the population as a whole across sessions. To answer this, we first plotted for each unit recorded in each session the significant 1Dir and 2Dir tuning directions (**Figure 39**). As can be seen in the figure, the answer is yes. There was an example of 2Dir tuning recorded from the first session in monkey G (POST 180° saccade modulated by a 90° saccade before). Further, the first example of 2Dir tuning by both the saccade before and the saccade after occurred in the second session of recording in monkey G (POST 0° saccade modulated by a 180° saccade before or after). There were a total of 11 units with 2Dir tuning by both the saccade before and the saccade after in the first ten sessions (out of 38 with 1Dir and 26 with 2Dir tuning by the saccade before or after). This result suggested that it was not the repetition of sequences per se that created 2Dir tuning, or that if 2Dir tuning was caused by repetition, it took less than a single session for units in the FEF to respond in this fashion.

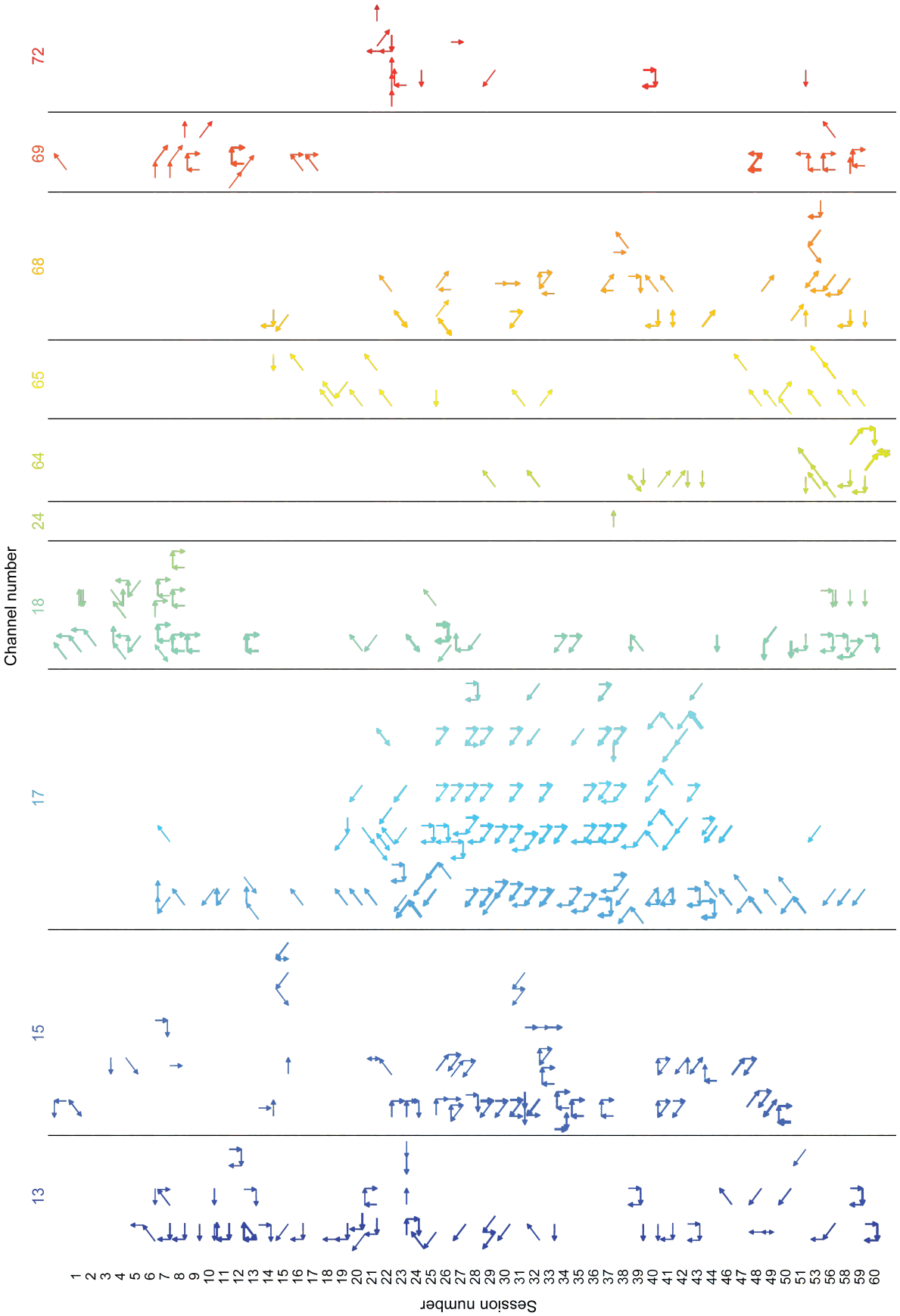
Channel number
72
69
68
65
64
24
18
17
15
13
Session number
1 2 3 4 5 6 7 8 9 10 11 12 13 14 15 16 17 18 19 20 21 22 23 24 25 26 27 28 29 30 31 32 33 34 35 36 37 38 39 40 41 42 43 44 46 47 48 49 50 51 53 56 58 59 60

Figure 39. All preferred saccade directions of all units in monkey G. Rows are sessions and columns are channels. Sub-columns indicated by color are different clusters on the same channel. Thickness of each vector indicates tuning score, though differences are difficult to see at this scale.

We next examined how single and double direction tuning related to the monkeys' most frequent loop sequences through all task performance sessions (*Chapter II: Behavior* **Figure 4**). Even if the existence of 1Dir or 2Dir tuning is not caused by the execution of sequences, the properties of this tuning could be influenced by the specific habitual sequences performed on each session. For each unit that was found to be significantly tuned in 1Dir or 2Dir, we found the fraction of the preferred direction(s) were members of the loop sequences on the session in which the unit was recorded. For example, during recording session number 7 in monkey G, a unit was found to have selectivity to 180° saccades modulated by a 270° saccade before. This sequence of two saccades (down then left), was found to be a member of one of the loop sequences on that session (going clockwise around in a square, **Figure 4A**). The fraction that a given direction or sequence of directions would be a member of a loop sequence by chance is the fraction of directions represented by the sequence itself. For example, if the most frequent sequence was going clockwise in a square, then there are 4 possible two direction sequences represented by the loop sequence for a 4/64 (0.0625) fraction of sequences represented. The mean number of directions represented by the loop sequences across sessions were used for comparison purposes (see *Chapter V: Methods*).

We found that neurons were more likely to be tuned for parts of the monkeys' habits than for any other random two saccade sequence. In other words, the fraction of units' whose preferred directions were members of the loop sequences were greater than the fraction of directions represented by the loop sequences. We found this to be true for both 1Dir and 2Dir tuning in monkey G in both the first half and second half of task performance sessions (**Figure 40**). Monkey Y showed the same trend (with a low number of units) for 2Dir tuning, but not for 1Dir tuning (**Figure 41**). Monkey G also possibly showed a slight increase in the fraction of units' preferred directions that were members of loop sequences, for both 1Dir and 2Dir tuning, across sessions. We found an 8.1% difference in the first half and 9.5% difference in the second half of sessions for 1Dir tuning, and a 46.9% difference in the first half and 52.7% difference in the second half of sessions for 2Dir tuning. Overall, 2Dir preferred directions showed a nearly 5-fold increase over chance for being members of the loop sequences. Thus in addition to showing a trend toward becoming more sharply tuned with training, units in the FEF preferentially represented those saccade directions that were habitually performed by the monkey.

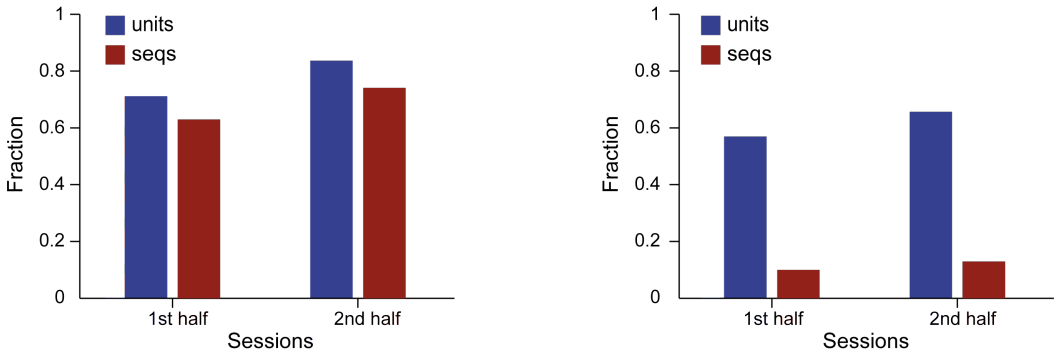

Figure 40. Fraction of tuning directions that are members of loop sequences in monkey G. Fractions are compared for the first half (sessions 1 to 30) and second half (sessions 31 to 60) of task performance sessions. Left: Fraction of all single direction tuned units that have their preferred directions members of the most frequent loop sequences compared with the fraction of single saccades that are represented by the most frequent loop sequences (the rate of single saccade membership expected by chance). Right: Fraction of all double direction tuned units that have their preferred directions members of the most frequent loop sequences compared with the fraction of sequences of two saccades that are represented by the most frequent loop sequences (the rate of two-saccade membership expected by chance).

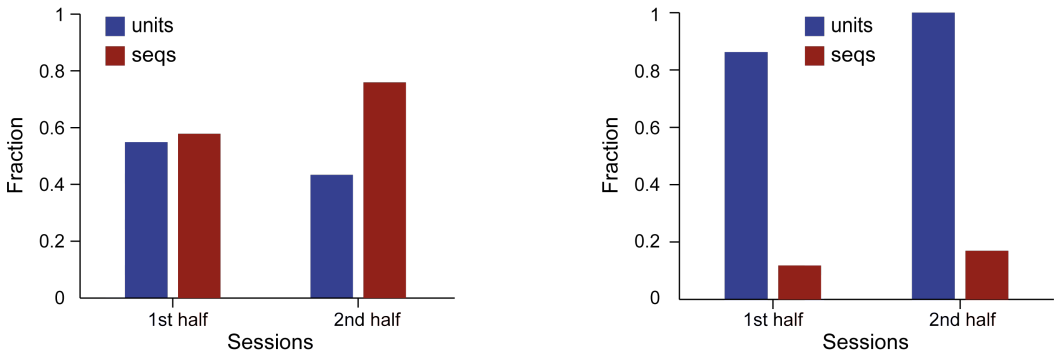

Figure 41. Fraction of tuning directions that are members of loop sequences in monkey Y. Fractions are compared for the first half (sessions 1 to 101) and second half (sessions 102 to 202) of task performance sessions. Left: Fraction of all single direction tuned units that have their preferred directions members of the most frequent loop sequences compared with the fraction of single saccades that are represented by the most frequent loop sequences (the rate of single saccade membership expected by chance). Right: Fraction of all double direction tuned units that have their preferred directions members of the most frequent loop sequences compared with the fraction of sequences of two saccades that are represented by the most frequent loop sequences (the rate of two-saccade membership expected by chance).

Discussion

These data replicate and extend existing knowledge of neural tuning in the FEF with respect to saccadic eye movements. As in previous studies, we observed high percentages of units that preferred a single direction of saccade, both pre- and post-saccadically along with cells that exhibited tuning that was less classical. The current findings extend current knowledge, suggesting a sub-class of FEF cells may provide a precise representation of habitual saccadic behavior. Prior to discussing the evidence for this suggestion, we highlight that these findings are mainly derived from recordings made in two hemispheres of one animal (G), with the same trends seen in a second animal (Y, discussed further below).

Four findings suggest that at least one class of FEF cells provide a precise representation of habitual behavior: 1) cells with single direction tuning (1Dir) modulated by the saccade before or after (2Dir tuned) were much more likely than chance to represent the monkey's habitual sequences of eye movements; 2) the most common type of 2Dir tuning were those cells modulated by the saccade before (2Dir Bf), and such cells have not been classified before and could suggest a role of the FEF in indexing the recent movements of the eyes to represent the pattern of saccades the monkey is expressing at a given time; 3) the direction tuning of 2Dir Bf cells was sharper than the 1Dir cells, suggesting a more precise representation by cells involved in habitual sequences over those that were not; and 4) the tuning of 2Dir Bf cells sharpened across task performance sessions, as the monkeys became more habitual in their patterns across

sessions (see *Chapter II: Behavior*). These results point to a role of the FEF in tracking habitual saccadic behaviors and suggest a mechanism by which the modulation of classic direction tuning could accomplish this.

To frame the following discussion and provide a reference point for the strength of our claims, we first discuss the relative contributions of data from the two monkeys used in this study. In calculations regarding the population of units in the FEF, recording sites from monkey G were primarily analyzed and discussed because the overall yield of direction tuned units was substantially lower in monkey Y (152) than in monkey G (312) even though similar numbers of overall units were recorded (538 G, 568 Y). This could be due to the anatomical location of the recordings. Though anatomical reconstruction has not yet been completed on monkey Y, it appeared from the surface inspection of the brain that recordings in one hemisphere of monkey Y that were targeting FEF may have been further from the genu of the arcuate sulcus and more along the upper limb. This localization is despite the fact that we elicited low-threshold (< 50 μA) saccades with pre-implantation microstimulation used for mapping potential electrode tracks. This anatomical region, even when localized using microstimulation evoked saccade thresholds greater than 50 μA, has been shown to have similar projections to other brain regions and neural responses that are largely the same as genual FEF (Parthasarathy et al. 1992; Balan and Ferrera 2003), but its inclusion as FEF varies. The other hemisphere of monkey Y was difficult to assess visually, as the principal and arcuate sulci followed an atypical pattern, however recording tracks were also placed according to where low threshold microstimulation elicited saccades. Despite possible differences in recording locations between monkey G and monkey Y, the same trends and patterns of neuronal activation were seen, and wherever possible units from both animals were included in analyses.

Our study replicated previous studies primarily by finding a high proportion of units in the FEF tuned to a particular direction of saccade. We found approximately half of the unique units we recorded from showed single direction tuning in the window either preceding or following saccades. Therefore, in this free-viewing scan task we found results similar to those in the well-trained animal performing instructed saccade tasks (Bruce and Goldberg 1985). This result is supported by work showing that the direction of tuning during free saccades is basically the same as during instructed saccades, with perhaps a lower gain (Balan and Ferrera 2003). However, a direct comparison cannot be made here, as units recorded during the free-viewing scan task were not also classified using classic instructed saccade paradigms. This task was designed such that nothing would compromise the naïve state of the animal performing it. Subsequent studies could include instructed saccade tasks, and indeed the original task design included a later phase of task performance that was instructed.

The main finding of the current study that extended previous work related the direction selectivity of cells in the FEF to habitual sequences of saccades that were uninstructed. Though there have been previous studies that used free eye movements (Burman and Segraves 1994) or instructed sequences (Isoda and Tanji 2003), there have not been any, to our knowledge, that examined activity in the FEF during freely formed habitual sequences of saccades. In this context, we found that 56% (25/45) of unique single direction tuned cells were also double direction tuned cells where the single direction selectivity was modulated by either the saccade before or the saccade after. Further, we found that approximately 5-fold more of these 2Dir units

than was expected by chance had preferred direction sequences that were members of the monkeys' habitual loop sequences. It is possible that this number is an underestimation in monkey G because only loop sequences from 4- and 9-target grids were used, not 16- and 25-targets. However, there were substantial similarities in the sequences of movements that monkey G executed, regardless of grid size. Monkey G had a tendency to recapitulate those saccade patterns that were effective on smaller grid sizes on a subset of targets on the larger grids. Therefore any correction for the saccade sequences in the 16-and 25-target tasks would not substantially change the current estimate. Cells in the FEF preferentially represented habitual sequences of eye movements.

Subpopulations of 2Dir tuned cells in the FEF discussed above varied in the amount that they have been previously studied and in their responsiveness to the free-viewing scan task. There are two main subpopulations: single direction tuning modulated by the saccade before (2Dir Bf) and single direction tuning modulated by the saccade after (2Dir Af). Both subpopulations could be further subdivided into those cells with 1Dir tuning that was presaccadic or postsaccadic.

One subpopulation of 2Dir activity, 2Dir Af, appears to have been described previously but was classified differently. Three similar kinds of activity have been studied before: 1) predictive activity during the fixation prior to a saccade that brought a target into the receptive field (Umeno and Goldberg 1997, 2001); 2) activity modulated by the direction of the upcoming saccade (Tian et al. 2000); and 3) predictive activity during the fixation before the second of two saccades in a particular direction or to a particular goal (Phillips and Segraves 2009). However, these studies all focused on cells with presaccadic responses, and of those, mostly focused on cells with visual (V) or visuomovement (VM) activity. Of the ~17 unique presaccadic units recorded from in the FEF of monkey G, four of them (24%) showed significant modulation by the next saccade, the saccade after. These results are comparable to previous studies if one assumes we have classified the same relative population of cells with different techniques.

These findings do not account for those cells that we recorded in the FEF with presaccadic 1Dir tuning that was modulated by the saccade before (PRE 2Dir Bf). Very little work has examined the modulation of presaccadic activity by previous saccades. One study examined sequence selectivity presaccadic cells in the FEF and found 5% of cells to be rank selective and 9% of cells to be sequence selective (Isoda and Tanji 2003). This kind of activity could be taken to be a modulation by the preceding saccade(s). It is possible that the ~41% (7/17) unique monkey G presaccadic units that were modulated by the saccade before (2Dir Bf) were a similar type of cell, but our classification was done without regard to rank or sequences greater than two saccades and suggests that this kind of modulation is more common in our task than previously seen in other studies.

The above discussion leaves out an entire subpopulation of cells in the FEF that has been rarely studied, postsaccadic cells. Indeed, the most common responses we found in the FEF were postsaccadic, with 62% (28/45) of unique units selective for POST in 1Dir. Very little previous work has classified postsaccadic responses, but those studies that have suggest that postsaccadic activity could be related to delay period activity found in the FEF (Balan and Ferrera 2003) or processing the outcomes of choices (Reppas and Newsome 2008). It is interesting to note some of the first recordings in the FEF found only postsaccadic responses (Bizzi 1967). Also, previous

work had found only postsaccadic cells were active during "spontaneous saccades" (Bruce and Goldberg 1985), presaccadic cells were active for scanning but not in the dark (Burman and Segraves 1994), and no presaccadic responses during free eye movements (Balan and Ferrera 2003). The larger proportion of cells that are postsaccadic in the FEF suggests the FEF may also serve a 'memory' function in addition to the well documented 'motor' and 'motor planning' functions ascribed to it in many studies.

The most common subpopulation of 2Dir tuning were those neurons modulated by the saccade before. Of all 2Dir unique units, 84% (21/25) were modulated by the saccade before (2Dir Bf; of the 21, 12 were also modulated by the saccade after). Previous studies utilizing free eye movements did not categorize modulation by the saccade before (Phillips and Segraves 2009), suggesting the authors potentially overlooked this category, or the specifics of the free-viewing scan task used in this study produced these cells. Regardless, this finding suggests that in addition to the saccade planning and visual field mapping functions, cells in the FEF play a role in indexing those eye movements already executed, particularly if those movements are habitual in nature.

Additionally, this same subpopulation of double direction tuned cells with modulation by the saccade before showed greater specificity of tuning in two different contexts. One is that the pool of all 2Dir Bf units across both monkeys showed sharper tuning (higher tuning scores), than all units with 1Dir tuning across all task performance sessions. The second is that this sharper tuning seemed to be experience-driven. Similar results have been seen in other cortical regions (Freedman et al. 2005). Units classified as 2Dir Bf showed the greatest proportion of positive increases in tuning score across recordings from sessions that were all made at the same location. Both these results support the hypothesis that this class of neurons provides a precise representation of habitual sequences of saccades. Further, it is possible that these neurons play a role in the refinement of habitual behavior across task performance sessions, as increases in tuning were paralleled by increases in the repetitiveness of the eye movement sequences executed by the monkeys (see *Chapter II: Behavior*).

This study shows that the FEF participates in sequences of two (or more) saccades in the context of free-viewing. FEF has been shown to participate in sequences before, but the relative level of participation in comparison with another frontal eye movement area, the supplementary or medial eye fields (SEF/MEF), has been debated. Lesions to the FEF produced greater deficits to sequences of eye movements than lesions to the MEF (Schiller and Chou 1998). However, the neural responses selective to sequences and the result of stimulation during sequences have been found to be greater in the SEF (Isoda and Tanji 2003; Histed and Miller 2006). Though this study does not directly address this apparent dichotomy, it does suggest that under the task conditions used for these recordings from the FEF, sequence selectivity may be more common than previously found.

The FEF has been shown to have a wide variety of properties. The present findings begin to show how such tuning and modulation properties could work in concert to produce natural sequences of eye movements. It is the unique properties of the free-viewing scan task that allowed for our two main findings. First, we found that in the naïve monkey the properties of neurons in the FEF are similar to those in well-trained animals. We also found that examples of

direction selectivity and modulation by the saccade before or after existed even very early (the first 10 sessions) in task acquisition. This result could have been hypothesized based on previous findings of the adaptability of neurons in the FEF (Bichot et al. 1996; Umeno and Goldberg 2001), but has not been previously shown in recordings of the naïve animal. This also suggests that any neuronal properties that do not exist in the FEF de novo rapidly develop on the sub-session time scale. These analyses are the primary follow up to those presented here, especially in light of the finding that the patterns of saccades the animal executes from trial-to-trial are shaped by the trial-to-trial difference in the distance that the monkey's eyes travel (see *Chapter II: Behavior*).

The second finding was that the direction tuning of the units in the FEF preferentially reflected those sequences of eye movements that were repeatedly and habitually performed by the animal. This, combined with the finding that this modulation existed for both saccades before and after and for cells that responded preferentially pre- or post-saccades, indicates that the FEF could play a role in not only selecting the targets of upcoming saccadic eye movement or behavioral relevance, but in the creation and tracking of habitual patterns of eye movements by biasing saccade selection in concert with connected areas in the striatum towards those saccades that are performed most efficiently if they are automatically repeated.

Chapter IV: Future Directions

In summary, there were 5 main findings presented here. The first 3 were behavioral, and the second 2 were neural. Behaviorally, we found that: 1) naïve monkeys that performed a free-viewing scan task produced habitual sequences of eye movements without instruction; 2) these habitual sequences gradually evolved to be more predictable and optimal through task performance and were not driven by overall reward or cost (eye movement distance), but were driven by extremely local, trial-by-trial changes in cost; 3) the majority of the monkeys' behavior on the free-viewing scan task was successfully modeled using a simple reinforcement learning algorithm.

For cells recorded in the FEF of the monkeys performing this free-viewing scan task, we found that: 1) the tuning properties of cells, including those recorded when the monkey was still relatively naïve and had performed only 10 sessions of the task, largely replicated previous findings from studies that primarily used highly trained animals performing instructed saccade tasks. The fact that we were able to classify units in the FEF as having many traditional responses during performance of the free-viewing scan task, despite the fact that cells in the FEF had previously been primarily studied under non-natural, instructed conditions, alleviates a general concern that the free-viewing scan task is too unconstrained and opens the door to future analyses.

2) We further found properties not traditionally reported in the FEF cells. Most important for the current research, a subclass of cells was tuned for sequences of two saccades. These cells were tuned for 2-saccade sequences that were members of the habitual saccade sequences at a rate 5-fold greater than chance, were overall more sharply tuned than cells tuned for only 1 saccade direction, and they showed a sharpening of tuning through task performance. These findings suggest that the FEF contains a particularly high fidelity representation of habitual sequences of movements, and may play a role in the creation and tracking of habitual sequences of eye movements.

The primary future direction will be the analysis of neural recordings from the caudate nucleus (CN) that were made alongside recordings in the FEF (and PFC) throughout the task performance of these two animals. Previous work has shown that the striatum dynamically changes its firing responses depending on the stage of habit formation (Jog et al. 1999; Matsumoto et al. 1999; Barnes et al. 2005; Thorn et al. 2010). Preliminary analyses have indicated that similar firing patterns exist in the striatum through the course of task performance on the free-viewing scan task.

The analysis of recordings from the CN in concert with those from the FEF will allow us to harness the power of the simultaneous recording system we developed (see *Appendix*). Such recordings allow the analysis of the interaction between and among areas that is not possible without simultaneous recordings. Frontal cortical areas and striatal areas are well connected, and these 'loops' are thought to participate in the formation of habitual action sequences (Alexander et al. 1986; Parthasarathy et al. 1992; Graybiel 2008). With this task we also have the unique opportunity to start with the naïve state. Other work has looked at the interplay between frontal cortical areas and the striatum during learning in the primate, but on a much shorter time scale (Pasupathy and Miller 2005). We will be able to examine learning, and specifically habit learning, on a time scale that is closer to the natural state: over the course of many days and months. Future analyses will also examine the role activity in the CN could play in biasing activity in the FEF, along with driving habitual behaviors. Such work will be crucial to understanding how both beneficial and pathological habits are formed, and consequently, how they can be broken.

To aid in the goal of elucidating the potential complementary roles of frontal cortex and the striatum in the formation of natural habits, local field potentials (LFPs), in addition to spiking activity, were recorded. The modulation and interaction of oscillations and spiking activity are powerful tools with which to examine the functioning of more than one brain region (e.g., Pesaran et al. 2008; Gregoriou et al. 2009). With simultaneous recordings from the PFC, FEF, and CN there exists the opportunity to examine many levels of interactions between multiple cortical and subcortical regions.

In the free-viewing scan task we have seen how very local and noisy changes in the in the trial-by-trial cost to the animal, the distance the eyes traveled, shaped habitual patterns of saccades. It is possible that this is the reason why it can be easy to pick up new habits. The implication is that a chance association between a particular behavior and a desired outcome could drive the habit learning machinery to quickly code the repetition of this action, without consciousness. Very little is known about the neural underpinnings of this process. Clues as to the participation of one frontal cortical region, the FEF, were provided by results of the current work. We found a general trend towards the sharpening of tuning through task performance and a subclass of cells that preferred habitual sequences, even very early in training. This latter result suggests that such selectivities are formed very rapidly or exist in the naïve state.

In closing, we have developed a novel free-viewing scan task which allowed us to observe natural habit formation and a recording system by which to record simultaneously from multiple cortical and subcortical structures. In concert, these tools were used to record both spiking units and LFPs simultaneously from the PFC, CN, and FEF. These recordings made from naïve monkeys performing the free viewing scan task provide a unique opportunity to perhaps catch the potentially rapid formation of habitual sequences 'in action' in this circuitry in the brain and illuminate the underlying mechanisms. We have thus made the first step towards understanding the neural mechanism underlying habit formation in this naturalistic context, which will hopefully provide insight into the habits that shape our every day life, for better and for worse, in sickness and in health.

Chapter V: Methods

Behavioral Data Acquisition

Two adult female monkeys (*macacca mulata*) were studied (~5.9 kg each). Eye position was monitored by infrared eye tracking (500 Hz, EyeLink II or EyeLink 1000, SR Research Ltd., Mississauga, Ontario, Canada) and recorded with a Cheetah Data Acquisition system (2 KHz, Neuralynx, Inc.). Horizontal and vertical eye position were simultaneously digitized at 1000 Hz (PCI-DAS6032, Measurement Computing, Norton, MA) by a second computer (Intel (R) Pentium (R) 4 CPU 2.40GHz 2.40 GHz, 1.00 GB of RAM, Dell, Round Rock, TX) used for behavior control. Custom behavior control software was designed in Delphi III (Borland Software Corporation, Austin, TX now CodeGear as part of Embarcadero Technologies, San Francisco, CA), a development environment similar to Object Pascal. The behavior control computer also transmitted digital byte codes via an analog to digital card (PCI-DIO48H, Measurement Computing, Norton, MA) to the Neuralynx recording system to be recorded with a common time stamp indicating the occurrence of task events for purposes of correlating with recorded data.

The monkey was seated approximately 50 cm from the LCD screen (17", ViewPanel VG181b, View Sonic, Walnut, CA), and a "hot" mirror that passed visual light and reflected infrared light to the camera above was placed at a 45-degree angle in front of the monkey's nose such that the monkey could view the screen through the mirror and the infrared light would be reflected to the camera above. The EyeLink camera assembly and the hot mirror were all held in place using bars and clamps positioned by an x-y-z stage (Edmund Optics, Barrington, NJ).

Prior to behavioral data acquisition, a head post and recording chamber (see *Electrophysiological Method, General Procedures* for further details) were surgically implanted under pentobarbital anesthesia using sterile methods according to National Institutes of Health guidelines and as approved by Massachusetts Institute of Technology's Committee on Animal Care.

Behavioral Procedures

Each free-viewing scan trial consisted of task epochs as shown in **Figure 1**. The dimensions and spacing of the monkey's display are shown in **Figure 42**. The gray target grids had either 49 (1.6° diameter, 4.1° spacing, monkey G, not illustrated) or 36 (2.0° diameter, 5.4° spacing, monkey Y, illustrated in **Figure 42**) targets. The green target grid replaced the inner portion of the gray grid leaving a perimeter of gray targets and consisted of either 4 or 9 targets (diameters:

4.0°, 2.7°; center-to-center spacing: 13.9°, 7.7° respectively) depending on task acquisition and performance. Both grids spanned the central 17.6° of the screen, and the sum of the total area of green was equal.

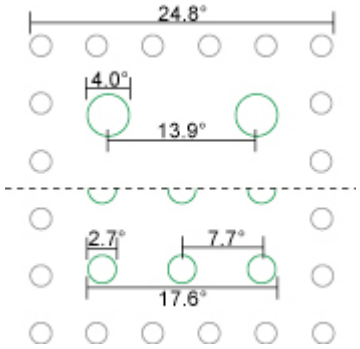

Figure 42. Scan task target spacing. Upper half of figure illustrates 4-target task, lower half 9-target task.

Once the green target grid appeared at the end of the Start Delay, the monkey had 5 s to enter the green grid space, though the monkey's eye position was usually already within that space or became so on the next saccade. On the rare occasion when the monkey's eye position did not enter the green grid space, the trial was aborted. During the Reward Scan, the start of which was not signaled to the monkey, the baited target could be captured by the monkey's gaze either fixating on or saccading through the target. The baited target was chosen by a pseudorandom schedule from the grid of targets such that in a given block of trials each target in the green grid would be chosen an approximately equal number of times (±1 due to the number of trials in a block not being evenly divisible by the number of targets or by premature block termination because the monkey refused to perform any longer). The only constraint placed upon the monkey's eye position throughout the Total Scan Time was that it had to remain within the area defined by the green target grid when it was displayed. There was no upper limit on the duration of the Scan Time as long as this condition was met. Exiting the green target grid resulted in the trial being aborted by extinguishing the green grid and proceeding directly to the ITI with no reward delivered.

After the monkey captured the rewarded target, the green target grid turned off and was immediately replaced by the original gray target grid. In a small number of training sessions, the green target grid turning off would be preceded by the rewarded target briefly blinking (200ms for the target to turn from green to gray and back to green again) to provide feedback to the monkey as to which was the rewarded target. This, however, was not incorporated into the final task design. There were no requirements placed on the monkey's eye position for the remaining task periods. The Reward Delay began immediately following the disappearance of the green target grid (targets off) and was a variable delay of 400-800ms for monkey G and 600-1,200ms for monkey Y. The reward was delivered via a tube inserted into the monkey's mouth during the Reward Time immediately after the Reward Delay and lasted for ~200ms (liquid juice delivered) for monkey G and 250ms (monkey food reward delivered) for monkey Y. Once the optimal amount of reward per trial was found for each animal, the amount was occasionally adjusted slightly according to the monkey's motivation level during a particular session. Reward delivery

was followed by the ITI which was 2s (monkey G) or 3s (monkey Y). Following the ITI another trial of the same size target grid with another pseudoranomly chosen target location would proceed until all the trials for that block were completed.

The first session of task acquisition required an initial estimate of the eye position in relation to the targets. The 4-target scan grid was displayed and a treat (e.g., a raisin) was placed in front of one of the targets. The gain and offset of the eye position signal was adjusted so that when the monkey's eye position was near the treat/target, it was rewarded via the tube in front of its mouth. This procedure was repeated for all four targets. Subsequent recording sessions also included a short period of calibration using the 4-target task, but without the assistance of treats.

Throughout task acquisition, three parameters were manipulated to shape the monkey's behavior: 1) rewarding any target that was captured after the Delay Scan (**Figure 2B**); 2) adjusting the size of the window around each target that would trigger capture (**Figure 2C**); and 3) adjusting the duration of the Delay Scan (**Figure 2D**). This third parameter was the main one used for shaping. During initial task acquisition the Delay Scan was negligible (1-2 ms) but was increased in increments of ca. 50 ms (e.g., 50-100 ms, 100-200 ms) as guided by the monkey's task performance. In general, the monkey's performance was considered suitable for an increase in Delay Scan time if in the two preceding groups of 50 trials the monkey had attained 80% rewarded trials or better. The observation that the monkeys continued to move their eyes during the Delay Scan when they were not required to do so (see **Figure 18** and **Figure 19**) could be result of this shaping procedure. However, it could also indicate that the automatic execution of saccade sequences in a habitual manner was "easier" than timing when the baited target would become available for capture.

Each session consisting of approximately 1,000 rewarded trials was divided into the following blocks: rest, calibration, 5 scan task blocks, rest, 5 scan task blocks, and rest. In the rest block the monkey sat passively in front of a black screen for a period of time approximately equal to 40 trials (c.a. 5 s each). The calibration block was typically 5-15 trials and was occasionally repeated later in the task session if drift of the eye position was suspected. Each scan block consisted of c.a. 100 rewarded trials of a single grid size with each target chosen to be baited an approximately equal number of times. Monkeys first acquired the 4-target task. When more than one grid size was used, monkey G had one block per half-session of the smaller grid size(s) and the remaining blocks were the largest grid size (e.g., 40 4-target trials, 460 9-target trials in a half-session). A sample recording day for monkey G would thus be:

Block	*Rest*	*Calib*	*4-targ*	*9-targ*	*Rest*	*4-targ*	*9-targ*	*Rest*
Num. trials	40	5-15	40	460	40	40	460	40

This structure was simplified for monkey Y so that all scan blocks would be the same target grid size with the exception of one session per week where half the scan blocks were 4-target and the other half were 9-target (e.g., 250 4-target trials, 250 9-target trials in a half-session). That training structure is represented below:

Block	*Rest*	*Calib*	*4-targ*	*9-targ*	*Rest*	*4-targ*	*9-targ*	*Rest*
Num. trials	40	5-15	250	250	40	250	250	40

Grid sizes with more than 9 targets were attempted with monkey G (16 and 25 targets), but were not included for analysis or performed with monkey Y, due to the difficulty the monkeys had in scanning them.

The overall number of sessions spent on each task for each animal was as follows. monkey G spent a total of 13 sessions on the 4-target task before beginning to learn the 9-target task on session 14. Monkey G finished acquisition of the 9-target task in 8 sessions (session 21 overall) and then while attempting to learn larger grid sizes not used in analysis completed another 38 sessions (60 sessions total) which sometimes included some small blocks both the 4- and 9-target tasks. Monkey Y completed acquisition of the 4-target task in a total of 49 sessions and the 9-target task in 61 sessions and performed a total of 202 sessions.

Behavioral Data Analysis

One Y4 and one Y9 session were excluded due to data loss. Session blocks with fewer than 55% rewarded trials were only included if performance on other blocks indicated the monkey was sufficiently motivated to perform the task, and session blocks with fewer than 40 rewarded trials were not included in analyses (~ 4% excluded overall). All eye movement analysis was done in Matlab.

Eye movement parsing

Horizontal and vertical eye position traces were post-processed offline in preparation for data analysis as follows. 1) Event markers were added to indicate the true beginning and end of each trial and compensate for breaks in recording during a session. 2) The data were fragmented by block type to create smaller files for handling in Matlab. 3) The horizontal (or x) and vertical (or y) eye position traces were then "deglitched" to remove the large, high-velocity transitions in eye position that can occur when the eye tracker momentarily (on the order of 2ms) is unable to track the eye. These large "glitches" typically occurred only around the time when the animal blinked, as there are intermediate steps between eye completely open and eye completely closed which are difficult for the camera based eye tracker to properly track. The parameters for large glitch removal were: there was a 500mV difference between two directly following samples and the difference took 1-12 to fall samples back to within 100mV of the starting value. 4) The x and y eye traces were then deglitched twice more to remove much smaller glitches that occurred when there was a slight mismatch between the timing of the output from the eye tracker and the recording. These glitches were a single sample in duration and were first removed only if they were greater than 20mV different from the preceding and following samples and then only if they were greater than 11mV different. 5) Both eye traces were then smoothed using a 33 sample wide Hanning window. All of the preceding steps were performed automatically after setting the initial parameters.

In the next step (6), calibration, slight adjustments were made by hand to ensure the eye traces were in proper register with the displayed targets. X and Y eye traces were plotted simultaneously in two dimensions, superimposed on the locations of the targets on the screen. The previously recorded online calibrations were applied and adjusted according to markers in the data indicating target entrances and exits and visual inspection of the eye traces and their relationship to all the targets present. This process was performed for the task period when the green targets were on for all scan trials in a given session either by inspecting each one, or a large random sample of all the trials depending on the number of trials of a given type in that day. Once the correct calibration was decided upon for a session, it had to be adjusted very little

through the course of that session and could be retrospectively applied to trials earlier in the session where the calibration was less certain (this was especially true earlier in training). New X and Y eye traces were then saved with the applied calibration thus eliminating the necessity to calibrate that session again in the future. 7) The velocity and acceleration of the calibrated eye traces were then calculated.

The final step (8) was to parse the eye traces into saccades, fixations, blinks and "other". This was a challenge, both because we began with naïve animals and because we were interested in the monkey's eye movement behavior throughout an entire training session, not just in the periods while the monkey was actively performing the task (while the green targets were on). This contains a number of sub-processes. a) Histogram the velocity to find thresholds for saccades and blinks. b) Find the maximum value of the x and y eye position traces that indicates where the tracker saturated during a blink. c) Find blinks by finding spans of time that exceed the blink velocity thresholds and/or the x and y eye position maximums. Blinks can have a maximum duration of 500ms. d) If the eye movement traces were found to have oscillatory noise at this point the blinks would be removed from the x and y eye traces and then the desired frequency would be filtered out. e) Saccades and fixations were then marked by identifying those velocity peaks that crossed threshold and then fitting them with a Gaussian. All times that were not categorized as a blink or saccade at the end of this process were marked as a fixation. f) Fixation and saccade event markers were then "cleaned" to prevent impossibilities such as durations that were too short or too long or many overlapping events in a short period (>30 events per sec in a 200 ms sliding window).

Eye movements were then tabulated trial by trial for import into a database (Microsoft Access or Post GRE SQL) and subsequent data analyses. For the purposes of generating these tables, a fixation or saccade was said to have been in or passed through a given target if it fell within a window around the target defined such that the window was as large as it could be around each target without overlapping with adjoining windows.

Sequences

The most frequent eye movement paths or 'loop' sequences were assembled by identifying the top 20 unique sequences of 5 fixations with greater than 20 occurrences and an incidence of greater than 1% in a single session. Sequences of length 5 were used after examining all sequence lengths and obtaining similar results; there were a manageable number of 5-fixation sequences. These were pooled and inspected for overlapping fixation sequences that completed a full loop (began and ended on the same target). The percentage of trials that contained any of the permutations of the full loop (regardless of start or stop position and, if applicable, regardless of whether or not a middle target was stopped on or passed through) was tallied.

The session at which behavioral measures reached asymptote was determined as follows. Starting with all sessions and then one-by-one subtracting beginning sessions (e.g., sessions 1-60, 2-60, 3-60, etc.), data were fitted with regression lines. The slope of each resulting line was tested with a t-test to determine whether it was significantly ($P < 0.01$) different from zero. The data were said to have reached asymptote when the slope of the resulting line fit was not significantly different from zero.

The fraction of trial fixations that were members of the loop sequences was calculated by first determining whether each fixation in each trial was a member of any of the loop sequences for that condition as shown in **Figure 4**. Then the fraction of fixations that were members of the loop sequences over all fixations in that trial was calculated. This fraction was averaged session-by-session for all rewarded trials.

The most probable loop for each session was based first on a single-step Markov model which used each target fixation as a state, as well as start of trial, end of trial, and fixation on a non-target. The state transitions were tallied for an entire session to populate the transition matrix which held the probability of transitioning from any one target to any other target (thus excluding start, stop, and non-target fixations). This transition matrix was then used to attempt to find a loop that began at the lower left corner target and ended at the same target in 15 steps or less.

Transition probabilities used for nonnegative matrix factorization (NMF) were calculated as the probability of a saccade from one target to the next (given fixation on the start target). The number of factors for NMF was determined by computing the root mean square (rms) residual of the factorization using up to 10 (4-target) or 20 (9-target) factors and determining the number of factors necessary for the residuals to complete an initial drop (an "elbow method"). Two NMF decomposition algorithms were applied, an alternating least squares algorithm and Seung's multiplicative update algorithm (Lee and Seung 1999), and the result with smallest residual was chosen (as this best optimizes the NMF objective function). The component factors were normalized.

The statistical dispersion of each NMF factor was assessed by multiplying the absolute value of distance from the median by the height (value) at each session. The value of each factor at each session was then shuffled and the same statistic computed again. This process was repeated 10,000 times and the *P*-value was the fraction of runs with a statistic less than that of the non-shuffled factor.

The entropy of the transition probabilities for each session was defined as:

$$E = -\sum_i q_i \sum_j q_{ij} \log_2 q_{ij} \qquad [1]$$

where q_i is the probability of observing target i, and q_{ij} is the probability of observing target j followed by target i. This measure of entropy was based on Shannon entropy and characterizes how predictable the target transitions are. Entropy is a measure that ranges from zero to one, and the minimum entropy sequences were defined as sequences that were periodic and contained each target exactly once.

The most optimal deterministic patterns were determined using an exhaustive search algorithm with the following three criteria: 1) the solution must be the shortest path length; 2) it must cover all targets in the grid; 3) it must start and end on the same target to form a closed "loop".

Reinforcement test

To reduce variability in the distance calculation due to behavioral shaping for the reinforcement test and inter-sequence interval (ISI) analyses, we calculated the geometric distance the

monkey's eyes traveled during the Total Scan period using only those trials in which the Delay Scan was > 1s and the Reward Scan had >1 saccade. After this initial elimination of trials, analysis was restricted to those trials that remained consecutive. In addition, saccades (distance traveled) in error trials were added to the next rewarded trial, as there was no reward delivered during error trials.

Formally, the reinforcement test was calculated as follows. Reward was calculated as the negative of total distance. The delta distance is defined as

$$D_k = d_k - d_{k-1} \quad [2]$$

where d_k is the total geometric distance of the saccades in the kth trial. Positive D_k is punishment, while negative D_k is reward. To measure the difference in saccade patterns, we compute the transition probabilities P_k between the targets in the kth trial. Note this will be a vector with N^2 components ($N = 4$ or 9 targets). The change in the scan pattern is then defined as

$$\Delta(k,k-1) = P(k) - P(k-1) \quad [3]$$

We then computed the delta pattern dissimilarity using the cosine distance measure:

$$S_k = \frac{\Delta(k,k-1)\cdot(P(k+1) - \Delta(k,k-1))}{|\Delta(k,k-1)||P(k+1) - \Delta(k,k-1)|} \quad [4]$$

Here $|\Delta(k,k\text{-}1)|$ and $|P(k+1)\text{-}\Delta(k, k\text{-}1)|$ are the lengths of the vectors. To detect the correlation between D_k and S_k, we selected all trails with $|D_k| < D_{max}$, where D_{max} is equal to the median of $|D_k|$ plus three times the standard deviation. This selection eliminated ca. 2-3% of the points in D_k at the extremes. The resulting selected trials were then pooled into ten equal-size bins and the median change in distance (D) and pattern dissimilarity (S) was calculated for each bin. A regression line was fit to those data. To determine if the slope of the line was significant, we randomly shuffled S 500 times and computed the slope of the resulting regression line after binning by the same procedure. The P-value is given by the fraction of times the actual slope is less than that of one of the shuffles.

The correlation between the change in distance (D) and the inter-sequence interval (ISI) was calculated in the same manner as for the reinforcement test. The data were pooled into ten equal-size bins and the mean change in distance and ISI was calculated for each bin. A regression line was fit to those data. To determine if the slope of the line was significant, we randomly shuffled ISI 500 times and computed the slope of the resulting regression line after binning by the same procedure. The P-value is given by the fraction of times the actual slope is less than that of one of the shuffles.

REINFORCE algorithm

We constructed the REINFORCE algorithm as follows. The agent followed a Markovian decision mechanism to generate saccades. From target j, the probability of a saccade to target i was p_{ij}. Here $i, j = 1, \ldots, N$, where $N = 4$ or 9 targets. A "start target" was designated as $j = 0$ that corresponded to the initial state of the agent outside of the targets. The transition probabilities were determined from the values m_{ij} associated with the transition from j to i. To determine the probabilities from the values in a manner that would balance discouraging the appearance of suboptimal stereotypical patterns too early, and allowing enough exploration without slow exploitation, we used the following method:

$$p_{ij} = \frac{m_{ij}^4}{\sum_j m_{ij}^4} \quad [5]$$

We generated exploration in m_{ij} through sampling a Gaussian distribution:

$$p(m_{ij}) = N(M_{ij}, \sigma) = \frac{1}{\sqrt{2\pi\sigma^2}} e^{-\frac{(m_{ij} - M_{ij})^2}{2\sigma^2}} \quad [6]$$

Here M_{ij} is the mean of the action values, and σ is the standard deviation. To keep the size of the exploration comparable to the mean, we scaled uniformly at each trial:

$$M_{ij} \rightarrow (1 - \delta) M_{ij} \quad [7]$$

Note that a uniform scaling of M_{ij} does not change the averaged transition probabilities. The constant reduction of M_{ij} balanced the growth of M_{ij} through learning, which kept exploration greater than a minimal level. The learning rule used so that reward would influence how the mean values changed for the exploit step was as follows:

$$M_{ij} \rightarrow M_{ij} + \alpha(r(t) - \bar{r})(m_{ij} - M_{ij}) \quad [8]$$

where $r(t)$ is the reward at time step t; $\bar{r}$ is the averaged reward of past trials; and α is the learning rate. The averaged reward of past trials can be estimated using:

$$\bar{r}(t) = \gamma r(t-1) + (1 - \gamma)\bar{r}(t-1) \quad [9]$$

This is a discrete version of the differential equation:

$$\frac{d\bar{r}(t)}{dt} = \gamma(r(t) - \bar{r}(t)) \quad [10]$$

The above learning mechanism can be mathematically derived from the REINFORCE mechanisms proposed by Williams (Williams 1992).

Our agent had random action values to start with. At each trial, new action values were sampled from the Gaussian distribution and these values determined the transition probabilities from which the sequence of saccades was generated following the same task constraints as the monkeys (1-2 s delay scan and a randomly baited target). The parameters used in the simulations were: $\sigma = 0.1$; $\gamma = 0.5$; $\delta = 10\text{-}5$; $\alpha = 10\text{-}2$ for 4 targets and $\alpha = 2 \times 10\text{-}3$ for 9 targets. These parameters were selected to ensure fast convergence of the saccade patterns to the optimal patterns. Additionally, at each saccade there was a 1% chance that the simulation would make an "error" and abort the trial (11-13% of trials, similar to error rate of monkeys). This allowed the termination of saccade patterns which did not cover all the targets. The distance or time spent in an error trial was added to the next trial's values.

Electrophysiological Method

Note that the method of recording is presented here in brief and elaborated in the *Appendix*.

General Procedures

Prior to behavioral training and data acquisition, a head post and recording chamber (interior dimensions 30x40mm, Specialty Machining, Wayland, MA) were surgically implanted under pentobarbital anesthesia using sterile methods according to National Institutes of Health

guidelines and as approved by Massachusetts Institute of Technology's Committee on Animal Care. Chamber placement was guided using pre-operative structural magnetic resonance images (T1 or T2 weighted images from a 1.5 or 3T magnet) to bilaterally target the prefrontal cortex (PFC), frontal eye fields (FEF), and caudate nucleus (CN). For monkey G the center of the chamber was placed at ML 0, AP 22 and parallel to the horizontal plane of the stereotaxic device. Prior to chamber placement for monkey Y, a mold of the exposed skull was taken using light vinylpolysiloxane impression material (Henry Schein, VP Mix, light body, regular set, orange color), reinforced with Blu-Bite (Henry Schein, Blu-Bite bite registration material, regular set, blue color), and then a positive cast was made using Resinrock (Henry Schein). This skull cast, in addition to precise measurements of skull height, was used to guide the shaping of the underside of the chamber thus enabling a better fit to the skull surface. The center of the chamber for monkey Y was placed at ML 0, AP 22.5 and tilted slightly (~9.4° from the AP horizontal plane).

The location of the implanted chamber was confirmed prior to initial recordings and the start of behavioral training using daily electrode penetrations of four to eight electrodes (Epoxylite coated tungsten, 125 μm shank diameter, impedance 800k-1.2 MΩ, FHC) to map the electrophysiological response properties of the underlying brain structures using the same grid that would later be used for chronic electrode recordings. Microstimulation was used to identify candidate FEF tracks along with determining landmarks in premotor and supplementary motor areas (24-96 pulses, biphasic, 350 Hz, 250 μs/phase, 10-200 μA stimulation current, thresholds ~20-100 μA, (Sommer and Wurtz 2000). The depth of the CN was determined initially using the MR images as a guide and then by guiding one or two electrodes to just above the projected depth and locating the boundary between the internal capsule and the CN.

Electrophysiological Recording

After initial chair training, but before behavioral training of any kind, 72-96 single electrodes were implanted chronically for 6-12 months at a time. We developed a novel recording method to allow chronic recording from ~100 independently moveable electrodes which could be both raised and lowered to allow the isolation of single units. A full description of this method along with the details of how the chronic implant was prepared and implanted is presented in the *Appendix*.

The implant procedure was performed with the monkey under general anesthesia. Custom screw-drive manipulators were loaded with three, six, or nine electrodes (Epoxylite coated tungsten, 125 μm shank diameter, impedance 800k-1.2 MΩ, FHC). During the implant procedure, one manipulator at a time, each manipulator was carefully positioned above the target grid holes and each sharp, inner 27G guide tube covering the electrode was threaded into the outer 23G guide tube already inserted in the grid. Once the guide tubes were properly situated, then each inner guide tube was used to punch through the dura. When all the tracks for the current manipulator had been punched, the manipulator was slowly lowered into position and the pressure-fit pins on the bottom of each manipulator were lowered into the corresponding grid holes to secure the manipulator in place. Upon completion of the placement of all the manipulators and the implantation of all the electrodes, all of the pins from the ends of the electrodes, references, and ground wires were plugged into the connector in such a manner as to interface with the chosen channel on the preamplifier. Once they were plugged in a coat of insulating varnish was applied

to prevent cross-talk between the channels and the wires were carefully bent in order to secure the connectors to the edge of the chamber.

No behavioral training occurred during the first one to two weeks of the chronic implant, during which electrodes were slowly lowered to their initial recording positions in the brain, the points at which putative single units could be identified in the target structures. It was only at this point at which behavioral training commenced. Throughout the duration of the chronic implant, electrodes were raised or lowered only if single units could no longer be isolated from a given recording site. On any given recording day no more than approximately 1/3 to 1/4 of the total electrodes in the implant were moved, and an effort was made not to move electrodes at nearby recording sites (~1 mm away) to promote the stability of recordings. Each recording day a subset of the channels with unit activity were chosen to simultaneously be recorded as local field potentials (LFPs), up to 32. Later recording sessions (starting 1/8/05) utilized a script to dynamically reconfigure amplifiers originally designated to record spike data to record LFP data instead. Therefore any recording electrode that did not have unit activity was recorded as an LFP in addition to the up to 32 LFPs chosen from the channels with units. LFP channels were filtered from 1 to 475 Hz and digitized and recorded at ~2 KHz, and spike channels were filtered 600 to 6000 Hz and were digitized and recorded at 32 KHz using a Cheetah 160 channel system (Neuralynx Inc., Bozeman, MT).

Recording site localization

Electrodes were localized to the FEF using a combination of physiological and anatomical criteria. A track was considered to be a candidate track in the FEF if during mapping sessions prior to the chronic implant of electrodes, microstimulation succeeded in eliciting low-threshold (< 50 μA) eye movements. Tracks nearby (~1mm from stimulated sites), were also considered candidate tracks.

In monkey G electrode placements in the FEF were confirmed via reconstruction from 60 μm thick coronal slices which were then stained with cresyl violet and mounted on slides (**Figure 28** right). Reconstruction was performed by making measurements by hand on a light dissecting microscope and then photographing the sections containing visible electrode tracks of interest for further, more exact reconstruction of electrode position based on daily recording electrode depths. Localization of FEF tracks were then completed by importing photographs of slide-mounted sections into Neurolucida (MicroBrightField, Inc., Williston, VT), an anatomical tracing program (**Figure 29**). Recording locations in the anterior bank of the arcuate suclus near the spur (Brodmann's area 8) that were in or near a track that had microstimulation-induced saccades was said to be in the FEF.

Due to the fact that monkey Y's brain had not yet been sectioned, recording locations in monkey Y's brain were reconstructed using structural magnetic resonance (MR) images. MR images were taken on either a 1.5 or 3 tesla scanner (Siemens, Germany) and the chamber and grid were visualized by filling the chamber and grid with saline while taking T2-weighted images. Images were then imported into Neurolucida and the recording locations on each day of data acquisition were estimated using the grid as a reference point.

FEF Data Analysis

Behavioral task

The behavioral task the monkey performed was the same as for the *Behavioral Data Analysis*. However, due to low numbers of correct trials in the 4- and 9-target tasks for monkey G in sessions where additional grid sizes were performed, correct trials from those larger grid sizes (16- and 25-targets) were included in analyses performed on cells in the FEF. This enabled a larger sampling of all the possible saccade directions. No grid sizes other than 4 and 9 targets were performed by monkey Y.

The behavioral task design was the same for the 16- and 25-target grids as it was for the 4- and 9-target grids; the sole modification was the number and positioning of targets. All target grid sizes spanned the same 17.6° square at the center of the screen. In other words, the edges of the corner targets for the 4-, 9-, 16-, and 25-target grids were all at the same eccentricity. Additionally, the area of the targets was adjusted so that there was always the same amount of green area on the screen, regardless of the number of the targets. This resulted in diameters of 2.0° and center-to-center spacing of 5.4° for the 16 green targets, and diameters of 1.6° and center-to-center spacing of 4.1° for the 25 green targets (see **Figure 42** and *Behavioral Procedures* for details of the 4- and 9-target tasks).

As monkey G acquired each new grid size, the monkey continued to perform smaller blocks of previously acquired grid sizes at the start of recording and at the midpoint of recording each day. For example, if the monkey had completed acquisition of the 4- and 9-target tasks and was acquiring the 16 target task, the money was asked to perform 40 trials of the 4-target task and 90 trials of the 9-target task before it began the approximately 500 total rewarded trials that would be performed of the 16 target task. This block sequence repeated again after a rest block half way through the recording session. When monkey G began acquisition of the 25-target task, smaller blocks of 160 trials of the 16-target task were added on to the beginning and middle points of recording sessions. There were 34 recording sessions that included the 16-target task and 17 sessions that included the 25-target task that were analyzed as part of this data set.

Spike sorting and Unit selection

Spiking units were separated from noise offline using Offline Sorter (Plexon Systems Inc, Dallas, TX). The most common parameters to sort on were principle components one and two, peak, valley, and timestamp. Electrodes generally had between one and five units that could be isolated each recording session, but electrodes that had one or maybe two units were the most common. Each recording channel was sorted from the beginning of training to the end of training sequentially to help maintain consistency in the day-to-day sorting of units.

Often a single electrode was recorded from through many recording sessions without moving that electrode. In order to obtain a non-overlapping sample of units by which to make population estimates, it was necessary to select a representative unit from each stretch of recordings made at the same electrode location. To avoid introducing any bias into the population estimates by the selection process, we bootstrapped by first selecting at random a single cluster to represent each stretch of recordings. Then for each set of randomly selected clusters we tallied the types of units and calculated the population statistics. This process was repeated 1000 times. The number and

types of units and their statistics representing the population were then taken to be the mean of these 1000 bootstrapping runs. This was referred to as the unique unit population.

The unique unit population means were found to be qualitatively similar to population statistics computed by picking the unit with the highest signal-to-noise ratio (SNR) from the second day of each stretch of recording if there was more than one day in a stretch. If there was only one session where the electrode was at a given depth, then the unit with the highest SNR was taken from that day. These "second day" unique units were used to illustrate the properties of the population found via the bootstrapping method.

Single direction tuning

All saccades through all task periods were binned into one of eight 45-degree direction bins centered at 0°, 45°, 90°, 135°, 180°, 225°, 270°, and 315°. Single direction tuning curves were then constructed by taking the mean firing rate for all saccades in each bin through three periods surrounding individual saccades: 1) PRE: from the onset of the fixation preceding the saccade to the onset of the saccade; 2) PERI: from half-way through the fixation preceding the saccade to half-way through the time following saccade onset (saccade duration plus the duration of the following saccade; and 3) POST: from the onset of the saccade to the offset of the fixation following the saccade. All subsequent analyses only used the pre- or post-saccade distinction, as the PERI window was found to not be useful in classifying units; the PRE and POST periods had higher firing rates.

The significance of tuning was assessed using a one-way ANOVA of firing rate across directions corrected for multiple comparisons ($p \leq 0.01 / 28$ comparisons). However, the ANOVA alone was not enough to determine if there was a significant preferred direction. Multiple comparisons of the means were performed using the Tukey-Kramer honestly significant difference criterion. The maximum mean firing rate was required to be significantly different from at least 5 of the other directions. Additionally, if the firing rate mean for the maximum direction was not significantly different from all 7 other bins, then the bins that it was not significantly different from had to be adjacent bins; e.g. if 90° bin was the maximum bin, it was only allowable to not be significantly different from the 45° or 135° bins. This was to permit the existence of broad tuning for a single direction, but not multiple, disparate direction tuning.

For cells that were found to be significantly tuned according to the ANOVA and multiple comparisons criteria in both the PRE and POST windows, we utilized the tuning in relation to sequences of two saccades to disambiguate the two and choose a preferred tuning window. We calculated the correlations between two sets of tuning curves: the windows PRE saccade one (s1) and PRE saccade two (s2), and the windows POST s1 and POST s2. The set with the higher *R*-value (PRE vs. POST) was chosen to be the preferred single-direction tuning window.

The single direction tuning score for each unit was calculated by dividing the firing rate for the maximum direction bin by the mean of the firing rates in all the direction bins for the preferred single direction window.

Double direction tuning

The significance of double-direction tuning using sequences of two saccades was assessed in much the same way as single-direction tuning. First a two-way ANOVA was performed on the 8x8 matrix of possible two-saccade sequences. If there was a significant interaction effect (factors: s1 direction and s2 direction, $p \leq 0.01/ 2016$ comparisons), then the significance of the modulation of the preferred single-direction tuning was assessed. This was done in two possible windows: PRE/POST s1 and PRE/POST s2 depending on the single-direction preference (PRE or POST). A slice through the 8x8 space of all possible sequences was taken that held either s1 or s2 to be the preferred single direction. The significance of the modulation of the firing rate in response to a saccade in the preferred single direction was then assessed in the same manner as for single-direction tuning: using a one-way ANOVA and multiple comparisons of the means.

The double direction tuning score for each unit was calculated separately for modulation by the saccade before and the saccade after. While the first (after) or second (before) saccade in the sequence was held as the preferred 1Dir direction to create a slice through the 8x8 space of all possible two saccade sequences, the firing rate for the maximum bin in that slice was divided by the mean of the firing rates in all bins of that slice.

Task period modulation

The modulation of a unit's 1Dir or 2Dir tuning was analyzed across three task periods: 1) before the scan targets turned on ("pre-scan", during the Start Delay); 2) while the green scan targets were on ("scan", Total Scan Time); and 3) after the green scan turned off ("post-scan", Reward Delay, Reward Time, and ITI; see **Figure 1** for illustration of task periods). A unit's 1Dir or 2Dir tuning was said to have significant modulation by task period if when comparing the firing rate in response to the preferred 1Dir or 2Dir direction, a one-way ANOVA was significant at the $p \leq 0.01$ level, corrected for multiple comparisons. By definition, this would mean that firing in response to the preferred direction(s) in one task period was significantly greater than at least one other task period. The preferred task period was taken to be the period with the maximum firing rate.

Tuning across sessions

Each stretch of recording where a given electrode was not moved across two or more sessions was first examined. A linear regression was fit to the tuning scores across sessions for all units with significant tuning on that channel during each stationary recording stretch. The slope of the line for each stationary recording stretch on each channel was recorded. This process was repeated separately for 1Dir and 2Dir before and after tuning scores. The weighted mean tuning score across all sessions was computed by taking the mean slope of each stretch, weighted by the number of tuning scores that were fit to calculate that slope.

To assess the relationship between the most frequent loop sequences and 1Dir and 2Dir tuning, for each significantly tuned unit (1Dir or 2Dir), we found whether the preferred direction(s) were members of any of the directions represented by the loop sequences on the session in which the unit was recorded. The total fraction of direction selective units that had sequences that were members of the loop sequences were then compared to the fraction of directions represented by the sequences themselves. On each day that there was a unit with significant tuning (1Dir or 2Dir) the number of 1Dir directions (8 possible) or 2Dir combinations of directions (64 possible)

that were represented by the sequences on that day were tallied. To estimate the chance over sessions, the mean of the number of possible directions or combinations of directions was taken for each epoch of comparison (first half of recording sessions and second half of recording sessions). We also performed the same calculation weighting this average of directions represented by the number of units found in the session to be direction tuned and did not find it to qualitatively change the result.

References

Emmons quote from [http://thinkexist.com/quotations/habit/2.html]

Adams, C. D. (1982). "Variations in the sensitivity of instrumental responding to reinforcer devaluation." The Quarterly Journal of Experimental Psychology Section B **34**(2): 77-98.

Alexander, G. E., M. R. DeLong and P. L. Strick (1986). "Parallel organization of functionally segregated circuits linking basal ganglia and cortex." Annu Rev Neurosci **9**: 357-81.

Applegate, D. L. (2006). The traveling salesman problem : a computational study. Princeton, Princeton University Press.

Araujo, C., E. Kowler and M. Pavel (2001). "Eye movements during visual search: the costs of choosing the optimal path." Vision Res **41**(25-26): 3613-25.

Armstrong, K. M., M. H. Chang and T. Moore (2009). "Selection and maintenance of spatial information by frontal eye field neurons." J Neurosci **29**(50): 15621-9.

Bahill, A. T., D. Adler and L. Stark (1975). "Most naturally occurring human saccades have magnitudes of 15 degrees or less." Invest Ophthalmol **14**(6): 468-9.

Balan, P. F. and V. P. Ferrera (2003). "Effects of spontaneous eye movements on spatial memory in macaque periarcuate cortex." J Neurosci **23**(36): 11392-401.

Balleine, B. W. and A. Dickinson (1998). "Goal-directed instrumental action: contingency and incentive learning and their cortical substrates." Neuropharmacology **37**(4-5): 407-19.

Barnes, T. D., Y. Kubota, D. Hu, D. Z. Jin and A. M. Graybiel (2005). "Activity of striatal neurons reflects dynamic encoding and recoding of procedural memories." Nature **437**(7062): 1158-61.

Barraclough, D. J., M. L. Conroy and D. Lee (2004). "Prefrontal cortex and decision making in a mixed-strategy game." Nat Neurosci **7**: 404-10.

Bayer, H. M. and P. W. Glimcher (2005). "Midbrain dopamine neurons encode a quantitative reward prediction error signal." Neuron **47**: 129-41.

Bichot, N. P., J. D. Schall and K. G. Thompson (1996). "Visual feature selectivity in frontal eye fields induced by experience in mature macaques." Nature **381**(6584): 697-9.

Bindra, D. (1974). "A motivational view of learning, performance, and behavior modification." Psychol Rev **81**(3): 199-213.

Bizzi, E. (1967). "Discharge of frontal eye field neurons during eye movements in unanesthetized monkeys." Science **157**(796): 1588-90.

Bizzi, E. and P. H. Schiller (1970). "Single unit activity in the frontal eye fields of unanesthetized monkeys during eye and head movement." Experimental Brain Research **10**(2): 151-158.

Bruce, C. J. and M. E. Goldberg (1985). "Primate frontal eye fields. I. Single neurons discharging before saccades." J Neurophysiol **53**(3): 603-35.

Burman, D. D. and M. A. Segraves (1994). "Primate frontal eye field activity during natural scanning eye movements." J Neurophysiol **71**(3): 1266-71.

Buschman, T. J. and E. K. Miller (2009). "Serial, covert shifts of attention during visual search are reflected by the frontal eye fields and correlated with population oscillations." Neuron **63**(3): 386-96.

Buttner-Ennever, J. A. and A. K. Horn (1997). "Anatomical substrates of oculomotor control." Curr Opin Neurobiol **7**(6): 872-9.
Chomsky, N. (1959). "Review: [untitled]." Language **35**(1): 26-58.
Daw, N. D., Y. Niv and P. Dayan (2005). "Uncertainty-based competition between prefrontal and dorsolateral striatal systems for behavioral control." Nat Neurosci **8**(12): 1704-11.
Daw, N. D., J. P. O'Doherty, P. Dayan, B. Seymour and R. J. Dolan (2006). "Cortical substrates for exploratory decisions in humans." Nature **441**: 876-9.
Dickinson, A. (1985). "Actions and Habits: The Development of Behavioural Autonomy." Philosophical Transactions of the Royal Society of London. B, Biological Sciences **308**: 67-78.
Dickinson, A., J. Campos, Z. I. Varga and B. Balleine (1996). "Bidirectional instrumental conditioning." Q J Exp Psychol B **49**(4): 289-306.
Ding, L. and O. Hikosaka (2006). "Comparison of reward modulation in the frontal eye field and caudate of the macaque." J Neurosci **26**(25): 6695-703.
Ferraina, S., M. Pare and R. H. Wurtz (2000). "Disparity sensitivity of frontal eye field neurons." J Neurophysiol **83**(1): 625-9.
Findlay, J. M. and V. Brown (2006). "Eye scanning of multi-element displays: I. Scanpath planning." Vision Res **46**(1-2): 179-95.
Foster, D. J., R. G. Morris and P. Dayan (2000). "A model of hippocampally dependent navigation, using the temporal difference learning rule." Hippocampus **10**: 1-16.
Freedman, D. J., M. Riesenhuber, T. Poggio and E. K. Miller (2005). "Experience-Dependent Sharpening of Visual Shape Selectivity in Inferior Temporal Cortex." Cereb Cortex.
Fujii, N. and A. M. Graybiel (2003). "Representation of action sequence boundaries by macaque prefrontal cortical neurons." Science **301**(5637): 1246-9.
Fujii, N. and A. M. Graybiel (2005). "Time-varying covariance of neural activities recorded in striatum and frontal cortex as monkeys perform sequential-saccade tasks." Proc Natl Acad Sci U S A **102**(25): 9032-7.
Fukushima, K., T. Yamanobe, Y. Shinmei, J. Fukushima, S. Kurkin and B. W. Peterson (2002). "Coding of smooth eye movements in three-dimensional space by frontal cortex." Nature **419**(6903): 157-62.
Gilchrist, I. D. and M. Harvey (2006). "Evidence for a systematic component within scan paths in visual search." Visual Cognition **14**(4): 704-715.
Goldberg, M. E. and C. J. Bruce (1990). "Primate frontal eye fields. III. Maintenance of a spatially accurate saccade signal." J Neurophysiol **64**(2): 489-508.
Gottlieb, J. P., M. G. MacAvoy and C. J. Bruce (1994). "Neural responses related to smooth-pursuit eye movements and their correspondence with electrically elicited smooth eye movements in the primate frontal eye field." J Neurophysiol **72**(4): 1634-53.
Graybiel, A. M. (2008). "Habits, rituals, and the evaluative brain." Annu Rev Neurosci **31**: 359-87.
Gregoriou, G. G., S. J. Gotts, H. Zhou and R. Desimone (2009). "High-frequency, long-range coupling between prefrontal and visual cortex during attention." Science **324**(5931): 1207-10.
Hammond, L. J. (1980). "The effect of contingency upon the appetitive conditioning of free-operant behavior." J Exp Anal Behav **34**(3): 297-304.
Hayhoe, M. and D. Ballard (2005). "Eye movements in natural behavior." Trends Cogn Sci **9**(4): 188-94.

Henn, V. and B. Cohen (1973). "Quantitative analysis of activity in eye muscle motoneurons during saccadic eye movements and positions of fixation." J Neurophysiol **36**(1): 115-26.
Hikosaka, O., M. K. Rand, S. Miyachi and K. Miyashita (1995). "Learning of sequential movements in the monkey: process of learning and retention of memory." J Neurophysiol **74**(4): 1652-61.
Hilario, M. R. and R. M. Costa (2008). "High on habits." Front Neurosci **2**(2): 208-17.
Histed, M. H. and E. K. Miller (2006). "Microstimulation of frontal cortex can reorder a remembered spatial sequence." PLoS Biol **4**(5): e134.
Isoda, M. and J. Tanji (2003). "Contrasting neuronal activity in the supplementary and frontal eye fields during temporal organization of multiple saccades." J Neurophysiol **90**(5): 3054-65.
Jog, M. S., Y. Kubota, C. I. Connolly, V. Hillegaart and A. M. Graybiel (1999). "Building neural representations of habits." Science **286**(5445): 1745-9.
Jovancevic-Misic, J. and M. Hayhoe (2009). "Adaptive gaze control in natural environments." J Neurosci **29**(19): 6234-8.
Kermadi, I. and J. P. Joseph (1995). "Activity in the caudate nucleus of monkey during spatial sequencing." J Neurophysiol **74**(3): 911-33.
Latto, R. (1978a). "The effects of bilateral frontal eye-field lesions on the learning of a visual search task by rhesus monkeys." Brain Res **147**(2): 370-6.
Latto, R. (1978b). "The effects of bilateral frontal eye-field, posterior parietal or superior collicular lesions on visual search in the rhesus monkeys." Brain Res **146**(1): 35-50.
Lee, D. D. and H. S. Seung (1999). "Learning the parts of objects by non-negative matrix factorization." Nature **401**: 788-91.
Matsumoto, N., T. Hanakawa, S. Maki, A. M. Graybiel and M. Kimura (1999). "Role of [corrected] nigrostriatal dopamine system in learning to perform sequential motor tasks in a predictive manner." J Neurophysiol **82**(2): 978-98.
Miyachi, S., O. Hikosaka, K. Miyashita, Z. Karadi and M. K. Rand (1997). "Differential roles of monkey striatum in learning of sequential hand movement." Exp Brain Res **115**(1): 1-5.
Miyashita, K., M. K. Rand, S. Miyachi and O. Hikosaka (1996). "Anticipatory saccades in sequential procedural learning in monkeys." J Neurophysiol **76**(2): 1361-6.
Mohler, C. W., M. E. Goldberg and R. H. Wurtz (1973). "Visual receptive fields of frontal eye field neurons." Brain Res **61**: 385-9.
Monosov, I. E., J. C. Trageser and K. G. Thompson (2008). "Measurements of simultaneously recorded spiking activity and local field potentials suggest that spatial selection emerges in the frontal eye field." Neuron **57**(4): 614-25.
Montague, P. R., P. Dayan, C. Person and T. J. Sejnowski (1995). "Bee foraging in uncertain environments using predictive hebbian learning." Nature **377**: 725-8.
Morris, G., A. Nevet, D. Arkadir, E. Vaadia and H. Bergman (2006). "Midbrain dopamine neurons encode decisions for future action." Nat Neurosci **9**: 1057-63.
Morse, W. H. and B. F. Skinner (1957). "A second type of superstition in the pigeon." Am J Psychol **70**(2): 308-11.
Najemnik, J. and W. S. Geisler (2005). "Optimal eye movement strategies in visual search." Nature **434**(7031): 387-91.
Najemnik, J. and W. S. Geisler (2008). "Eye movement statistics in humans are consistent with an optimal search strategy." J Vis **8**(3): 4 1-14.

Noser, R. and R. W. Byrne (2010). "How do wild baboons (Papio ursinus) plan their routes? Travel among multiple high-quality food sources with inter-group competition." Anim Cogn **13**: 145-55.
Noton, D. and L. Stark (1971a). "Scanpaths in eye movements during pattern perception." Science **171**(968): 308-11.
Noton, D. and L. Stark (1971b). "Scanpaths in saccadic eye movements while viewing and recognizing patterns." Vision Research **11**(9): 929-942, IN3-IN8.
Parthasarathy, H. B., J. D. Schall and A. M. Graybiel (1992). "Distributed but convergent ordering of corticostriatal projections: analysis of the frontal eye field and the supplementary eye field in the macaque monkey." J Neurosci **12**(11): 4468-88.
Pasupathy, A. and E. K. Miller (2005). "Different time courses of learning-related activity in the prefrontal cortex and striatum." Nature **433**(7028): 873-6.
Pesaran, B., M. J. Nelson and R. A. Andersen (2008). "Free choice activates a decision circuit between frontal and parietal cortex." Nature.
Phillips, A. N. and M. A. Segraves (2009). "Predictive Activity in Macaque Frontal Eye Field Neurons During Natural Scene Searching." J Neurophysiol.
Reppas, J. B. and W. T. Newsome (2008). Decision-outcome encoding in the primate prefrontal cortex. Society for Neuroscience. Washington, DC, Online Meeting Planner. **165.6**.
Ridley, R. M. (1994). "The psychology of perserverative and stereotyped behaviour." Prog Neurobiol **44**: 221-31.
Robinson, D. A. (1964). "The Mechanics of Human Saccadic Eye Movement." J Physiol **174**: 245-64.
Samejima, K., Y. Ueda, K. Doya and M. Kimura (2005). "Representation of action-specific reward values in the striatum." Science **310**: 1337-40.
Schall, J. D. (1991). "Neuronal activity related to visually guided saccades in the frontal eye fields of rhesus monkeys: comparison with supplementary eye fields." J Neurophysiol **66**(2): 559-79.
Schall, J. D. and D. P. Hanes (1993). "Neural basis of saccade target selection in frontal eye field during visual search." Nature **366**(6454): 467-9.
Schall, J. D., D. P. Hanes, K. G. Thompson and D. J. King (1995). "Saccade target selection in frontal eye field of macaque. I. Visual and premovement activation." J Neurosci **15**(10): 6905-18.
Schiller, P. H. (1998). The neural control of visually guided eye movements. Cognitive Neuroscience of Attention: A developmental perspective
J. Richards. Mahwah, NJ, Erlbaum**:** 3-50.
Schiller, P. H. and I. H. Chou (1998). "The effects of frontal eye field and dorsomedial frontal cortex lesions on visually guided eye movements." Nat Neurosci **1**(3): 248-53.
Schiller, P. H. and E. J. Tehovnik (2001). "Look and see: how the brain moves your eyes about." Prog Brain Res **134**: 127-42.
Schiller, P. H. and E. J. Tehovnik (2005). "Neural mechanisms underlying target selection with saccadic eye movements." Prog Brain Res **149**: 157-71.
Schiller, P. H., S. D. True and J. L. Conway (1979). "Effects of frontal eye field and superior colliculus ablations on eye movements." Science **206**(4418): 590-2.
Schultz, W., P. Dayan and P. R. Montague (1997). "A neural substrate of prediction and reward." Science **275**: 1593-9.
Skinner, B. F. (1948). "Superstition in the pigeon." J Exp Psychol **38**(2): 168-72.

Sommer, M. A. (1994). "Express saccades elicited during visual scan in the monkey." Vision Res **34**(15): 2023-38.
Sommer, M. A. (2006). Scan path repetition was seen, but not quantified while collecting data for Sommer, 1994 paper. Personal communication to. T. M. Desrochers. Society for Neuroscience, Atlanta, GA.
Sommer, M. A. and E. J. Tehovnik (1997). "Reversible inactivation of macaque frontal eye field." Exp Brain Res **116**(2): 229-49.
Sommer, M. A. and E. J. Tehovnik (1999). "Reversible inactivation of macaque dorsomedial frontal cortex: effects on saccades and fixations." Exp Brain Res **124**(4): 429-46.
Sommer, M. A. and R. H. Wurtz (2000). "Composition and topographic organization of signals sent from the frontal eye field to the superior colliculus." J Neurophysiol **83**(4): 1979-2001.
Song, C., Z. Qu, N. Blumm and A. L. Barabasi (2010). "Limits of predictability in human mobility." Science **327**: 1018-21.
Sutton, R. S. and A. G. Barto (1998). Reinforcement learning : an introduction. Cambridge, MA, MIT Press.
Tehovnik, E. J., M. A. Sommer, I. H. Chou, W. M. Slocum and P. H. Schiller (2000). "Eye fields in the frontal lobes of primates." Brain Res Brain Res Rev **32**(2-3): 413-48.
Thorn, C. A., H. Atallah, M. Howe and A. M. Graybiel (2010). "Differential dynamics of activity changes in dorsolateral and dorsomedial striatal loops during learning." Neuron **66**(5): 781-95.
Tian, J., J. Schlag and M. Schlag-Rey (2000). "Testing quasi-visual neurons in the monkey's frontal eye field with the triple-step paradigm." Exp Brain Res **130**(4): 433-40.
Umeno, M. M. and M. E. Goldberg (1997). "Spatial processing in the monkey frontal eye field. I. Predictive visual responses." J Neurophysiol **78**(3): 1373-83.
Umeno, M. M. and M. E. Goldberg (2001). "Spatial processing in the monkey frontal eye field. II. Memory responses." J Neurophysiol **86**(5): 2344-52.
Van den Bercken, J. H. and A. R. Cools (1982). "Evidence for a role of the caudate nucleus in the sequential organization of behavior." Behav Brain Res **4**(4): 319-27.
Whitson, J. A. and A. D. Galinsky (2008). "Lacking control increases illusory pattern perception." Science **322**(5898): 115-7.
Williams, D. R. and H. Williams (1969). "Auto-maintenance in the pigeon: sustained pecking despite contingent non-reinforcement." J Exp Anal Behav **12**(4): 511-520.
Williams, R. J. (1992). "Simple statistical gradient-following algorithms for connectionist reinforcement learning." Machine Learning **8**: 229-256.
Williams, Z. M. and E. N. Eskandar (2006). "Selective enhancement of associative learning by microstimulation of the anterior caudate." Nat Neurosci.
Wood, W. and D. T. Neal (2007). "A new look at habits and the habit-goal interface." Psychol Rev **114**(4): 843-63.
Yarbus, A. L. (1967). Eye movements and vision. New York,, Plenum Press.

Appendix: Recording System

The following Appendix is a manuscript in preparation for submission to *Nature Methods*:

A system for recording neural activity chronically and simultaneously from cortical and sub-cortical regions in non-human primates.

Joseph Feingold[1,2]*, Theresa M. Desrochers[2,3]*, Naotaka Fujii[4]*, Ray Harlan[5], and Ann M. Graybiel[2,3]

* These authors contributed equally to this work

[1]HST, MIT, Cambridge, MA, USA
[2]MIBR, MIT, Cambridge, MA, USA
[3]BCS, MIT, Cambridge, MA, USA
[4]BSI, RIKEN, Saitama, Japan
[5]Specialty Machining, Wayland, MA USA

Author Contributions:
JF, TMD, NF, RH, and AMG designed the implant system. JF, TMD, NF and RH manufactured and assembled the components. JF, TMD, NF and AMG performed the surgical procedures. JF, TMD, and NF tested and implemented the system and performed the experiments. JF and TMD wrote the manuscript, with advice and editorial help from NF and AMG.

Abstract

A major goal of neuroscience is to understand the functions of networks of neurons in cognition and behavior. Recent work has focused on implanting fixed arrays of ~100 electrodes or smaller numbers of individually adjustable electrodes, mainly designed to target a few cortical areas. We have developed a recording system that allows independent movement of hundreds of electrodes that can accommodate prolonged chronic recording periods. We have tested this system in macaque monkeys recording simultaneously from up to 127 electrodes in several cortical and subcortical structures for up to one year at a time. Because of the versatility of the system for sampling either the same or different brain sites during prolonged periods in single implants, this system can provide multiple snapshots of network activity across different combinations of sites. By combining microstimulation and injection modes along with recording in the implant designs, this system represents a powerful tool for studying neural network activity in the primate brain.

Introduction

Microelectrode-based recording techniques provide the most direct measure of electrical activity in the brains of behaving animals. Extracellular recordings of neural signals in the awake, behaving monkey, pioneered by Evarts (1968), have shaped our understanding of how the primate brain operates as animals perceive the world, make decisions, and select appropriate actions to reach goals. Despite their remarkable contributions to neuroscience, these classic single-electrode recording techniques by their nature were accompanied by problems, the most important being the inability to measure the activity of many neurons simultaneously. Solving this problem is critical, given the need to analyze brain circuits computing across distributed networks (Alexander et al. 1986; Pesaran et al. 2008; Cohen and Maunsell 2009). Many multi-electrode array and multi-site silicon probe electrode designs have begun to address this problem. There remains, however, a key need to extend these circuit-level designs (Contreras et al. 1996; Graybiel and Rauch 2000; Siapas et al. 2005; Rivlin-Etzion et al. 2006; Hammond et al. 2007; Sommer and Wurtz 2008; Pennartz et al. 2009) to permit independent movement of recording electrodes within the context of individual prolonged chronic periods while maintaining reliable recording at multiple cortical and subcortical sites and the possibility of independent manipulation of individual sites by stimulation or injection. We have addressed this problem in the work described here, with the aim of wide-scale and flexible monitoring neural circuits.

In order to increase the number of simultaneously recorded sites in the monkey brain, three approaches have been pursued. First, surgically implanted arrays of immovable electrodes have led to increased rates of data acquisition by at least one order of magnitude over acute single electrode techniques (Nordhausen et al. 1996; Nicolelis et al. 2003; Vetter et al. 2004; Suner et al. 2005; Ward et al. 2009). The pioneering use of these arrays has led to novel therapies centered on brain-machine interfaces for human patients (Carmena et al. 2003; Hochberg et al. 2006; Velliste et al. 2008). However, a major disadvantage of these arrays is that they do not enable adjustments of the position of the electrode tips over the lifetime of the implant. There is little control over signal quality or the types of cells recorded once they are implanted. It is difficult to obtain and maintain well-isolated units simultaneously on separate electrodes within an array, and the single-unit yield and signal quality decrease with time. Also, while arrays enable the simultaneous recording of activity from multiple sites, in most cases these sites are restricted to a few small regions of cortical surface (Chhatbar et al. 2010). Most importantly, arrays have not been used to study subcortical structures of the primate brain because of the limitations of the implantation technique and the substantial damage to the overlying cortex and white matter that this method would entail (McCreery et al. 2006).

Second, small numbers of chronically implanted adjustable electrodes have been used to gain control over the placement of electrodes post-implantation (Jackson and Fetz 2007). However, the independently movable microwire electrodes targeted only a restricted region of cortex, and adjusting their depths in the brain required anesthesia and hand-held forceps. Other techniques (Lei et al. 2004; Ecker et al. 2010), adapted from methods used in rodents (Wilson and McNaughton 1993; Jog et al. 2002), have begun to be scaled up to record simultaneously from more than one structure in the monkey. It has not been demonstrated whether they could be expanded to record from multiple cortical and deep structures, as this would require reducing the

physical footprint of the headstages substantially, and overcoming the challenge of traversing sulci with microwires.

Third, neuronal activity has been recorded simultaneously from multiple brain structures (Pasupathy and Miller 2005; Hernandez et al. 2008) or from multiple sites within a single structure (Baker et al. 1999; Courtemanche et al. 2003; Gray et al. 2007) in acute preparations. These acute multi-electrode methods can achieve higher rates of data acquisition than the single-electrode methods, but they are either limited to only a few independently movable channels per implant, or they require considerable preparation time prior to each recording session, constraining the duration and frequency of experimental recording sessions. These methods also suffer from the difficulty of maintaining stable signals following acute implantation of multiple electrodes in a confined region, potential for tissue damage from repeated daily penetrations, and the inability to track changes in the activity of a localized neural population over daily recording sessions.

We have developed a chronic multi-electrode recording system for implanting potentially hundreds of independently movable electrodes targeting cortical and subcortical sites in the monkey simultaneously, for periods of up to several months or a year at a time. We have used this system, the Chronic Independently Movable Electrode (ChIME) system, to record from up to 127 electrodes simultaneously in 14 brain regions with implants lasting up to a year, have incorporated microstimulation and reagent injection capabilities within the implants, and have found that this has major advantages by virtue of its flexibility and stability. We therefore describe this system in detail, together with evidence of its adaptability to the needs of circuit-level depth recording in primates. Like chronically implanted arrays, the ChIME system allows repeated sampling of the same sites from session to session, and like acute methods, it enables the sampling of multiple sites along individual recording tracks, providing an opportunity to improve the unit isolation at each site by adjusting the depth of the electrode. The implant procedure is reversible, and individual monkeys can receive multiple implants in succession, with different configurations of microdrives, targeting the same or different brain regions. The ChIME system is straightforward to use and highly flexible – the number and locations of the microdrives can be completely reconfigured implant-to-implant, and the microdrives can be used with many different types of electrodes and in combination with stimulation, injection and optogenetic techniques. We have published experimental results based on the use of pilot versions of the ChIME system(Fujii and Graybiel 2005; Fujii et al. 2007).

Results

Reconfigurable chronic electrode implant system

We designed and implemented the ChIME system to permit simultaneous recording of neural activity from multiple, individually movable microelectrodes chronically implanted in cortical and subcortical structures of the primate brain. The key components of the ChIME system are compact screw-based microdrives that can be placed in nearly any configuration on a grid (**Figure 43** & **Figure 44**). The grid can be inserted into a plastic chamber fixed to the skull, in order to deliver electrodes to the underlying brain. Structural magnetic resonance images (MRIs) are used (**Figure 45a**) to confirm the location of the grid holes relative to the target regions in the

brain. We describe here the use of the system based on results from 16 implants of electrodes placed in cortical and subcortical sites in seven monkeys (**Table 1**).

Monkey ID	*G*	*Y*	*H*	*J*	*K*	*L*	*M*	***Overall***
Chamber lifetime (yrs)	3.2	4.6	3.0	3.7	2.2	2.5	4.5	3.4
Implant duration (days)	189.5	265	121	264	36.3	53	40.5	130.9
Brain areas targeted	7	6	14	10	4	4	6	7.3
Implanted electrodes	84	87	119	115	38.7	39	36	74.8
Recording sessions	75	101.5	24	28	18	20.5	17.5	38.1
Unit-recording electrodes (total)	2196	1816.5	696	723	411	359	253	875.9
Yield:								
1st day of recording	50%	30%	35%	22%	30%	17%	24%	30%
Maximum	60%	36%	39%	32%	79%	78%	71%	57%
Minimum	24%	8%	10%	12%	21%	8%	24%	15%
Mean across all recording sessions ± s.d.	35% ±10%	21% ±6%	25% ±7%	23% ±7%	56% ±17%	47% ±21%	43% ±18%	31% ±16%
Mean unit-recording electrodes per session	29	19	29	25	21	19	18	23
Unit-recording electrodes with activity on at least one day	83%	81%	82%	67%	77%	73%	71%	77%

Table 1. Summary of implant statistics. Values for each monkey were averaged across implants. Overall values were calculated from grand averages across all monkeys and implants.

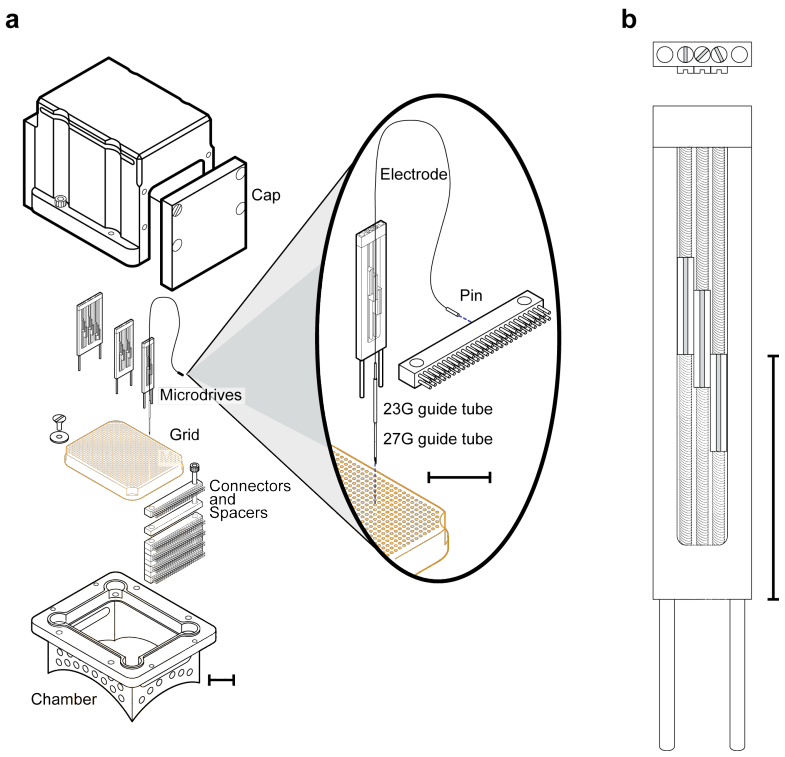

Figure 43. Reconfigurable chronic electrode implant system. (a) Exploded-view schematic of chamber cap, microdrives (left to right, 9, 6, or 3 screws for driving electrodes), grid, connector strips and chamber. Side ports in the chamber below the level of the grid provide access for cleaning and observation of the granulation tissue over the dura. A ridge along the top of the chamber prevents fluid from contaminating the microdrives and connector strips. The chamber cap has upper slots for ventilation and removable side panels for easy access to the connector strips. Inset, a three-screw microdrive loaded with a single electrode. A beveled 27-gauge guide-tube is used for punching through the dura and fits inside a shorter 23-gauge tube to minimize friction with the grid hole. (b) Top- and front-views of a non-loaded three-screw microdrive. Electrodes can be glued to the slotted plastic sled attached to each screw. When the screw is turned, the plastic sled moves along the screw shaft. Scale bars, 1 cm.

Figure 44. Key components of the chronic implant system. (a) The chamber is secured to the skull with bone cement anchored by ceramic bone screws. The chamber can be covered by a raised cap to protect the implanted electrodes (a flat cap, used when no electrodes are implanted, is not shown). (b) The grid (40 x 40 mm2) is prepared for insertion into the chamber by filling the holes with silicone sealant (white), in order to keep the space above the grid dry for the duration of the implant. (c) A six-screw microdrive with a conventional tungsten microelectrode glued to the plastic sled on each screw. Scale bar, 1 cm. (d) During the implant procedure, a beveled 27-gauge guide-tube can be used to punch through the dura, while protecting the electrode tip contained within it. (e) Front-view of an implant of 111 electrodes in monkey J. On the sides, five preamplifiers are connected to the electrode leads via black connector strips. White silicone covers the surface of the grid at the base of the microdrives to promote dryness above the grid. Reference wires, ground wires, and the exposed surfaces of pins are insulated with paint. The depth of each electrode can be manipulated independently by turning the appropriate microdrive screw with a small flat-head screwdriver. (f) Top-view of 117 electrodes in monkey H (implant 1). Insulating varnish is red. Black, red, yellow, and gray wires are the leads from tubes used for reference.

Figure 45. Localization of electrodes simultaneously implanted in cortical and subcortical structures. (a) Coronal section from a T2-weighted structural MR image of monkey D showing the saline-filled grid and chamber above granulation tissue covering the intact dura mater. (b) Dorsal view of right hemisphere of monkey J's brain (anterior at top, medial wall at left). Scale bar, 1 cm. (c) Coronal cresyl violet-stained section from monkey H showing tracks of three electrodes targeting the CN (left) and a fourth approaching the Put (right), all from implant 3, which was removed after the monkey was perfused. Note the remarkably straight approach to the deep targets. (d) Coronal

cresyl violet-stained section from monkey G showing tracks of electrodes that recorded from the CN (lower arrow) and dlPFC (upper arrow) in implant 2. Scale bar, 1 cm.

Microdrives loaded with 3, 6 or 9 individually moveable electrodes were placed on grid within the chamber, and the electrodes were lowered into the brain in a single implant procedure (see Methods). Subsequently, across multiple daily sessions, the electrodes were advanced to their intended target sites. The depth of each electrode was controlled by turning the microdrive screw (158.75 μm/turn) to which it was attached. Implants were left in place for periods of weeks to months, during which the depths of individual electrodes were continually adjusted (maximum travel distance: 13 mm from initial implant depth). Following completion of the recordings, histological analysis was performed to reconstruct the locations of the electrodes (**Figure 45b-d**).

Simultaneously recorded neural activity from multiple cortical and subcortical sites

To test this system, we have used implants that ranged in size from 27-127 electrodes and lasted 22-365 days. In each implant, single-unit spiking activity and local field potentials (LFPs) were recorded simultaneously from electrodes implanted in 6-14 brain structures bilaterally, including medial and dorsolateral prefrontal cortex (mPFC and dlPFC), frontal eye fields (FEF), supplementary eye fields (SEF), primary motor cortex (M1), premotor cortex (PM), supplementary and pre-supplementary motor areas (SMA and pSMA), anterior cingulate cortex (ACC), cingulate motor area, orbitofrontal cortex, parietal cortex, caudate nucleus (CN), putamen (Put), globus pallidus, thalamus and amygdala. Recording sessions occurred on up to 59% of the days an implant was in place. In a single session, up to 57 electrodes recorded unit activity simultaneously (**Table 2**) along with 84 LFP signals. Under the constraints of the data acquisition system that we used, when fewer units were recorded, up to 127 LFPs were recorded simultaneously.

Monkey ID/ Implant No.	*G1*	*G2*	*Y1*	*Y2*	*H1*	*H2*	*H3*	*J1*	*J2*	*K1*	*K2*	*K3*	*L1*	*L2*	*M1*	*M2*
Implant duration (days)	168	211	165	365	139	51	172	271	257	22	40	47	56	50	30	51
Brain areas targeted	8	6	6	6	14	14	14	10	10	4	4	4	4	4	6	6
Implanted electrodes	72	96	95	79	117	115	126	103	127	27	41	48	30	48	40	32
Recording sessions	76	74	65	138	20	23	28	35	21	13	18	23	25	16	6	29
Unit-recording electrodes (total)	2136	2256	1403	2230	591	635	861	957	488	199	313	721	329	389	140	366
Yield:																
1st day of recording	69%	31%	34%	27%	49%	32%	25%	17%	27%	11%	51%	29%	23%	10%	30%	19%
Maximum	72%	48%	39%	33%	49%	37%	32%	38%	27%	93%	63%	81%	80%	75%	70%	72%
Minimum	25%	23%	11%	5%	9%	9%	13%	16%	9%	11%	22%	29%	10%	6%	30%	19%
Mean across all recording sessions ± s.d.	39% ±12%	32% ±5%	23% ±6%	20% ±5%	25% ±9%	24% ±7%	24% ±6%	27% ±6%	18% ±5%	57% ±22%	42% ±10%	65% ±10%	44% ±20%	51% ±23%	58% ±15%	39% ±17%
Mean unit-recording electrodes per session	28	30	22	16	30	28	31	27	23	15	17	31	13	24	23	13
Unit-recording electrodes with activity on at least one day	82%	84%	79%	82%	84%	76%	87%	66%	69%	92%	63%	75%	70%	75%	70%	72%

Table 2. Detailed implant statistics.

We used the ChIME system to record neural signals simultaneously from several neocortical and subcortical regions participating in widely distributed brain networks. The left half of **Figure 46** gives examples of LFPs recorded simultaneously from the left hemisphere of a bilateral implant in monkey H, showing different activity patterns across regions, during performance of a joystick movement task. The right half of **Figure 46** shows examples of unit activity recorded simultaneously from the right hemisphere of a separate implant in monkey G, during performance of an oculomotor scan task. For each implant, all of the recording sites were accessed through a single craniotomy and grid.

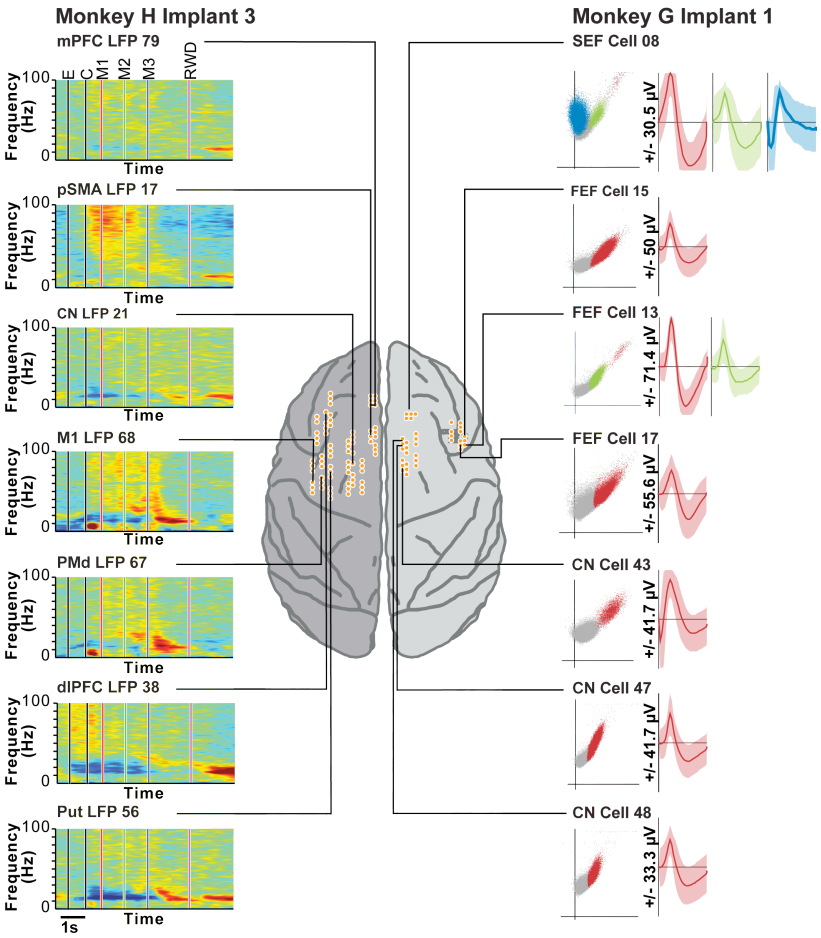

Figure 46. Simultaneously recorded neural activity from multiple cortical and subcortical sites. Center, top-down view of macaque brain showing configuration of electrodes implanted in one hemisphere of each of two chronic implants (left, monkey H, implant 3; right, monkey G, implant 1). Black lines identify the recording sites (projected onto the brain surface) for each sample neural signal shown. Left column, spectrograms of LFP power simultaneously recorded from example sites on day 159 of the implant, during joystick task performance. Spectrograms are aligned in windows on the following task events: trial start (E), cues onset (C), 1st-3rd joystick movement onset (M1-3) and reward delivery (R). The brain structure and electrode number are listed above each spectrogram (abbreviations as in main text). Power at each frequency indicated by color ranging from blue (-5 dB) to red (5 dB). Right column, feature plots and average wave-forms of units simultaneously recorded from the example sites on implant day 126, during performance of an oculomotor scan task. Feature plots show first principal component vs. peak-valley amplitude. Average wave-forms are 1 ms in duration and shading indicates ±3 s.d.

Session-to-session adjustment of individual electrodes' depths

We have found that electrode depths can be adjusted either immediately prior to a recording session or on a previous day. Manipulating the depths of individual electrodes at different times enabled us to monitor activity from different combinations of sites within multiple regions across the recording sessions performed during a single implant (**Figure 47a**). The vertical travel of the microdrives (up to 13 mm) enabled individual electrodes to progress through multiple brain structures over the course of a single chronic implant (**Figure 47b**). Within a given brain structure, it was possible to record from sites at which neurons exhibited different activity profiles along a single track (**Figure 47c**).

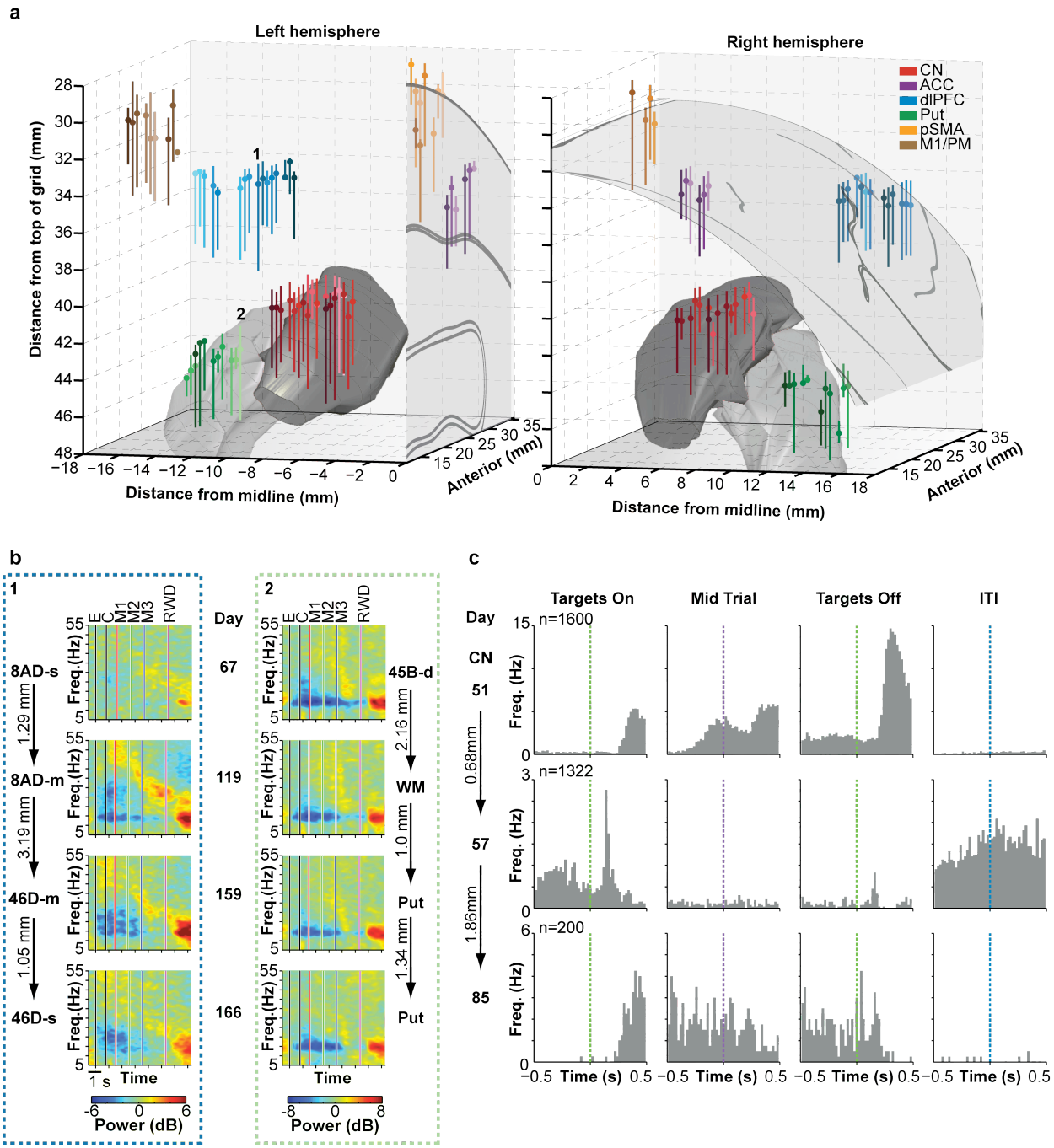

Figure 47. Sampling at different depths across recording sessions. (a) Three-dimensional schematic of all recording tracks for the duration of a single chronic bilateral implant (monkey H, implant 3, 172 days). Medial wall (left) and dorsal surface (right) of cortex shown in gray. Approximate locations of the CN (dark gray) and Put (light gray) also indicated. Vertical colored lines represent the trajectories of the tips of the electrodes from the first through the last recording session of the implant. Dots indicate the electrode tip locations in a recording session midway through the course of the implant (day 98). Color of each line indicates targeted brain structure. (b) Spectrograms of LFP power recorded from two electrodes (labeled 1 and 2 in left hemisphere of a) in four sessions at four depths. Spectrograms follow same conventions as in previous figure. Day of implant, session-to-session change in depth and brain structure shown for each recording site (s, m, d indicate superficial, middle and deep layers of cortex, respectively). (c) Peri-event time histograms of single-unit spiking activity recorded in three sessions at three depths from an electrode targeting the CN in the right hemisphere (monkey G, implant 1, oculomotor scan task, in which monkeys

freely scanned visual targets to find the baited one). Each row shows data from a single session and recording depth (implant day, number of trials and change in depth shown).

We defined the yield in each recording session as the fraction of electrodes that recorded unit activity. The average yield over all sessions was 31% (Mean Yield, **Table 1**), but the yield varied from implant to implant, ranging from 18% to 65% (**Table 2**). The yield averaged across all implants decreased over months (**Figure 48**), though the time-course of the yield differed across implants (**Figure 49**). Implants with fewer electrodes and of shorter durations were associated with higher yields (**Figure 49**, right vs. left columns; note difference in vertical scale). In most implants the yield converged within a few weeks to the overall mean value (31%).

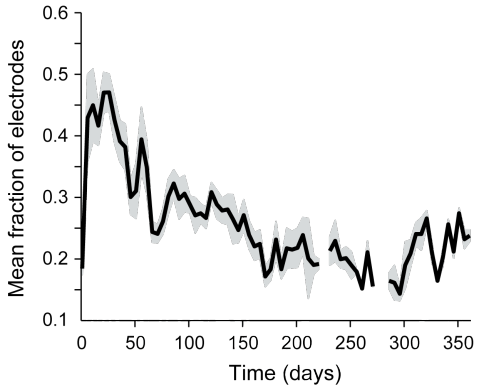

Figure 48. Mean yield over time across implants. The fraction of electrodes that recorded unit activity out of the total number of electrodes averaged over 16 implants in seven monkeys. All electrodes were implanted in the brain on day 0. Since not all implants have a yield measurement for each day of the implant (see next Figure), the mean yield (± s.e.m.) is shown for the pool of available data in five-day bins.

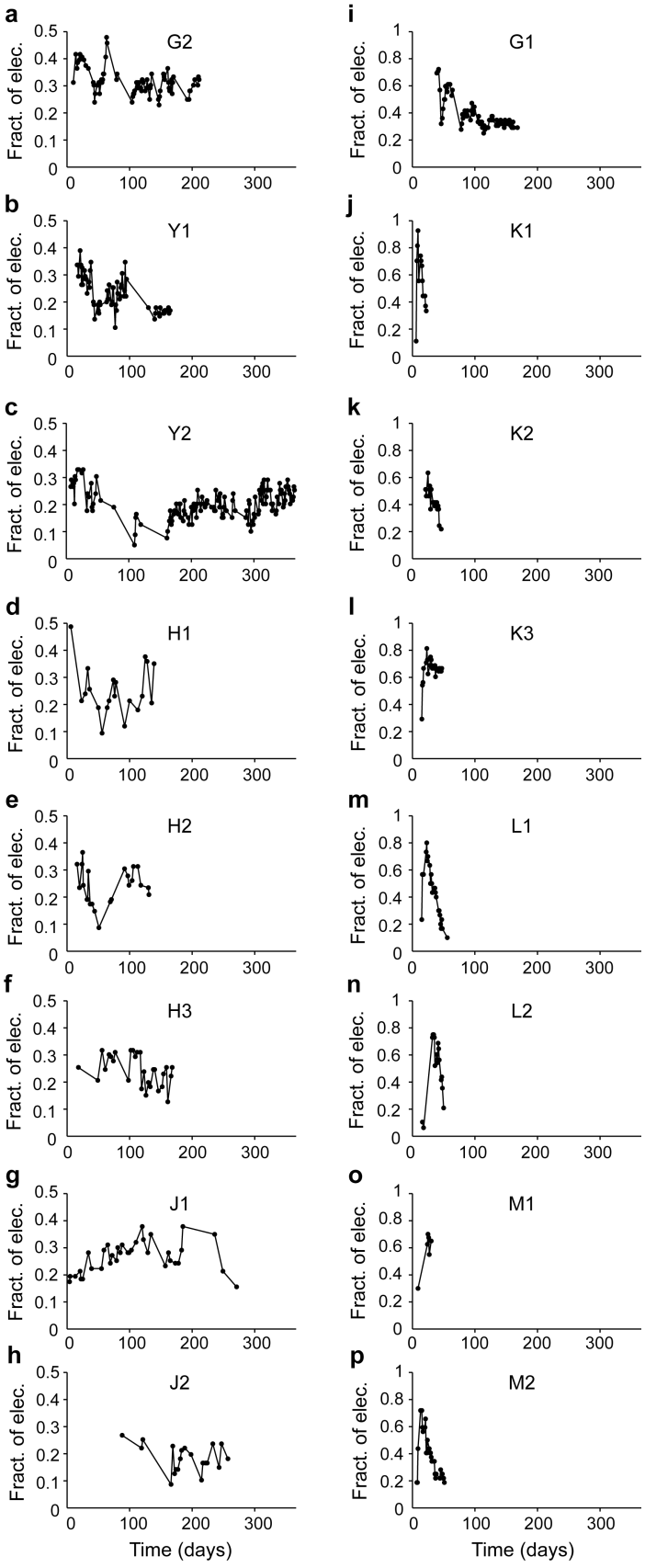
a
G2
b
Y1
c
Y2
d
H1
e
H2
f
H3
g
J1
h
J2
i
G1
j
K1
k
K2
l
K3
m
L1
n
L2
o
M1
p
M2
Fract. of elec.
Time (days)
0
100
200
300
0.1
0.2
0.3
0.4
0.5
0.6
0.8
1

Figure 49. Yield of individual implants across recording sessions. The fraction of electrodes with recorded unit activity out of the total number of electrodes in each of 16 total implants. All electrodes were implanted in the brain on day 0. Vertical scales in the left column (a-h) are half of those in the right column (i-p), in order to better illustrate differences in yield over time for those implants that had a lower maximum yield. The shorter and smaller implants had higher maximum yields.

To investigate the time-course of the yield in individual implants, in each recording session of two monkeys (H and J, 5 implants total), we classified the electrodes that recorded unit activity into two groups: electrodes that had recorded units in the preceding session and electrodes that had not (**Figure 50**). These two groups both contributed persistently to the yield over the course of each implant. Of the electrodes that recorded at least one unit in a given session, 35% ± 18% (mean ± s.d. unless otherwise noted) recorded new unit activity, that is, they had not recorded any units in the previous session (means for each implant in Monkey H: 43% ± 16%, 35% ± 21% and 44% ± 12%; in Monkey J: 25% ± 13% and 32% ± 20%). The emergence of new activity on many electrodes represents a key advantage of the ChIME system over fixed multi-electrode arrays, and new unit activity can continue to arise for several months after the start of an implant.

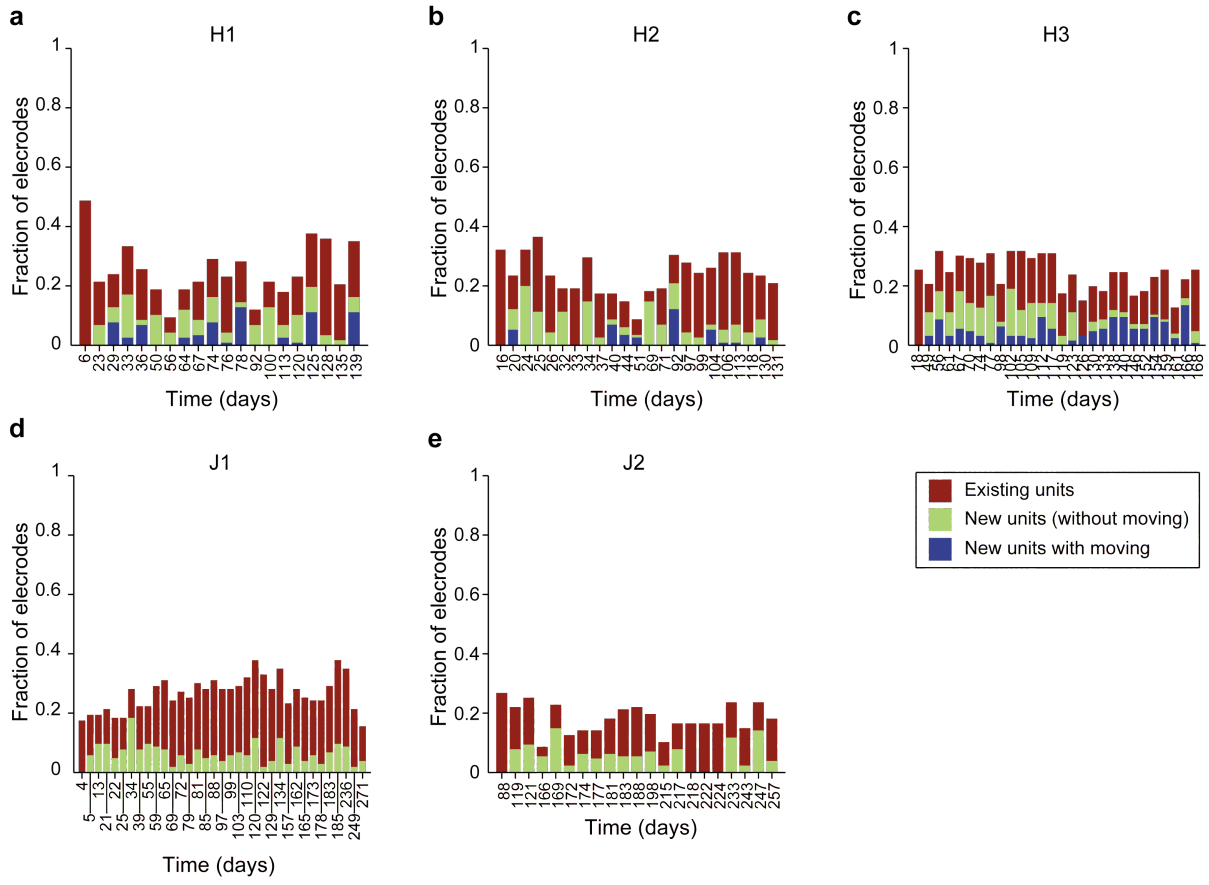

Figure 50. Yield of new and existing units across recording sessions. (a-c) For each session of implants 1-3 of monkey H, the fraction of electrodes that recorded unit activity and had recorded unit activity in the preceding recording session is shown in red (existing units). Also shown are the fractions of all electrodes that recorded new unit activity and that either had been moved since the preceding recording session (new units with moving, blue) or had not (green). All electrodes were implanted in the brain on day 0. (d, e) Same as a-c, except that the electrodes recording new unit activity have not been subdivided into moved vs. not-moved since the preceding session.

To assess the effect of manipulating the depths of the implanted electrodes on the yield, we present an analysis of data from monkey H, because session yields did not differ significantly across all three implants in this monkey (chi-square test, $P > 0.5$). Of the electrodes that recorded new unit activity in a given session, on average 37% ± 32% had been moved since the preceding session (**Figure 50a-c**). As this percentage varied with the rate at which electrodes were moved, it does not imply a causal relationship between moving electrodes and recording new unit activity. Focusing on the electrodes that had not recorded units in a given session, we asked whether moving them increased the likelihood of recording new units in the following session. In each of the three implants, we found that it did. Electrodes that had been moved were significantly more likely to record new units in the following session than electrodes that had not been moved (chi-square test, $P < 10^{-15}$). This comparison likely underestimates the effect of moving electrodes on the yield, as we examined the probability of obtaining unit activity only in the recording session immediately following a session in which an electrode was moved, and we did not take into account the cumulative effects of moving electrodes multiple times before new units were recorded.

Session-to-session stability of neural activity

We tested the ability of the ChIME system to record stable activity over days from multiple electrodes that were not moved in the interim (**Figure 51**). We analyzed the durations of such stretches in 6 implants across 3 monkeys. On average, an electrode recorded unit activity in 2.1 ± 2.8 consecutive sessions (3.9 ± 8.5 days), without being moved. Stationary electrodes that recorded unit activity in at least 2 consecutive sessions recorded unit activity in a total of 4.2 ± 4.1 consecutive sessions (9.7 ± 12.8 days), on average. Such activity was not only stable, but typically exhibited striking similarities in wave-shape, inter-spike interval distribution and responses to task events across sessions (**Figure 51a,** Days 106-115). LFPs recorded from stationary electrodes also showed extraordinary stability over periods of several weeks to months (**Figure 51b**). When the electrodes were moved, the recorded signals changed (**Figure 47b,c**; **Figure 51a** first and last day; **Figure 51b**, last day), suggesting that the preceding recordings were likely obtained from small volumes of brain with similar functional properties.

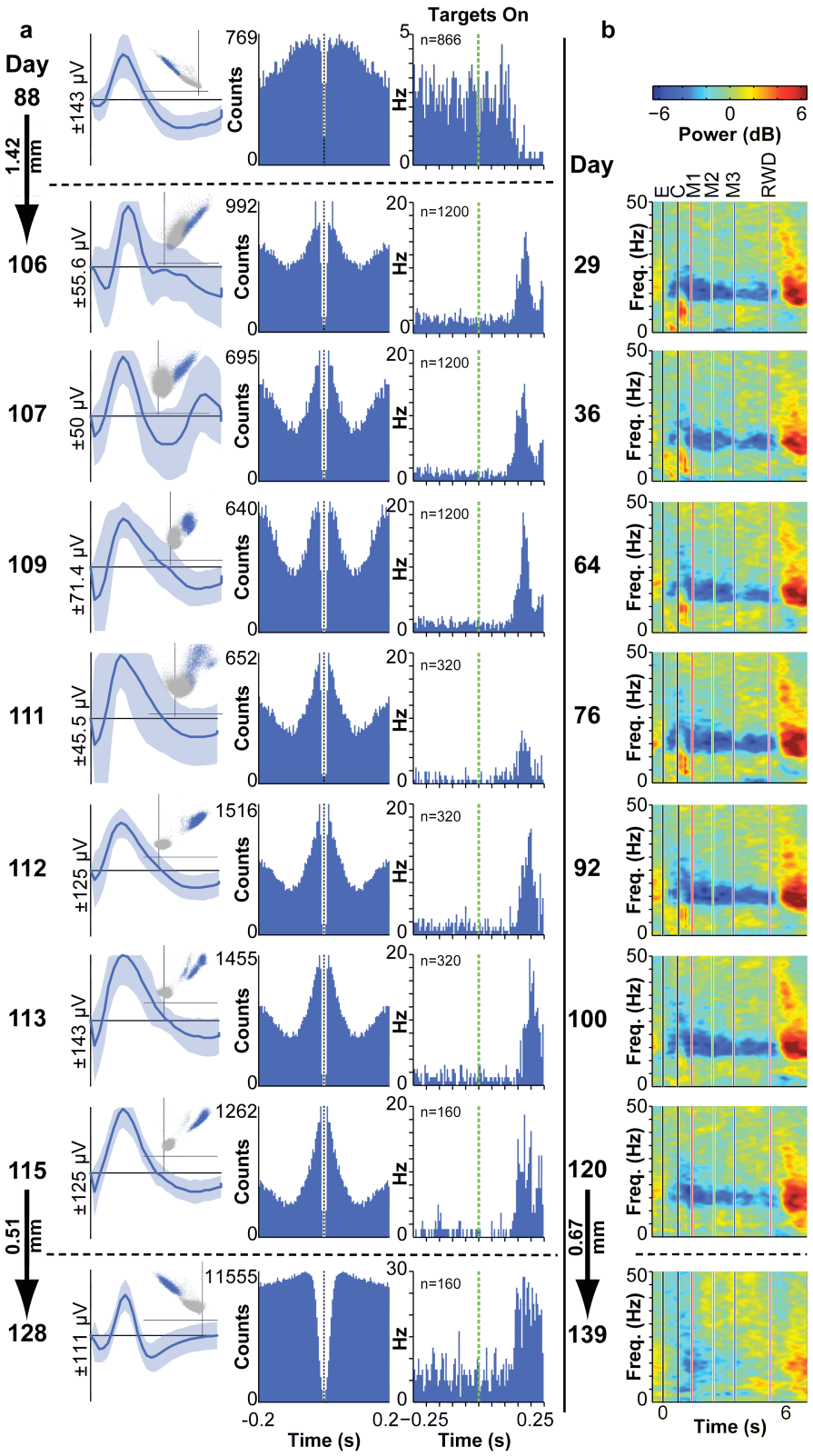

Figure 51. Session-to-session stability of neural recordings. (a) Day of implant, mean wave shape (± 3 s.d.) with inset of first principle component vs. peak-valley feature plot, autocorrelogram and PETH aligned on visual targets on (green line) for a single electrode targeting the CN in the chronic implant of monkey G during performance of the

oculomotor scan task. Each row corresponds to a different recording session. Electrode was moved between day 88 and 106 and again between day 115 and 128. The reduction in phasic unit firing in the PETH on day 111 may be due to the introduction of a new visual task on that day. (b) Spectrograms from an electrode in the dlPFC of monkey H (implant 2) during performance of the joystick task. Spectrograms are aligned in windows on the following task events: trial start (E), cues onset (C), 1st-3rd joystick movement onset (M1-3) and reward delivery (R). Responses from the middle layers of area 9/46 are shown in recording sessions spanning 92 days. Electrode was moved to the deeper layers of 9/46 between day 120 and 139.

Discussion

Large-scale simultaneous recordings from multiple superficial and deep brain structures test the limits of existing methods for extracellular recordings in alert non-human primates. We developed the ChIME system to meet this need. The most important advantage of our system is the opportunity it provides to sample neural activity at multiple depths chronically and flexibly. The ability to move individual electrodes can dramatically improve the yield of single units, as demonstrated by the comparison of the unit activity between electrodes that had or had not been moved across pairs of successive sessions. In addition to its critical effect on the yield, the independent manipulation of electrodes enabled recordings from different combinations of depths across the recording tracks of a single implant (**Figure 47**). This cannot be done using silicon probes with multiple contacts, the distances between which are fixed (Kipke et al. 2003). Finally, by adjusting the depths of electrodes independently, cells that are anatomically connected or that belong to specific classes can be targeted and studied selectively. The ChIME system thus provides a unique opportunity to collect neural data for analyzing circuits spanning cortical and deep structures.

The neural signals on many electrodes were stable across numerous sessions (**Figure 51** and **Figure 50**). The durations of periods of stable activity recorded by individual electrodes were likely limited by the fact that most of the electrodes in an implant were moved periodically, in order to sample new sites along each track. Moving electrodes could have reduced the stability of signals recorded on stationary neighboring electrodes. We suspect that the long-term stability of signals recorded with the ChIME system is due to the combination of continued growth of granulation tissue overlying the exposed dura mater within the chamber and to the multiple guide-tubes stabilizing the dural surface. It is possible for the dura mater and overlying calvarium to re-grow over the course of several weeks, providing even further stabilization of the electrodes. Indeed, we found evidence for dural adhesions to the guide-tubes in at least one monkey that was perfused with the implanted electrodes left in place (see Methods).

As signal quality was often maintained day-to-day, minimal pre-recording preparation time was required, with the bulk of it spent adjusting electrode depths in order to improve single-unit isolation. On any given day, we only adjusted the depths of a fraction of the electrodes. With implants of greater numbers of electrodes, we moved electrodes only on non-recording days. This made the system essentially “plug-and-play” on recording days, maximizing the length of recording sessions.

The number of electrodes used in our experiments to date has been limited only by the capacity of available data acquisition systems. We have demonstrated the capabilities of the ChIME system using commercially available, epoxy-coated tungsten or parylene-coated

platinum/iridium microelectrodes, but we have successfully tested the use of microwire bundles to increase the density of recording sites by increasing the number of recording channels per track. These could be substituted by tetrodes or multi-contact probes, either of which can be attached to a microdrive screw. The number of simultaneously recorded channels could also be increased by adding more microdrives, which can drive ~9 tracks per 30 grid holes, allowing up to ~450 tracks in a single implant (using a 40 mm x 40 mm grid).

The flexibility of the ChIME system permits the incorporation of other methods in conjunction with electrode-based recordings. Microinjections can be made through the grid for pharmacological manipulations and anatomical labeling. Fiber optics can be passed through the grid for use with optogenetic methods, which have recently been extended to the monkey brain (Han et al. 2009). With minor changes (e.g., replacing the microdrive screws with plastic ones), the ChIME system could also be used in paired recording and functional MR-imaging experiments. Using these and other innovative techniques with the ChIME system should make it possible to manipulate and record chemical, electrical and optical signals in nearby tracks simultaneously over long periods of time, giving unprecedented insight into the function of cortical and subcortical networks.

The gradual deterioration of signal quality is a challenge facing all chronic recording methods. The fall-off in yield and accompanying increase in the impedance of many electrodes over the course of an implant has been attributed to the process of gliosis (Stice and Muthuswamy 2009). The ChIME system can be used to reduce the effects of gliosis by moving the electrodes. Nevertheless, in our experience, the signal-to-noise ratio tended to degrade over the duration of the implant along with the proportion of well-isolated single units. Using platinum/iridum electrodes, we have been able to reduce electrode impedances by stimulating frequently to "clean" the electrode tips (Otto et al. 2006). The stimulation paradigm effectively reduced even high impedances (> 2 MOhm) to pre-implant levels. However, stimulation typically did not lead to new unit activity unless the electrodes were subsequently moved.

A potential drawback of the ChIME system, shared by other implant systems, is that the approach of some of the electrodes is not orthogonal to the cortical surface (**Figure 45d**). This can present a challenge for targeting some cortical areas. When necessary, we have addressed this issue by implanting some chambers above a single hemisphere, targeting structures along up to 50 mm of the anterior-posterior axis. This orients most of the grid in parallel to the underlying cortical surface. We have also used smaller chambers (e.g., 30 mm x 30 mm), placed at an angle and offset from the midline.

The ChIME system successfully resolves two major problems associated with current recording techniques: a low rate of data acquisition and the inability to measure the activity of many neurons simultaneously across superficial and deep brain structures. The main advantages of our system include: the ability to sample from a variety of cortical and sub-cortical locations simultaneously; the possibility of changing the recording locations over days; the increased yield resulting from moving electrodes; the ability to sample activity from small volumes of brain with excellent stability over weeks; minimal daily preparation and maintenance; the ability to re-implant monkeys in the same or different brain regions; and the possibility of interfacing with a variety of electrodes and experimental techniques. These key features combine to make a

powerful, simple to use, chronic recording system that we anticipate will contribute to an understanding of the function of multiple interacting circuits widely distributed across the brain.

Acknowledgements

This work was supported by the National Institutes of Health Javits Merit Grant NS025529, National Eye Institute Grant EY012848, Office of Naval Research Grant N000140710903, DARPA Grant NBCHC070105 and the Stanley H. and Sheila G. Sydney Fund (AMG), MIT Zakhartchenko Fellowship (JF) and NDSEG Fellowship (TMD). We thank P. Blazquez, H.F. Hall, M. Cantor, N. Hasegawa, B. DePasquale, A. Quach, P. Harlan, R. Marini, C. Keller-McGandy, M. Histed, Y. Kubota, B. Baker, G. Fakterman, E. Romano, P. Tierney and M.C. Brown.

Methods

Surgical procedures

Procedures were performed under sterile conditions on anesthetized monkeys placed in a standard stereotaxic apparatus, in accordance with National Institutes of Health guidelines and as approved by the Massachusetts Institute of Technology's Committee on Animal Care. Prior to the chamber implant procedure, a mold of the skull was made (VP Mix, Henry Schein) and subsequently used to create a plastic chamber (Delrin, DuPont, DE; Specialty Machining, Wayland, MA). The curved bottom surface of the chamber was machined to fit the contours of the skull precisely. Based on pre-operative MRI of the monkey (T1 and T2 weighted structural images, 1.5-3 Tesla, Siemens, Germany) and in accordance with Rhesus monkey atlases, the chamber was positioned under stereotaxic guidance to facilitate recordings from target brain areas. During the initial procedure, a portion (10 mm x 20 mm) of the skull was removed over the intended recording area in each hemisphere. The chamber was then secured to the skull with radiopaque bone cement (Palacos, Zimmer, OH), anchored by ceramic screws (Thomas Recording, Germany). Divots around the outside of the lower portion of the chamber facilitated the adhesion of the bone cement. The chamber was designed so that the bottom of the removable grid into which the microdrives can be inserted would be ~10 mm above the highest point on the skull, leaving room for fluid to escape through the side ports, rather than rise above the grid. The placement of the chamber was confirmed post-operatively with structural MRI.

At least one month after the chamber implant, the remaining bone covered by the chamber was removed in one or more procedures. Ultimately, sufficient bone was removed to allow access to the entire volume of brain beneath the chamber, resulting in a single opening in the skull of up to 1600 mm^2. Following recovery, additional physiological mapping was performed to reconfirm the 3D coordinates of the brain in relation to the grid. Additional procedures were performed periodically in order to remove growing bone and to thin the dura mater and overlying granulation tissue.

Electrophysiological mapping

Initially, under the guidance of structural MRIs, the cortex and striatum of each monkey was mapped to determine the locations relative to the grid of known brain landmarks. In each mapping session, a 7 mm thick rectangular plastic grid (area: 30 x 30 mm^2, 30 x 40 mm^2, 30 x 50 mm^2 or 40 x 40 mm^2, Specialty Machining, Wayland, MA, **Figure 43a**, **Figure 44b**) was inserted into the recording chamber and secured in place with a screw in each corner. Depending on the size of the grid, its holes (0.025 in diam., spaced 1 mm center-to-center) could provide access to the brain across an area of up to 1600 mm^2. The holes in some grids were offset such that a 90° rotation would provide access to tracks that are shifted by 0.5 mm from those accessible in the original orientation. This design enabled sampling from non-overlapping recording tracks when accessing the underlying brain through the same grid holes in successive chronic implants.

In each mapping session, up to 12 epoxy-insulated tungsten microelectrodes (Frederick Haer, Inc., ME, 1-2 MOhm at 1 kHz, 110 to 130 mm long, 125 μm shank, ~3 μm diam. tip) glued to screw microdrives (**Figure 43a**) were acutely implanted in the brain, using sharp stainless steel

guide-tubes to penetrate the dura mater while protecting the tips of the electrodes. Neuronal responses were characterized by standard somatosensory, visual and auditory tests and by manipulation of the limbs and electrical microstimulation (Master-8, A.M.P.I., Israel, and Bak Electronics, MD, trains of 24-64 250 μs wide biphasic pulses, 333 Hz, 10-150 μA). Several sessions were performed to map the somatotopic organization of the motor and oculomotor cortical areas, including M1(Strick and Preston 1982), FEF(Funahashi et al. 1989; Sommer and Wurtz 2000), SMA and pSMA(Mitz and Wise 1987; Luppino et al. 1991; Matsuzaka et al. 1992), and to confirm the depths of the CN, Put and other subcortical targets, as needed. The dlPFC was defined as the area rostral to the FEF, surrounding the principal sulcus and corresponding to Brodmann Area 9/46.

Chronic implant preparation

Depending on the experiment and based on the MRIs and the results of electrophysiological mapping, the desired number and locations of electrodes were selected. The electrodes were loaded onto custom-made screw-based microdrives (Specialty Machining, Wayland, MA). Each microdrive consisted of 1-3 groups of three adjacent screws each (length, 0.825 in; 160 threads per inch, so that six 360° turns = 0.9525 mm of vertical travel distance), spaced 1 mm apart, and supported by a plastic frame. A pair of stainless steel pins on the bottom of the microdrive frame fit into grid holes and was used to secure the microdrive to the grid inside the chamber rigidly. The microdrive was designed so that the heads of the screws were flush with the top of the microdrive, and could be turned with a flat-head screwdriver (**Figure 43b** top, **Figure 44e**). Each screw was threaded through a 5 mm-long plastic sled with a slot to which one or more electrodes could be glued. The screws rested on the bottom of the microdrive frame, so that turning a screw would cause the attached sled to move along the screw's shaft. The microdrive's plastic frame provided friction to prevent the sleds on the outer screws of each group of three from twisting around the screw threads. The sleds on neighboring screws provided additional stabilizing friction, so long as the center-points of the sleds were less than a sled's length apart in height.

Prior to an implant procedure, the grid was prepared in the following manner. First, the entire top and under side of the grid was covered in a general purpose silicone sealant to prevent fluid from below the grid from contaminating the space above the grid. After curing, the silicone was cleared with a 23-gauge needle from the grid holes needed for the implant. Bare copper wire for carrying the ground was looped below the grid and the free ends were fed through the cleared grid holes and capped with pins to interface with the connectors. In some implants, the copper wire was soldered to a piece of flattened copper mesh, designed to rest over as large a portion of the granulation tissue as possible (without obstructing the path of the electrodes). The outer guide-tubes (23-gauge, extra thin wall) of a set of two telescoping guide-tubes designed to protect each electrode were then inserted into the holes cleared for electrode tracks. These tubes were short enough so that they would not touch the surface of the granulation tissue above the dura. To carry reference signals, a number of electrodes or 23-gauge stainless steel tubes that could reach the tissue under the grid were inserted through cleared grid holes. The entire grid construct was bathed in 70% ethyl alcohol prior to the implant procedure.

The microdrives and electrodes were prepared in parallel with the grid. First, connector pins were crimped onto the ends of the electrodes (same as mapping electrodes or Parylene-coated tungsten or platinum/iridium, 125 μm shank diameter, impedance < 1.5 MΩ, WeSense, Israel)

and then glued (2-hour epoxy, extra slow cure). Second, the impedance of each electrode was tested to confirm that it fell within the acceptable range (0.5-1.5 MOhms). Third, each electrode was glued to a slotted sled on one microdrive screw, so that, upon implanting, the recording tip of the electrode would be at the desired depth relative to the grid. After the glue cured, securing the electrodes to the microdrive, a sharp-edged stainless-steel guide-tube (27-gauge, regular wall hypodermic disposable needle or custom cut and beveled tubing) was slipped over the shank of each electrode and left covering the tip to protect it during the implant procedure. The guide-tubes were filled with mineral oil to keep out blood and other fluids. The electrode leads of each loaded microdrive were grouped together by microdrive using labeled, folded paper slips, intended to prevent the leads from tangling during the implant procedure.

Chronic implant procedure

The implant procedure was performed under aseptic conditions, with the monkey under light general anesthesia (ketamine, xylazine and atropine) and the head fixed within a stereotaxic apparatus. After thoroughly cleaning and drying the chamber and the grid, silicone sealant was applied around the outer edge of the grid. The grid was inserted into the chamber and secured to it with four screws and washers in the corners. Then, one by one working from the center of the implant outward, each microdrive was carefully positioned above the target grid holes. The 27-gauge guide-tubes covering the electrode tips were lowered into the 23-gauge guide-tubes that had already been inserted into the grid. Once all the sharp guide-tubes for a given microdrive were properly situated, they were used to punch small holes through the dura mater, using forceps or fine needle holders. The microdrive was then slowly lowered into position and its bottom pins were fit into the grid holes, so that the bottom of the microdrive frame was flush with the surface of the grid. Openings in the sides of the chamber were used to monitor the tissue underlying the grid and remove any excess fluid during this process.

Upon completion of the implantation of all the electrodes, a bead of silicon sealant was applied along the upper junction of the chamber and grid and the grid anchor screws covered. Any cleared holes in the grid not filled by implant components were also filled in. Then the pins from the ends of the electrode leads, references, and ground wires were plugged into the appropriate spots along the connector strips. Efforts were made to minimize crisscrossing of the leads above the microdrives. Finally, all the wires were carefully bent with forceps in order to accommodate the connectors fastened to the edges of the chamber, and a thick coat of varnish was applied to protect and insulate them (completed implant, **Figure 44e,f**).

Recording sessions and implant maintenance

During the first few weeks of a chronic implant, electrodes were slowly lowered to their initial recording positions in the brain, the earliest points at which unit activity could be detected in the target structures. Once a sufficiently large fraction of electrodes had reached their targets, recordings commenced in daily sessions. Either at the start of recording sessions or in between them (on non-recording days), a subset of electrodes was advanced carefully in ~20 μm steps to isolate units. Typically, on any given day no more than approximately 1/3 of the total electrodes in the implant were moved, and an effort was made not to move adjacent electrodes in order to promote the stability of recordings.

Large slots in the lower portion of the chamber (**Figure 43a**, **Figure 44a**) provided access to the underside of the grid for daily cleaning and observation of the surface of the granulation tissue. At the start of each session, the chamber beneath the grid was flushed thoroughly with sterile saline via these side ports. Depending on the monkey and the chronic implant, this was followed by diluted (20:1) Novalsan Solution (chlorhexidine diacetate 2%) or Betadine Solution (povidone-iodine 10%) 2-5 times per week. The chamber beneath the grid was filled with saline for the duration of the session. Prior to some sessions, the saline was mixed with viscous methyl cellulose, in order to reduce noise resulting from the motion of the saline. When necessary, application of petroleum jelly or silicon grease to the electrode leads between the tops of the microdrives and the connectors effectively dampened mechanical vibrations of the electrodes.

Over the course of the implant, the space above the grid was kept as dry and clean as possible, in order to preserve the quality of recorded signals and the ability to manipulate the depths of electrodes with the microdrives. The grid was sealed with silicone and the side slots in the chamber beneath the grid were left partially open, as needed, to minimize fluid build-up. Further protection from fluid was provided by a raised ridge around the top of the inner surface of the chamber (surrounding the grid) that served as a dam.

In between experimental sessions, the chamber was covered with either a raised cap, while electrodes were implanted in the brain, or a flat cap, otherwise (**Figure 43a** top, **Figure 44a** top). The side panels on the raised cap could be removed to connect pre-amplifiers to the connector strips without having to remove the main portion of the cap. Ventilation slots along the non-removable ends of the raised cap helped to keep the space above the grid dry.

Neuronal signals were amplified and filtered (600-6000 Hz for spikes, and 1-475 Hz for LFPs) by the Cheetah system (Neuralynx Inc., Bozeman, MT). Spike waveforms (32 kHz sampling rate) and LFP signals (2 kHz) were continuously collected during daily recording sessions. The Cheetah system was configured to accommodate up to 128 single electrodes along with 8 analog input channels (for behavioral data). At the start of each recording session, custom software was used to configure each electrode channel to record either spike or LFP data. Spike and LFP signals could be recorded simultaneously from up to 32 electrodes. Each neural (spike or LFP) data channel was stored to a separate file for offline analysis.

In some implants, the impedance of the electrodes was measured periodically and those with high impedance (> 2 MOhm) were stimulated (Master-8, A.M.P.I., Israel, and Bak Electronics, MD, 100-200 ms trains of biphasic pulses at 1 kHz, < 20 μA). Stimulation was repeated up to five times or until the impedance fell below 2 MOhm. Post-stimulation impedance values were measured and recorded.

Implant removal

At the end of a chronic implant, the electrodes were slowly raised to their initial depths, over a few sessions. With the alert monkey head-fixed, the implant was then removed in a single procedure. First, the electrode leads above the microdrives and reference and ground wires were cut, and the connector strips unscrewed from the chamber. Then, each microdrive was removed by first ensuring the electrodes are retracted as far as possible, if possible using forceps to raise guide-tubes and then gently using force perpendicular to the grid to extract the manipulator.

Once all the manipulators have been removed in this manner, the silicon sealing the grid was stripped away and the grid itself removed by unscrewing the corner screws. The chamber was then thoroughly rinsed with sterile saline. The monkey was allowed to recover for at least a few weeks before the next implant. The grid, microdrives and most 23-gauge guide-tubes that could be recovered for use in subsequent implants were cleaned with ethanol, bleach and acetone.

Histology

After experiments were completed, the monkey was perfused intracardially with fixative (0.9% NaCl followed by 4% paraformaldehyde in 0.1 M Na^{2+}/K^{-} PO_4 buffer, pH 7.4). Whenever possible, this was done before removing the final chronic implant. In some cases, electrolytic lesions (10 μA DC for 10 s, < 15 sites) were made to mark locations in the brain relative to the grid. Conventional Nissl staining (60 μm thick slices) was performed to visualize electrode tracks. The slices were analyzed to reconstruct the location of each electrode in each recording session. Tracks from earlier chronic implants were reconstructed on the assumption that the distance from the grid to the surface of the brain was constant across implants. In some monkeys, anatomical tracing software and 3D reconstruction (Neurolucida, MicroBrightField, Inc., Williston, VT) was used.

Appendix References

Alexander, G. E., M. R. DeLong and P. L. Strick (1986). "Parallel organization of functionally segregated circuits linking basal ganglia and cortex." Annu Rev Neurosci **9**: 357-81.

Baker, S. N., N. Philbin, R. Spinks, E. M. Pinches, D. M. Wolpert, D. G. MacManus, Q. Pauluis and R. N. Lemon (1999). "Multiple single unit recording in the cortex of monkeys using independently moveable microelectrodes." J Neurosci Methods **94**(1): 5-17.

Carmena, J. M., M. A. Lebedev, R. E. Crist, J. E. O'Doherty, D. M. Santucci, D. F. Dimitrov, P. G. Patil, C. S. Henriquez and M. A. Nicolelis (2003). "Learning to control a brain-machine interface for reaching and grasping by primates." PLoS Biol **1**(2): E42.

Chhatbar, P. Y., L. M. von Kraus, M. Semework and J. T. Francis (2010). "A bio-friendly and economical technique for chronic implantation of multiple microelectrode arrays." J Neurosci Methods **188**(2): 187-94.

Cohen, M. R. and J. H. Maunsell (2009). "Attention improves performance primarily by reducing interneuronal correlations." Nat Neurosci **12**(12): 1594-600.

Contreras, D., A. Destexhe, T. J. Sejnowski and M. Steriade (1996). "Control of spatiotemporal coherence of a thalamic oscillation by corticothalamic feedback." Science **274**(5288): 771-4.

Courtemanche, R., N. Fujii and A. M. Graybiel (2003). "Synchronous, focally modulated beta-band oscillations characterize local field potential activity in the striatum of awake behaving monkeys." J Neurosci **23**(37): 11741-52.

Ecker, A. S., P. Berens, G. A. Keliris, M. Bethge, N. K. Logothetis and A. S. Tolias (2010). "Decorrelated neuronal firing in cortical microcircuits." Science **327**(5965): 584-7.

Evarts, E. V. (1968). "Relation of pyramidal tract activity to force exerted during voluntary movement." J Neurophysiol **31**(1): 14-27.

Fujii, N. and A. M. Graybiel (2005). "Time-varying covariance of neural activities recorded in striatum and frontal cortex as monkeys perform sequential-saccade tasks." Proc Natl Acad Sci U S A **102**(25): 9032-7.

Fujii, N., S. Hihara and A. Iriki (2007). "Dynamic social adaptation of motion-related neurons in primate parietal cortex." PLoS ONE **2**: e397.

Funahashi, S., C. J. Bruce and P. S. Goldman-Rakic (1989). "Mnemonic coding of visual space in the monkey's dorsolateral prefrontal cortex." J Neurophysiol **61**(2): 331-49.

Gray, C. M., B. Goodell and A. Lear (2007). "Multichannel micromanipulator and chamber system for recording multineuronal activity in alert, non-human primates." J Neurophysiol **98**(1): 527-36.

Graybiel, A. M. and S. L. Rauch (2000). "Toward a neurobiology of obsessive-compulsive disorder." Neuron **28**(2): 343-7.

Hammond, C., H. Bergman and P. Brown (2007). "Pathological synchronization in Parkinson's disease: networks, models and treatments." Trends Neurosci **30**(7): 357-64.

Han, X., X. Qian, J. G. Bernstein, H. H. Zhou, G. T. Franzesi, P. Stern, R. T. Bronson, A. M. Graybiel, R. Desimone and E. S. Boyden (2009). "Millisecond-timescale optical control of neural dynamics in the nonhuman primate brain." Neuron **62**(2): 191-8.

Hernandez, A., V. Nacher, R. Luna, M. Alvarez, A. Zainos, S. Cordero, L. Camarillo, Y. Vazquez, L. Lemus and R. Romo (2008). "Procedure for recording the simultaneous

activity of single neurons distributed across cortical areas during sensory discrimination." Proc Natl Acad Sci U S A **105**(43): 16785-90.
Hochberg, L. R., M. D. Serruya, G. M. Friehs, J. A. Mukand, M. Saleh, A. H. Caplan, A. Branner, D. Chen, R. D. Penn and J. P. Donoghue (2006). "Neuronal ensemble control of prosthetic devices by a human with tetraplegia." Nature **442**(7099): 164-71.
Jackson, A. and E. E. Fetz (2007). "Compact movable microwire array for long-term chronic unit recording in cerebral cortex of primates." J Neurophysiol **98**(5): 3109-18.
Jog, M. S., C. I. Connolly, Y. Kubota, D. R. Iyengar, L. Garrido, R. Harlan and A. M. Graybiel (2002). "Tetrode technology: advances in implantable hardware, neuroimaging, and data analysis techniques." J Neurosci Methods **117**(2): 141-52.
Kipke, D. R., R. J. Vetter, J. C. Williams and J. F. Hetke (2003). "Silicon-substrate intracortical microelectrode arrays for long-term recording of neuronal spike activity in cerebral cortex." IEEE Trans Neural Syst Rehabil Eng **11**(2): 151-5.
Lei, Y., N. Sun, F. A. Wilson, X. Wang, N. Chen, J. Yang, Y. Peng, J. Wang, S. Tian, M. Wang, Y. Miao, W. Zhu, H. Qi and Y. Ma (2004). "Telemetric recordings of single neuron activity and visual scenes in monkeys walking in an open field." J. Neurosci. Methods **135**(1-2): 35-41.
Luppino, G., M. Matelli, R. M. Camarda, V. Gallese and G. Rizzolatti (1991). "Multiple representations of body movements in mesial area 6 and the adjacent cingulate cortex: an intracortical microstimulation study in the macaque monkey." J Comp Neurol **311**(4): 463-82.
Matsuzaka, Y., H. Aizawa and J. Tanji (1992). "A motor area rostral to the supplementary motor area (presupplementary motor area) in the monkey: neuronal activity during a learned motor task." J Neurophysiol **68**(3): 653-62.
McCreery, D., A. Lossinsky, V. Pikov and X. Liu (2006). "Microelectrode array for chronic deep-brain microstimulation and recording." IEEE Trans Biomed Eng **53**(4): 726-37.
Mitz, A. R. and S. P. Wise (1987). "The somatotopic organization of the supplementary motor area: intracortical microstimulation mapping." J Neurosci **7**(4): 1010-21.
Nicolelis, M. A., D. Dimitrov, J. M. Carmena, R. Crist, G. Lehew, J. D. Kralik and S. P. Wise (2003). "Chronic, multisite, multielectrode recordings in macaque monkeys." Proc. Natl. Acad. Sci. U.S.A. **100**(19): 11041-6.
Nordhausen, C. T., E. M. Maynard and R. A. Normann (1996). "Single unit recording capabilities of a 100 microelectrode array." Brain Res. **726**(1-2): 129-40.
Otto, K. J., M. D. Johnson and D. R. Kipke (2006). "Voltage pulses change neural interface properties and improve unit recordings with chronically implanted microelectrodes." I.E.E.E. Trans. Biomed. Eng. **53**(2): 333-40.
Pasupathy, A. and E. K. Miller (2005). "Different time courses of learning-related activity in the prefrontal cortex and striatum." Nature **433**(7028): 873-6.
Pennartz, C. M., J. D. Berke, A. M. Graybiel, R. Ito, C. S. Lansink, M. van der Meer, A. D. Redish, K. S. Smith and P. Voorn (2009). "Corticostriatal Interactions during Learning, Memory Processing, and Decision Making." J Neurosci **29**(41): 12831-8.
Pesaran, B., M. J. Nelson and R. A. Andersen (2008). "Free choice activates a decision circuit between frontal and parietal cortex." Nature.
Rivlin-Etzion, M., O. Marmor, G. Heimer, A. Raz, A. Nini and H. Bergman (2006). "Basal ganglia oscillations and pathophysiology of movement disorders." Curr Opin Neurobiol **16**(6): 629-37.

Siapas, A. G., E. V. Lubenov and M. A. Wilson (2005). "Prefrontal phase locking to hippocampal theta oscillations." Neuron **46**(1): 141-51.
Sommer, M. A. and R. H. Wurtz (2000). "Composition and topographic organization of signals sent from the frontal eye field to the superior colliculus." J Neurophysiol **83**(4): 1979-2001.
Sommer, M. A. and R. H. Wurtz (2008). "Brain circuits for the internal monitoring of movements." Annu Rev Neurosci **31**: 317-38.
Stice, P. and J. Muthuswamy (2009). "Assessment of gliosis around moveable implants in the brain." J. Neural. Eng. **6**(4): 046004.
Strick, P. L. and J. B. Preston (1982). "Two representations of the hand in area 4 of a primate. I. Motor output organization." J Neurophysiol **48**(1): 139-49.
Suner, S., M. R. Fellows, C. Vargas-Irwin, G. K. Nakata and J. P. Donoghue (2005). "Reliability of signals from a chronically implanted, silicon-based electrode array in non-human primate primary motor cortex." IEEE Trans Neural Syst Rehabil Eng **13**(4): 524-41.
Velliste, M., S. Perel, M. C. Spalding, A. S. Whitford and A. B. Schwartz (2008). "Cortical control of a prosthetic arm for self-feeding." Nature **453**(7198): 1098-101.
Vetter, R. J., J. C. Williams, J. F. Hetke, E. A. Nunamaker and D. R. Kipke (2004). "Chronic neural recording using silicon-substrate microelectrode arrays implanted in cerebral cortex." I.E.E.E. Trans. Biomed. Eng. **51**(6): 896-904.
Ward, M. P., P. Rajdev, C. Ellison and P. P. Irazoqui (2009). "Toward a comparison of microelectrodes for acute and chronic recordings." Brain Res.
Wilson, M. A. and B. L. McNaughton (1993). "Dynamics of the hippocampal ensemble code for space." Science **261**(5124): 1055-8.